PROCESSING-STRUCTURE-PROPERTY RELATIONSHIP IN ELECTROSPUN POLYMER NANOFIBERS

RYUJI INAI
(M. Eng), KIT

A THESIS SUBMITTED

FOR THE DEGREE OF Ph.D. OF ENGINEERING

DEPARTMENT OF MECHANICAL ENGINEERING

NATIONAL UNIVERSITY OF SINGAPORE

2007

ACKNOWLEDGEMENT

I would like to express my deep gratitude and great respect to my supervisor, Prof. Seeram Ramakrishna, for his inspiration and encouragement during my Ph.D. study. I also greatly appreciate the discussions and guidance from my co-supervisor, Dr. Chan Kwan-Ho, Casey. I am deeply grateful to Prof. Masaya Kotaki for his valuable discussions and support.

Special thanks are given to Dr Kazutoshi Fujihara, Chan Kok Ho Kent and Tan Si Hui for their instructions with the experimental supports. Throughout my study, I have greatly benefited from working with my colleagues- Dr. Thomas Yong, Dr. Ma Zuwei, Teo Wee Eong, Renuga Gopal, Satinderpal Kaur, Teo Chieh Yin Karen, Wang Yanping Karen, He Wei and Ramakrishnan Ramaseshan. To Steffen Ng and Kelly Low Puay Joo for handling all administrative work related to this thesis. Their friendship and unconditional support will always be remembered. I wish them the best in all their future endeavors. Finally, I would like to show my appreciation to my wife and parents. Thanks to their love and kindest supports, I could overcome the facing problems and complete Ph.D. study.

Table of Contents

Acknowledgements i

Table of Contents ii

Summary vi

List of Tables x

List of Figures xii

List of Publications xvii

Chapter I INTRODUCTION 1

Chapter II Literature Review 5

2-1. Overview of Polymer Micronfibers 5

2-1-1. Melt-spinning Process 5

2-1-2. Solution-spinning Process 7

2-1-3. Post-drawing Process 7

2-1-4. Structure Formation during Processing 9

2-1-5. Structure-Property Relationship 13

2-2. Overview of PLLA Micronfibers 17

2-2-1. Processing-related Parameters Effects on Molecular Structure of PLLA Fibers 17

2-2-2. Structure Formation of PLLA Fibers 19

2-2-3. Structure-property Relationship of PLLA Fibers 20

2-3. Polymer Nanofibers 22

2-3-1. Processing of Polymer Nanofibers 22

2-3-2. Processing-Fiber Morphology Relationship 24

2-3-3. Processing-Molecular Structure Relationship 33

2-3-4. Structure-Property Relationship 34

Chapter III FIBER MORPHOLOGY OF ELECTROSPUN POLYMER FIBERS AND THEIR ARCHITECTURE **36**

3-1. Introduction 36

3-2. Experimental 38

3-2-1. Design of Electrospinning Setup 40

3-2-2. Materials Selection 41

3-2-3. Control of Humidity Level 41

3-2-4. Conductivity Meter and Rheometer 41

3-2-5. Scanning Electron Microscopy (SEM) and Transmission Electron Microscopy (TEM) 42

3-3. Results and Discussion 42

3-3-1. Fiber Morphology 42

(1) Solution Properties Effect 42

(2) Processing Conditions Effect 49

(3) Ambient Conditions Effect 53

(4) Processing Map 57

(5) Electrospinning of Ultra-fine Polymer Fibers 60

3-3-2. Fibers Patterning 60

(1) Effect of Table Material 60

(2) Effect of Take-up Velocity 63

(3) Electrospinning of 3-D architecture with aligned nanofibers 64

3-4. Summary 65

Chapter IV STRUCTURE AND PROPERTIES OF AS-SPUN FIBERS **67**

4-1. Introduction 67

4-2. Experimental 69

4-2-1. Materials 69
4-2-2. Solvent-cast Film 70
4-2-3. Annealing 71
4-2-4. X-ray Diffraction (XRD) 71
4-2-5. Differential Scanning Calorimetry (DSC) 71
4-2-6. Tensile Test of Electrospun Nanofiber Membranes 72
4-2-7. Tensile Test of Electrospun Single Nanofibers 73
4-3. Results 75
4-3-1. Evaluation of Tensile Test Method using Nanofiber Membranes 75
4-3-2. As-spun PLLA Nanofibers 79
4-3-3. As-spun PCL Nanofibers 94
4-3-4. As-spun P(LLA-r-CL) Copolymer Nanofibers 99
4-4. Discussion 102
4-5. Summary 106

Chapter V STRUCTURE AND PROPERTIES OF ELECTROSPUN FIBERS VIA POST-PROCESSING 109

5-1. Introduction 109
5-2. Experimental 110
5-2-1. Material Selection 110
5-2-2. Post-processing 111
5-2-3. Tensile Test of Electrospun Single Nanofibers 114
5-3. Results 114
5-3-1. Annealing Effects 114
5-3-2. Hot-drawing Effects 118
5-4. Discussion 128

5-5. Summary 137

Chapter VI CONCLUDING REMARKS AND RECOMMENDATIONS 140

6-1. Summary and Results 140

6-2. Review of Contributions 145

6-3. Recommendations for Future Works 146

6-4. Conclusion 148

REFERENCES 149

SUMMARY

In this study, processing-structure-properties relationship in electrospun biodegradable polymer nanofibers was investigated. In order to study the relationship, an electrospinning setup was designed and developed (chap. 3). Unlike the standard setup, ambient conditions can be controlled using the developed setup.

The purpose in the first part of the work (processing studies) was to discuss the effects of electrospinning parameters on electrospun fiber morphology (fiber diameter and fiber uniformity). It was found that electrospun fiber diameter is determined by mass of polymer in the spinning jet and the jet drawing ratio. The tendencies to change fiber morphology were summarized in the processing map. Based on the systematic parameter studies, polymer nanofibers as small as 9nm in diameter were successfully produced. With the electrospinning setup developed in this study, 2D and 3D structures with electrospun aligned nanofibers were successfully produced (Chap. 3).

Structure formation / development in electrospun nanofibers were discussed using semi-crystalline rigid (PLLA), ductile (PCL) homopolymers and their block and

random copolymers (Chap. 4). XRD and DSC analysis were conducted to investigate processing condition effects on the molecular structure.

For electrospun rigid polymer (PLLA) nanofibers, parameters which contribute to an electrical drawing of a jet, were found to affect molecular structure in amorphous region. Parameter which is associated with the mechanical drawing of the jet was the dominant parameter to develop crystalline structure. On the other hand, crystalline structure was developed in electrospun ductile polymer (PCL) nanofibers via electrospinning process, but the crystallinity was independent of processing parameters. Structure formation of electrospun nanofibers seems to be dependent on polymer properties.

It was found that structure development of rigid (- LLA) units and ductile (- CL) is different in their block and random copolymers. Crystalline structure attributed to rigid (- LLA) units was developed in random units sequence (P(LLA-r-CL)) copolymer, while ductile (- CL) units were transformed into crystalline structure in block units sequence (P(LLA-b-CL) copolymer. The structure formation of ductile or rigid units is highly reflected by their mobility.

A disc collector was developed to conduct tensile tests using electrospun single nanofibers. As the results of tensile tests, crystallized PLLA nanofibers showed higher tensile modulus, strength but lower strain at break than that of amorphous PLLA nanofibers.

To further study structure formation of polymer nanofibers, post-processing was applied to the as-spun PLLA nanofibers. Based on XRD and DSC analysis, the model of structure formation in hot-drawn nanofibers was suggested. The results of structure analysis indicated that crystalline formation via post-processing is highly dependent on initial molecular structure before the post-processing. Via annealing process, amorphous fibers have a high potential for the development of highly crystallized structure which is corresponding to isotropic crystalline structure.

On the other hand, crystallized fibers have a preferential structure to facilitate crystallization via hot-drawing. The crystalline structure in hot-drawn fibers seems to be crystal lamella oriented along the fiber axis. The lamellae break-up induced crystalline orientation along the fiber axis at higher drawing ratio, accompanying a decrease in ΔH. It is noteworthy that 91 % crystallinity was obtained by hot-drawing nanofibers (with around 500nm in a fiber diameter) at small drawing ratio of 1.5.

In addition to large scale nanofibers (500nm) used in the above studies, molecular structure of hot-drawn small scale nanofibers (< 100nm) was investigated. As the results, 80 % crystallinity was obtained in the small scale nanofibers at drawing ratio of 1.4. The high efficiency of hot-drawing on structure development might be due to nanometer scale effects. The packed molecular chains in small dimension induce high molecular interaction / shear force between molecular chains, affecting polymer crystallization kinetics.

Structure-properties of hot-drawn nanofibers were discussed by tensile tests using single nanofibers. Hot-drawing was successfully conducted using amorphous nanofibers with 540nm in a diameter. The resultant hot-drawn nanofibers showed a significant increase in tensile properties, i.e. 6.6 GPa in modulus, 230 MPa in strength and 0.26 in strain at break.

List of Tables

Table 3-1.	Parameters related electrospinning process.	36
Table 3-2.	Solvent Properties.	41
Table 3-3.	PLLA polymer solutions used for processing studies.	43
Table 3-4.	P(LLA-r-CL) solutions used to study electrical conductivity effects.	47
Table 4-1.	Materials used in molecular structure studies.	69
Table 4-2.	Solvent Properties.	70
Table 4-3.	Polymer solutions used for solvent-casting.	70
Table 4-4.	Solution and processing conditions for electrospinning of P(LLA-b-CL).	75
Table 4-5.	Tensile properties of electrospun P(LLA-b-CL) nanofiber membrane.	77
Figure 4-6.	Solution and processing conditions applied to study polymer concentration effects on PLLA fibers.	80
Table 4-7.	The corresponding thermal properties of PLLA fibers as a function of polymer concentration.	81
Table 4-8.	Solution and processing conditions applied to study effects of solvents properties on PLLA fibers.	83
Table 4-9.	The corresponding thermal properties of PLLA fibers as a function of solvents properties.	85
Table 4-10.	Solution and processing conditions applied to study solution temperature effects on PLLA fibers.	86
Table 4-11.	The corresponding thermal properties of PLLA fibers as a function of solution temperature.	87
Table 4-12.	Solution and processing conditions applied to study take-up velocity effects on PLLA fibers.	89
Table 4-13.	The corresponding thermal properties of PLLA fibers as a function of take-up velocity.	90
Table 4-14.	Tensile properties of electrospun PLLA single nanofibers.	92
Table 4-15.	Solution and processing conditions applied to study effects of solvents properties of PCL fibers.	95

Table 4-16.	The corresponding thermal properties of PCL fibers as a function of solvents properties.	96
Table 4-17.	Solution and processing conditions applied to study take-up velocity effects on PCL fibers.	97
Table 4-18.	The corresponding thermal properties of PCL fibers as a function of take-up velocity.	99
Table 4-19.	Solution and processing conditions for electrospinning of P(LLA-r-CL) at different take-up velocity.	101
Table 4-20.	Summary of structure analysis of electrospun nanofibers.	103
Table 5-1.	Solution and processing conditions applied to study hot-drawing effects on PLLA fibers.	112
Table 5-2.	PLLA nanofiber samples used for post-processing studies.	112
Table 5-3.	The corresponding thermal properties of annealed fibers.	116
Table 5-4.	Tensile properties of annealed PLLA single nanofibers.	118
Table 5-5.	The corresponding thermal properties of PLLA fibers spun at 63m/min, followed by hot-drawing.	121
Table 5-6.	Tensile properties of hot-drawn PLLA single nanofibers.	123
Table 5-7.	The corresponding thermal properties of PLLA fibers spun at 630m/min, followed by hot-drawing.	124
Table 5-8.	The corresponding thermal properties of annealed PLLA fibers spun at 630m/min, followed by hot-drawing.	126
Table 5-9.	Solution and processing conditions applied to study nanometer scale effects on PLLA fibers.	135
Table 5-10.	PLLA nanofiber samples used for nanometer scale effects studies.	135
Table 5-11.	The corresponding thermal properties of small scale PLLA fibers spun at 630m/min, followed by hot-drawing.	136

List of Figures

Figure 2-1.	The melt spinning process	6
Figure 2-2.	Model of structure development in polymers: (a)amorphous, (b) crystallization nuclei, (c) crystal lamellar and (d) spherulite	10
Figure 2-3	Model of molecular structure developed in as-melt spun HDPE fibers [7].	11
Figure 2-4.	Molecular mechanism of plastic deformation of parallel lamellae in a polymer crystal [19].	12
Figure 2-5.	Typical stress-extension curve for as-melt spun iPP fibers.	14
Figure 2-6.	True stress-draw ratio curves as a function off strain rate (E1: the onset of crystallization, E2: the onset of regime 2 crystallization [25].	14
Figure 2-7.	Mechanism of translational slippage between groups of crystallites [4].	15
Figure 2-8.	Model illustrating reversible deformation of raw structure exiting in highly oriented as-melt spun iPP fibers [26].	16
Figure 2-9.	WAXD pattern of PLLA α-crystalline [34].	19
Figure 2-10.	WAXD patterns of: (a) α-crystalline structure in as-melt spun PLLA fibers, (b) β-crystalline structure in as-solution spun PLLA fibers [36].	20
Figure 2-11.	FESEM images of PS fibers electrospun from THF (35wt% PS/THF) at different relative humidity: (a) 50% relative humidity, (b) 30% relative humidity.	29
Figure 2-12.	Beaded PEO fibers [47].	29
Figure 2-13.	(a) Poly(ether imide) ribbons fibers, (b) a wrinkled bend [67].	30
Figure 2-14.	SEM images of branched (a) HEMA fibers, (b) PS fibers and (c) Poly(ester imide) [67].	30
Figure 2-15.	A rotating hollow drum collector with a sharp pin [72].	31
Figure 2-16.	A rotating wire drum collector [73].	32
Figure 2-17.	A knife-edged bar-induced diagonally aligned fibers on the tube (a) microphotograph at lower magnification, (b) SEM photo at higher magnification [77].	32
Figure 3-1.	Schematic drawing of electrospinning setup.	39

Figure 3-2.	Disc collector developed for electrospinning of aligned fibers.	40
Figure 3-3.	Polymer concentration effects on the diameter of the electrospun PLLA fibers.	43
Figure 3-4.	Molecular weight effects on the morphology of the electrospun PLLA fibers.	45
Figure 3-5.	Solution conductivity effects on the diameter of the electrospun P(LLA-r-CL) fibers.	47
Figure 3-6.	Solution temperature effects on the diameter of the electrospun PLLA fibers.	49
Figure 3-7.	Applied voltage effects on the diameter of the PLLA (Mw: 300K) fibers electrospun from solutions with different polymer concentration.	51
Figure 3-8.	Volume feed rate effects on the diameter of the PLLA (Mw: 300K) fibers electrospun from solutions with different polymer concentration.	51
Figure 3-9.	Electrospun fiber diameter as a function of take-up velocity.	53
Figure 3-10.	SEM images of PLLA fibers electrospun at different humidity level; (a) flat fibers electrospun at below humidity of 48%, (b) uniform fibers electrospun between 48 and 85%.	54
Figure 3-11.	Diameter of electrospun uniform PLLA fibers as a function of humidity level.	54
Figure 3-12.	Processing map obtained based on the systematic parameter study: (a) jet drawability (affected by solvent properties, applied voltage, take-up velocity), (b) mass of polymer (affected by polymer concentration, applied voltage, volume feed rate)	58
Figure 3-13.	The jet drawing-related parameters.	59
Figure 3-14.	TEM image of ultra-fine PLLA fibers: (a) at lower magnification, (b) at higher magnification.	61
Figure 3-15.	Disc collectors developed for electrospinning of aligned fibers: (a) conductive square-shaped table, (b) non-conductive tubular-shaped table fixed on the edge of a disc collector.	62
Figure 3-16.	Fiber orientation as a function of table materials: PCL fibers electrospun on tables made from (a) conductive materials, (b) non-conductive material.	62

Figure 3-17.	Fiber orientation as a function of take-up velocity: PLLA fibers electrospun at (a) 63m/min, (b) 630m/min.	63
Figure 3-18.	SEM image of 3-D architecture with PCL aligned nanofibers directed at 0^o, -45^o and $+45^o$.	64
Figure 3-13.	The jet drawing-related parameters.	69
Figure 3-14.	TEM image of ultra-fine PLLA fibers: (a) at lower magnification, (b) at higher magnification.	71
Figure 3-15.	Disc collectors developed for electrospinning of aligned fibers: (a) conductive square-shaped table, (b) non-conductive tubular-shaped table fixed on the edge of a disc collector.	72
Figure 3-16.	Fiber orientation as a function of table materials: PCL fibers electrospun on tables made from (a) conductive materials, (b) non-conductive material.	72
Figure 3-17.	Fiber orientation as a function of take-up velocity: PLLA fibers electrospun at (a) 63m/min, (b) 630m/min.	63
Figure 3-18.	SEM image of 3-D architecture with PCL aligned nanofibers directed at 0^o, -45^o and $+45^o$.	64
Figure 4-1.	Disc collector for single nanofibers.	74
Figure 4-2.	Procedures to prepare single nanofiber sample: (a) short time electrospinning, (b) pick aligned nanofibers onto a paper frame, (c) removing non-required nanofibers and (d) single nanofiber sample.	74
Figure 4-3.	SEM images of electrospun P(LLA-b-CL) fibers.	76
Figure 4-4.	(a) XRD diagram and (b) DSC thermogram of electrospun P(LLA-b-CL) fibers.	76
Figure 4-5.	Typical stress-strain curves of electrospun P(LLA-b-CL) nanofiber membrane under tensile loading.	77
Figure 4-6.	Fiber orientation angles in the P(LLA-b-CL) membranes during the tensile deformation.	78
Figure 4-7.	SEM micrograph of an electrospun P(LLA-b-CL) (75/25wt%) membrane during the tensile deformation (at point C).	78
Figure 4-8.	SEM images of PLLA fibers electrospun from solutions with different polymer concentration of: (a) 7.5wt% and (b) 12.5wt%.	80

Figure 4-9.	Polymer concentration effects: (a) XRD diagram and (b) DSC thermogram of PLLA fibers electrospun from 7.5wt% and 12.5wt% solutions.	81
Figure 4-10.	SEM images of PLLA fibers electrospun from solutions consisting of: (a) DCM/Pyridine (60/40wt%) and (b) DCM/Methanol (80/20wt%).	83
Figure 4-11.	Effects of solvents properties: (a) XRD diagram and (b) DSC thermogram of PLLA fibers electrospun from 7.5wt% solutions with DCM/Pyridine (60/40wt%) and DCM/Methanol (80/20wt%).	85
Figure 4-12.	SEM images of PLLA fibers electrospun from solutions at: (a) room temperature, and (b) 40^{o}C and (c) 70^{o}C.	86
Figure 4-13.	Solution temperature effects: (a) XRD diagram and (b) DSC thermogram of PLLA fibers electrospun from solutions at room temperature, and 40^{o}C and 70^{o}C.	87
Figure 4-14.	SEM images of PLLA fibers electrospun at different take-up velocity of: (a) 63m/min, (b) 630m/min, (c) 1,260m/min and (d) 1,890m/min.	89
Figure 4-15.	Take-up velocity effects: (a) XRD diagram and (b) DSC thermogram of PLLA fibers electrospun at 63m/min, 630m/min, 1,260m/min and 1,890m/min.	90
Figure 4-16.	WAXD pattern of PLLA fibers electrospun at: (a) 63m/min, (b) 630m/min and (c) 1,890m/min.	91
Figure 4-17.	Tensile stress-strain curves of PLLA single nanofibers electrospun at take-up velocity of 63, 630 and 1,890m/min.	92
Figure 4-18.	SEM micrographs of fractured PLLA single nanofibers after tensile tests: (a) 63m/min and (b) 630m/min.	92
Figure 4-19.	SEM images of PCL fibers electrospun from solutions consisting of: (a) $CHCl_3$/Pyridine (60/40wt%) and (b) $CHCl_3$/Methanol (80/20wt%).	95
Figure 4-20.	Effects of solvents properties: (a) XRD diagram and (b) DSC thermogram of PCL fibers electrospun from 10wt% solutions in $CHCl_3$/Pyridine (60/40wt%) and $CHCl_3$/Methanol (80/20wt%).	96
Figure 4-21.	SEM images of PCL fibers electrospun at: (a) 63m/min and (b) 630m/min.	98

Figure 4-22.	Take-up velocity effects: (a) XRD diagram and (b) DSC thermogram of PCL fibers electrospun at 63 and 630m/min.	99
Figure 4-23.	SEM images of P(LLA-r-CL) fibers electrospun at: (a) 63m/min and (b) 630m/min.	101
Figure 4-24.	XRD diagram of electrospun P(LLA-r-CL) fibers at 63 and 630 m/min.	101
Figure 5-1.	SEM images of as-spun, annealed fibers spun at 63, 630, 1,260 and 1,890m/min.	115
Figure 5-2.	Annealing effects on PLLA fibers electrospun at different take-up velocity: (a) XRD diagram and (b) DSC thermogram.	116
Figure 5-3.	Tensile stress-strain curves of annealed PLLA single nanofibers electrospun at 630 and 1,890m/min.	118
Figure 5-4.	SEM images of as-spun, annealed and hot-drawn PLLA fiber bundles.	119
Figure 5-5.	Hot-drawing effects on PLLA nanofibers spun at 63m/min: (a) XRD diagram and (b) DSC thermogram.	121
Figure 5-6.	Tensile stress-strain curves of hot-drawn PLLA single nanofibers electrospun at take-up velocity of 63m/min.	122
Figure 5-7.	Hot-drawing effects on PLLA nanofibers spun at 630m/min: (a) XRD diagram and (b) DSC thermogram.	124
Figure 5-8.	Hot-drawing effects on annealed PLLA nanofibers spun at 630m/min: (a) XRD diagram and (b) DSC thermogram.	126
Figure 5-9.	WAXD patterns of as-spun, annealed and hot-drawn PLLA fiber bundles.	127
Figure 5-10.	Structural model of electrospun PLLA nanofibers followed by hot-drawing.	129
Figure 5-11.	SEM images of as-spun, annealed and hot-drawn PLLA fiber bundles with small scale diameter.	136
Figure 5-12.	Hot-drawing effects on small scale PLLA nanofiber bundles spun at 630m/min: (a) XRD diagram and (b) DSC thermogram.	136
Figure 5-13.	WAXD patterns of as-spun, annealed and hot-drawn PLLA fiber bundles with small scale diameter.	137

Publication lists

1) Wei He, Thomas Yong, Zu Wei Ma, ***Ryuji Inai***, Wee Eong Teo, Seeram Ramakrishna, "Biodegradable Polymer Nanofiber Mesh to Maintain Functions of Endothelial Cells", Tissue Engineering, *accepted*

2) S. Ramakrishana, T.C. Lim, ***R. Inai***, K. Fujihara, "Modified Halpin-Tsai Equation for Clay-Reinforced Polymer Nanofiber", Mechanics of Advanced Materials and Structures, 13 (2006) pp.77-81

3) ***R. Inai***, M. Kotaki, S. Ramakrishna, " Structure and Property of Electrospun Single Nanofibers", *Nanotechnology*, 16 (2005) pp.208-213, *selected as featured article and cover page of the journal*

4) S-H, Tan, ***R. Inai***, M. Kotaki, S. Ramakrishna, "Systematic Parameter Study for Ultra-Fine Fiber Fabrication via Electrospinning Process", *Polymer*, 46 (2005) pp.6128-6134

5) ***R. Inai***, M. Kotaki, S. Ramakrishna, "Deformation Behavior of Electrospun P(LLA-CL) Nonwoven Membranes under Uniaxial Tensile Loading", *Journal of Polymer Science: Polymer Physics*, *43(22)* (2005) pp. 3205-3212

6) C.Y. Xu, ***R. Inai***, M. Kotaki, S. Ramakrishna, "Electrospun Nanofiber Fabrication as Synthetic Extra Cellular Matrix and Its Potential for Vascular Tissue Engineering", *Tissue Engineering*, 10 (2004) pp. 1160-1168

7) C.Y. Xu, ***R. Inai***, M. Kotaki, S. Ramakrishna, "Aligned Biodegradable Nanofibrous Structure: A Potential Scaffold for Blood Vessel Engineering", *Biomaterials*, *25* (2004) pp.877-886

CHAPTER I

INTRODUCTION

In the 1950s and 60s, properties of polymers were found to be strongly related to their molecular arrangement and chemical constitutes. Therefore, it became essential to make clear how an assembly of macromolecules develops structures; how specific molecular arrangement can be induced; and how these structures are related to properties. Researches to study the processing-structure-property relationship (PSP relathionship) of polymer fibers are particularly important since they show a potential for their mechanical property. Such high mechanical properties are obtained with their ordered molecular structure which is formed as a result of drawing of the fibers during the spinning process. Recently, some processing have attracted attention to produce polymer nanofibers since the polymer nanofibers are good candidates in many application fields such as tissue engineering scaffolds, filtration media, protective cloth, and so on. This has given rise to a great interest in researches to study the PSP relationship in polymer nanofibers.

Objectives of This Research

The main aim of the research was to investigate processing-structure-property

relationship in electrospun polymer fibers. The objectives were addressed separately in processing, structure and properties studies.

In the processing studies, the objectives were

1) To control electrospun fiber dimension by studying processing parameters systematically. The dimension was observed under SEM and TEM.
2) To fabricate 2-D and 3-D architecture with electrospun aligned nanofibers by developing a collector

The objective of the structure studies was

3) To investigate how a specific molecular arrangement or highly ordered structure is formed into the electrospun polymer nanofibers. Molecular structures of the electrospun nanofibers were characterized using XRD and DSC. The studies particularly focused on the effects of the processing parameters (dominant parameters found in processing-fiber dimension studies and take-up velocity) and post-processing parameters (hot-drawing ratio) on the development of the molecular structure.

In the properties studies, the objective was

4) To develop a method to collect electrospun single nanofibers, and make clear the relationship between mechanical properties and the molecular structure developed in the nanofibers. Tensile test of the single nanofibers was conducted

using a nano tensile testing system (Nano Bionix, MTS) with 500 mN load range, and 50nN load resolution

The research was conducted mainly using poly($_L$-lactide acid) (PLLA) which has potential tissue engineering applications as a suture in microsurgery, tissue engineering scaffolds due to its good biocompatibility and biodegradability. The polymer nanofibers can also be good candidates as reinforcement in composite materials. In the electrospinning, there are a number of parameters and most of which were investigated in the processing studies. The results of the processing studies were used to identify some parameters that have an important role in the development of the molecular structure in the electrospun nanofibers. Subsequently, the structure studies focused on only these more important parameters. The results of studies in the PSP relationship in the electrospun nanofibers should offer a way to engineer polymer nanofibers to meet the specific demands such as dimension and properties, of the nanofiber applications, and the results, hence, should contribute to further expansion of the nanofiber applications. The results of the studies may also contribute to a better understanding of how an assembly of molecules develops structure if a scale of fiber diameter is in the nanometer range and how the molecular structure affects mechanical properties. More details of the structure development and the structure-properties relationship in micron scale of melt-spun / dry-spun

fibers will be described in chapter 2. The description would provide the useful information to understand the significant finding in the thesis, that is, the development of the molecular structure and its effects on the mechanical properties in the polymer nanofibers,

CHAPTER II

LITERATURE REVIEW

2-1. Overview of Polymer Micronfibers Processing

In the polymer fibers based industries, a micro scale of polymer fibers (micronfibers) produced by either melt-spinning or solution-spinning have been widely used. Past research works based on these micronfibers have gave us the idea that how to control molecular structure by processing; and how the molecular structure affects mechanical properties of the fibers. Literature review of the above works would provide fundamental knowledge to investigate processing-structure-properties relationship in electrospun nanofibers.

2-1-1. Melt-spinning Process

The idea of the melt spinning process was given by R. A. Brooman in 1845 [1]. The melt spinning process involves melting and extrusion of the material to be processed through a multi-hole capillary die (called a spinneret), followed by cooling and solidification to form filaments. The produced filaments can be wound on a bobbin. In this process, tensile force is usually applied to draw the filaments and results in a decrease in a fiber diameter.

A standard setup of melt-spinning is illustrated in Figure 2-1. Pellets formed polymer is fed into an extruder where it is melt and delivered to metering pump and ejected from spin pack with a multifilament spinneret. The extruded filaments are drawn down to smaller diameter, while they are simultaneously cooled / quenched by air blowing across the filament bundle. The resulting filaments are either wound onto a bobbin or they are passed directly to another processing step such as drawing or texturing.

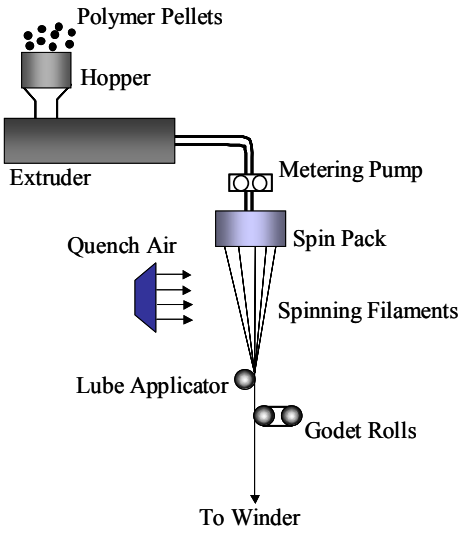

Figure 2-1. The melt spinning process.

The major parameters for melt-spinning are as follows,

Processing parameters

- extrusion temperature
- mass flow rate of polymer through each spinneret hole
- take-up velocity of the wound-up or deposited filaments
- the spinline cooling conditions
- spinneret orifice shape, dimensions and spacing
- the length of spinline

Material parameters

- variables that affect the rheology of the polymer melt

- variables that affect the solidification behavior of the polymer

One of the most important parameters of the melt-spinning process is take-up velocity. This has marked effects on not only the productivity of the spinline but also the structure and properties of the melt spun filaments.

2-1-2. Solution-spinning Process

The setup is similar to the melting setup. In the solution-spinning, semi-dilute solutions are used and it is ejected from a spinneret to form fibers. Usually the elongation of chains is performed by drawing in the semi-solid state at below the melting, dissolution temperature. Thus the process of spinning and drawing are separated, respectively above and below the melting, dissolution temperature.

2-1-3. Post-drawing Process

Post-drawing process is well known to produce high-modulus and high-strength polymer fibers. Post-drawing of fibers after spinning at low / high take-up velocity show higher molecular orientation compared to one found in noncrystalline region

of fibers spun at high-speed melt spinning [2-4]. The tensile modulus and tenacity of fibers required for high performance and advanced engineering applications can be generally obtained only by extending and orienting the molecules in a drawing operation following spinning.

Traditionally, chain orientation and extension is generated in melt- and solution-spun fibers by two different methods as follows,

1) applying a draw-down to the fibers during or immediately after spinning (in the molten state or super cooled melt)
2) drawing of fibers at temperatures close to but below the melting or dissolution temperature.

A draw-down in the molten state or in solution is usually less effective to generate chain-extension due to extensive relaxation process. Drawing in the (semi-)solid state, i.e. below the melting and/or dissolution temperature is usually much more effective since relaxation processes are restricted, due to reduced thermal motions and because the chains are trapped into crystals which act as physical network junctions.

2-1-4. Structure Formation during Processing

Processing and Materials-related Parameters Effects

Molecular orientation is generated as a result of polymer deformation. The deformation is carried out in the melt or the solid state, affected by parameters which have the greatest effect on spinline stress, namely polymer viscosity (i.e., molecular weight), spinning speed and mass throughput. Stress would also be expected to increase the temperature at which crystallization takes place. Crystallization kinetics is determined, primary, by the nature of the polymer and the level of molecular orientation developed.

The polymer viscosity is increased with an increase in the molecular weigh. The higher polymer viscosity leads to a greater stress and molecular orientation in the spinline. Take-up velocity is also an important parameter to encourage fibers to form highly ordered structure [5-13]. However, there seems to be an upper limit on the take-up velocity to increase and above the limit, which depends on a type of polymer, no further development of molecular structure occur. For example, Poly(ethylene terephthalate) (PET) filaments was found to show no increase in molecular orientation and crystallinity at the take-up velocity above 3,500 m/min [14].

Crystalline Structural Model

An unoriented, crystalline polymer generally consists of spherulitic structures, which are formed by radial growth of stacks of parallel crystal lamellae from a central nucleus (Figure 2-2 [15]). Chains fold back at the surface of each lamellae, and their extension in the direction along the chain axis is in the region of 10 nm. The noncrystalline component consists of crystal defects, free chain ends, chain folds and interlamellar tie-chains. Spherulite size varies from less than one micrometer to hundreds of micrometers, depending on the crystallization conditions, and spherulitic growth is often blocked by impingement with neighboring spherulites. The final shape truncated spherulites is usually polygonal [16].

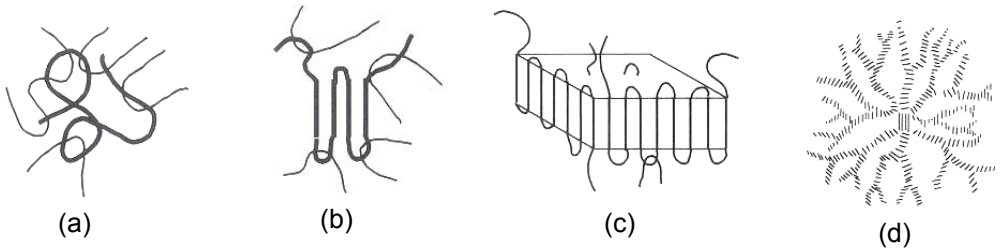

Figure 2-2. Model of structure development in polymers: (a) amorphous, (b) crystallization nuclei, (c) crystal lamellar and (d) spherulite.

When the nucleation density is very high, their development may not progress beyond the formation of randomly oriented stacks of parallel lamellae. If the stress in fiber spinning are high enough, but not too high, row nucleated crystal structure are formed (Figure 2-3 [7,17]. These consist of fibril nuclei oriented in the fiber axis

direction, onto which chain-folded crystals grow epitaxially, in a direction perpendicular to the fibril axis. The well-developed row structure was formed into the fibers spun from the broad molecular weight distribution of polymer [18]. In some instances, row-nucleated material and spherulites coexist. When the stress is higher there is less twisting of the lamellar crystals with the result that the x-axis becomes more aligned with the fiber axis while the a-axis tends to become more nearly perpendicular to it.

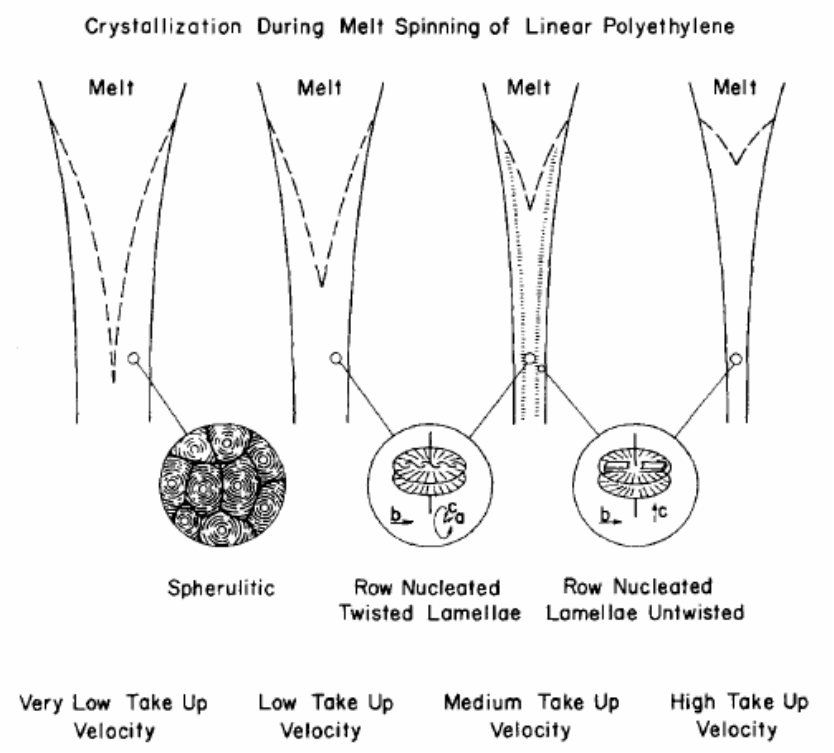

Figure 2-3. Model of molecular structure developed in as-melt spun HDPE fibers [7].

Microfibrillar structure was found from fibers via post-drawing process. In the process, the molecular arrangements of crystallined polymers are different from that of amorphous polymers (Figure 2-4 [19]). In the early stages of drawing an unoriented crystalline polymer, spherulites become elongated in the draw direction [20], and in the region of the yield point, chain tilting and slipping occur within the lamellae of the chain-folded crystals. Then if the drawing temperature is high enough, chains partially unfold and the lamellae break up into small crystallites connected to each other by uncrystallized tie molecules, forming 'microfibrillar' structures [15]. At high draw ratios, deformation involves the sliding motion of microfibrils past each other. The thinnest lamellar escape the breaking-up stage and are simply rotated and aligned, and that high draw temperature cause some chain refolding and crystal thickening during yield (and necking) process [21]. The fibrillar structure has been found to be a function of take-up velocity [22,23] and molecular weight distribution of polymer [18].

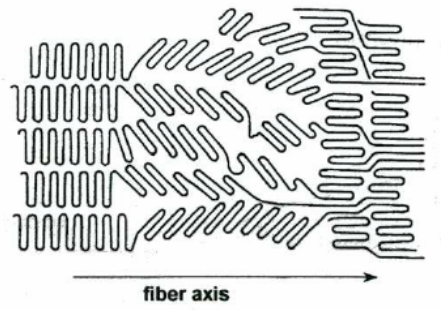

Figure 2-4. Molecular mechanism of plastic deformation of parallel lamellae in a polymer crystal [19].

2-1-5. Structure-Property Relationship

Overview

Misra et al. have studied structure-properties relationship of melt-spun polypropylene micronfibers. The studies revealed that tensile strength is little affected by crystallinity, but increases with increased molecular orientation as measured by birefringence. On the other hand, the modulus is a function of both molecular orientation and crystallinity. An increase in either causes an increase in modulus [24].

Typical stress-stain curves for as-meltspun polypropylene filaments are illustrated in Figure 2-5. The filament spun at low speed show rather low molecular orientation, which exhibits a “yield point”, filament necking and extension at essentially constant load to about 450 % elongation, followed by a period of work hardening and high elongation to break. The filament with higher orientation does not exhibit a marked yield point or neck down. It does have a higher yield strength, tenacity and lower elongation to break.

Amorphous-crystallizable Polymers

Typical stress-stain curve is shown in Figrue 2-6 [25]. The deformation of a network

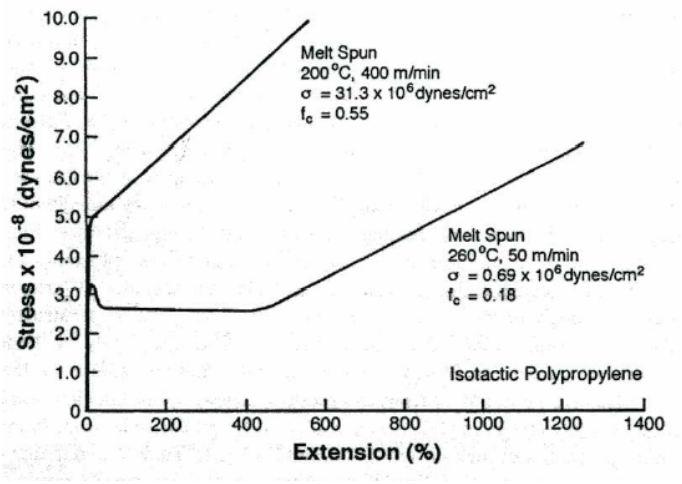

Figure 2-5. Typical stress-extension curve for as-melt spun iPP fibers.

of entangled chains occurs in the first rise in stress and results in molecular orientation. Crystallinity and molecular orientation develop rapidly between E1 and E2, while stress develops slowly. A crystalline network, which provides rigid junctions of polymer chains, is formed by E2. The increase in stress results from an increase in polymer viscosity contributed by the interconnection of crystallites. Entanglements act as impermanent crosslinks that can slip and relive stress in a time-dependent manner. The temperature in the range of above Tg provides sufficient chain mobility for slippage

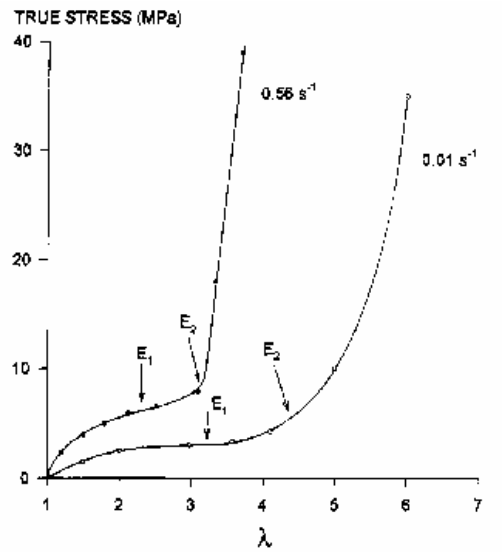

Figure 2-6. True stress – draw ratio curves as a function of strain rate (E1:the onset of crystallization, E2: the onset of regime 2 crystallization [25].

of entanglements to occur. Especially at sufficient high draw ratios, and if slippage is not constrained by crystallization, the upturn in stress would be much smaller. The slowing of orientation in the high-stress region may be due to the formation of taut intercrystalline tie chains, which would restrain the uncoiling of neighboring tie-chains that are not fully extended [4]. Then, deformation would proceed via translational slippage between groups of crystallites which were held together by extended tie-chains (Figure 2-7). On the other hand, below Tg, the polymer behaves like a brittle solid due to insufficient molecular mobility.

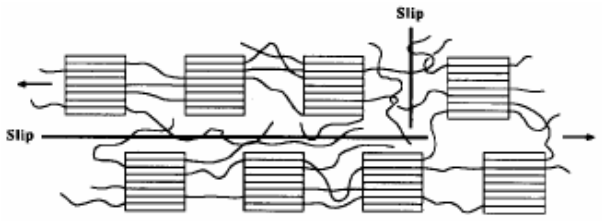

Figure 2-7. Mechanism of translational slippage between groups of crystallites [4].

Crystalline Polymers

The modulus of a polymer in crystalline state (in the direction of chain axis) is generally one to two orders of magnitude higher than its modulus in the amorphous state with randomly oriented chains. But not only crystalline regions but also unoriented amorphous regions would have the dominant influence on fiber modulus.

The more oriented sample with the well-developed row structure exhibits high elastic recovery, while the elastic recovery of the filament with low orientation is much smaller. The elastic filaments also exhibit a reversible decrease in density when stretched. The reversible decreased density is caused by the formation of numerous voids and surface connected pores. These features suggest that the elastic recovery of these filaments is “energy driven” rather than “entropy driven.” This behavior could be explained by a structural mode of the type illustrated schematically in Figure 2-8 [26]. The basic idea of the model is that a row structure exists in which lamellar are only connected to each other at certain tie points. When the stress is released the lamellae regain their original shape, producing the elastic recovery and reduction in void volume.

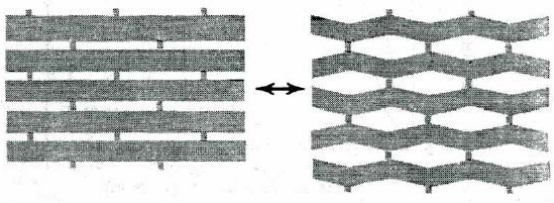

Figure 2-8. Model illustrating reversible deformation of raw structure exiting in highly oriented as-melt spun iPP fibers [26].

The past studies on melt-spun micronfibers indicated that the tensile properties of the polymer fibers can be controlled by arranging their molrcular structures. It is important to find the key parameters which strongly affect the development of

molecular structures during the processing. Therefore, systematic parameter studies are essential to engineer polymer fibers with desired properties. In the following sections, past studies on PLLA fibers which is mainly focused in this studies were focused.

2-2. Overview of PLLA Micronfibers

In recent years, the preparation of high-strength PLLA fibers has been studied because of its potential applications as a suture in microsurgery and in composite materials. In this section, past studies on melt-spun and solution-spun PLLA fibers are presented.

2-2-1. Processing-related Parameters Effects on Molecular Structure of PLLA Fibers

Due to demands from potential applications, a lot of efforts have been made to study: how the strong PLLA fibers with a highly ordered structure can be produced. There have been mainly two approaches, i.e., to investigate effects of spinning process related parameters, and effects of post-processing related parameters. Since a take-up velocity has been found to be one of dominant spinning process-related parameters to improve mechanical properties of as-spun fibers, high-speed melt

spinning of PLLA fibers has been investigated. Mezghani and Spruiell have studied high speed melt-spinning of PLLA fibers at take-up velocity up to 5,000 m/min [27]. The melt-spun PLLA fibers exhibited the highest crystallinity in the range from 40 to 50 % at take-up velocity between 2,000 and 3,000 m/min. Decreased crystallinity at take-up velocity above 3,000 m/min might be due to increased cooling rate of the fibers without a compensating increase in crystallization kinetics. On the other hand, high-speed solution-spinning of PLLA fibers is possible at take-up velocity only up to 1,500 m/min [28]. As another approach to develop molecular structure of PLLA micronfibers, hot-drawing effects were investigated. It has been reported that final molecular structure formed into melt-spun fibers depend on their drawability which is associated with the as-spun fibers initial crystallinity and diameter [29,30]. The fibers spun at lower take-up velocity, showing amorphous fibers, induced the higher the maximum drawing ratio. In the solution-spun fibers, the drawability was found to be a function of the solvent composition [31,32]. Postema and Pennings have found that the hot-drawing of solution-spun PLLA fibers can take place in two temperature regions [33]. One region up to 180 ^{o}C, in which deformation takes place in the semicrystalline state of the polymer, and one region between 180 and 190 ^{o}C in which the deformation proceeds in the liquid state of the polymer, leading to a semicrystalline state by strain hardening after displacement of topological defects.

2-2-2. Structure Formation of PLLA Fibers

De Santis et al has found for the first time α crystalline structure with an pseudoorthorhombic unit cell (a = 1.07, b = 0.65 and c = 2.78 nm; α = β = γ = 90^{o}), which is arising from chain folded lamella structure, from stretched PLLA polymer after annealing at 120 ^{o}C [34]. Figure 2-9 shows WAXD pattern of the α-form. Kalb et al. have further studied the dimension of the crystalline structure and found lamellar crystals about 10 nm in a thickness [35]. Modification from α-phase to β-phase of crystalline structure, in the form of extended chains, was first observed from hot-drawn solution-spun fibers by Eling et al [36]. The crystalline form can be determined using WAXD patters. As shown in Figure 2-10, the α-phase of PLLA fibers gives sharp reflections, whereas the β-phase gives only diffuse reflections seen as smeared layer lines in the diffraction patters. For β crystalline structure, an orthorhombic unit cell (a = 1.03, b = 1.82 and c = 0.9 nm) was reported by Hoogsten et al.

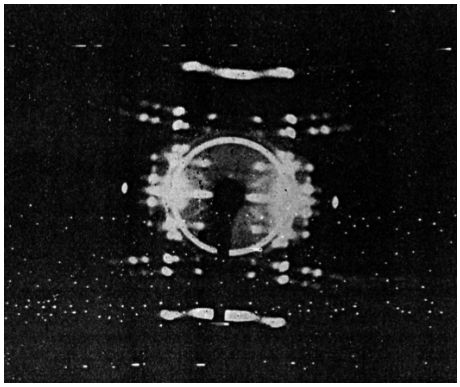

Figure 2-9. WAXD pattern of PLLA α-crystalline [34].

As a structural model for PLLA fibers, Postema et al. have suggested that a

shish-kebab-like structure is formed in solution-spun fibers, followed by hot-drawing process [28]. They also found skin-core structure of the solution-spun PLLA fibers, and the structure depend on ambient conditions and solvents used for spinning [30]. Evaporation of the good solvent from the upper layer of the fiber brings about a polymer distribution that is non-uniform over the cross-section. This distribution is determined by the evaporation step and results in a different morphology of the fiber skin and core.

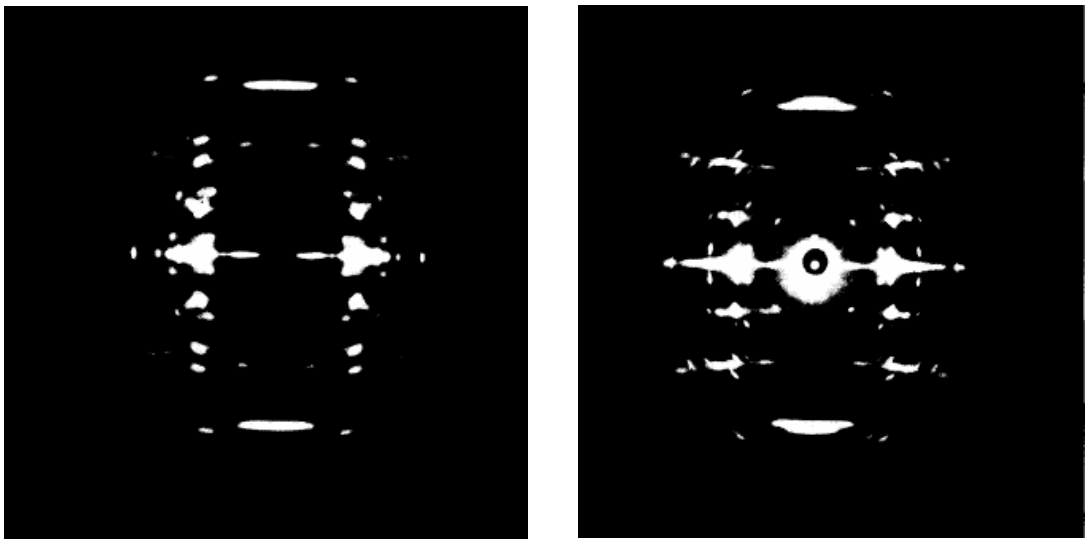

(a) (b)

Figure 2-10. WAXD patterns of: (a) α-crystalline structure in as-melt spun PLLA fibers, (b) β-crystalline structure in as-dry spun PLLA fibers [36].

2-2-3. Structure-property Relationship of PLLA Fibers

The strongest PLLA fibers exhibiting 2.3 GPa in tensile strength have been produced by low speed solution-spinning via high ratio of hot-drawing, i.e., 13 in a drawing

ratio [33]. Leenslag et al. have also successfully produced high strength of PLLA fibers, exhibiting 16 GPa in tensile modulus and 2.1 GPa in tensile strength, by solution-spinning, followed by hot-drawing [31]. It is found that the high strength of hot-drawn PLLA fibers is a result of the β-crystal modification. Eling et al. has reported that the β crystalline structure shows a potential for tensile properties rather than α crystalline structure [36]. On the other hand, low speed melt-spinning, followed by high ratio of hot-drawing results in PLLA fibers with only up to 9.2 in tensile modulus and 870 MPa in tensile strength. The solution-spinning has a potential for spinning amorphous structured polymer fibers which shows good drawability. The higher strength of solution-spun PLLA fibers via hot-drawing would be due to the good drawability. High-speed melt spinning between 2,000 and 3,000 m/min in take-up velocity resulted in PLLA fibers with 6 GPa in tensile modulus and 385 MPa in tensile strength, which are the maximum values achieved by changing take-up velocity.

There were no studies comparing the structure-properties relationship between micron fibers and nanofibers. The comparing studies might lead new findings to engineer polymer fibers. In the following sections, processing to produce nanofibers were investigated.

2-3. Polymer Nanofibers

2-3-1. Processing of Polymer Nanofibers

Several techniques such as Template Synthesis, Phase Separation, Self-Assembly, Electrospinning are known to be good method to produce polymer nanofibers [37]. In the Template Synthesis, nanofibers with different diameters and densities can be obtained by pouring precursor polymer solution on templates with different pore diameters. The Phase Separation provides nanofibers from a freeze-dried polymer gel. In this process, it is difficult to control the fiber diameter. In Self-Assembly, nanofibers are produced by assembling polymer molecules. Although this process has potential for controlling the diameter of nanofibers and their architecture, the process is technical and complicated. Electrospinning, invented by Formals in 1934 [38], shows good spinnability of continuous nanofibers from most polymers and the spinnability cannot be achieved via other processing. Since the process also shows potential in terms of low cost and simplicity of the setup, it has attracted a great deal of attention as a superior method to produce polymer nanofibers / nanofiber sheets. Particular interests have been displayed in tissue engineering to produce biocompatible scaffolds for tissue repair and replacement, and filtration application to produce filter media. 2-D and 3-D architecture are suitable for the biocompatible scaffolds and the filter media since the structures induce better cell activities and

filtration rate. The cell activities and the filtration rate also depend on the fiber orientation in the structures. Fabrication of the 2-D and 3-D architecture with desired fiber orientation, therefore, has been an area of interest. It is also noted that fiber morphology (diameter, uniformity and surface profile) of the nanofibers is one of the important parameters to determine the cell activities and the filtration rate. Due to the interest in such application fields, great efforts have been made in researches for electrospinning process to study how the processing affects the fiber morphology of electrospun nanofibers. In the electrospinning process, polymer solution with polymers dissolved in organic solvents is used as materials. Electrospinning setup mainly consists of a voltage power supplier, a spinneret with a tinny nozzle attached to a syringe, a syringe pump, and a collector. In the electrospinning process, high voltage is applied to polymer solution and results in reveling an electrostatic field between a spinneret and a collector. Once an electrostatic force overcomes surface tension of polymer solution at tip of spinneret, a jet of polymer solution is ejected from the spinneret, and the resultant charged jet goes towards the grounded collector. While the jet flies between the spinneret and the collector, the solution jet is formed into polymer nanofibers via solvent evaporation. There are many parameters associated with the electrospinning process and the parameters can be divided into three groups, i.e. solution conditions / properties / properties, processing conditions

and ambient conditions.

2-3-2. Processing-Fiber Morphology Relationship

Solution conditions / properties

Parameters of solution conditions / properties include polymer elasticity, molecular weight, polymer concentration, polymer solubility in solvent, boiling temperature of solvent and solution conductivity. According to past studies, it has been found that various fiber morphology of electrospun nanofibers can be produced by changing parameters of solution conditions / properties.

Molecular weight reflects the number of chain entanglements within a polymer solution, thus solution viscosity, which determines electrospun fiber uniformity and fiber spinnaility. Too low viscosity of a solution jet, resulted from low molecular weight of polymer, does not encourage to form fibers, results in formation of droplets / particles [39]. If the solution is too viscous, clogging resulted from solidified polymer solution occur at the tip of spinneret [40]. Under spinning of sufficient viscosity of polymer solution, uniform fibers are produced.

Solution viscosity is also a function of *polymer concentration*. If polymer

concentration is too low, leading to lower viscosity, an influence of surface tension on the solution jet is increased and consequently beaded fibers are electrospun [41,42]. In the sufficient range of viscosity to produce uniform fibers, an increased polymer concentration results in an increase in fiber diameter [41,43-46].

Higher *solution conductivity* has been found to result in formation of smaller diameter of electrospun fibers [47]. Due to an applied high voltage to polymer solution, a charged solution jet is ejected from the tip of spinneret during electrospinning. The charges at the jet surface would be repulsed, resulting in stretching the solution jet. The level of charges is increased with higher conductivity which may induce highly stretched jet. The smaller diameter of fibers spun from highly conductive solution might be a result of high stretching of the jet. Although solution conductivity has been reported to affect fiber diameter, some researchers claimed that a reduction of fibers is due to *dielectric constant* [48,49]. When solvent with either higher electrical conductivity or dielectric constant is added, the solubility of a polymer into the solvent must be paid attention. If *the solubility* of a polymer is decreased due to excessive the solvent added, beaded fibers are formed [50]. It noted that additional solvent into the polymer solution also changes total solution viscosity and surface tension.

Processing Conditions

In addition to solution conditions / properties-related paremeters, processing condition including applied voltage, distance from a spinneret to a collector (S-C distance), feed rate of a syringe pump and solution temperature, have been found to affect the electrospun fiber morphology.

In the electrospinning process, both negative and positive voltage can be applied for forming a solution jet [51]. *Applied voltage* is associated with the amount of charges on a solution jet. Higher voltage results in the more charges on a solution jet and the resultant solution jet will be highly stretched during electrospinning due to the charges-induced repulsive force. The stretching of the solution jet is further encouraged by interaction with an external electric field. Hence, higher voltage was found to induce electrospinning of fibers with smaller diameter [41,52,53]. However, opposite trends that fibers with larger diameter were spun at higher applied voltage, was also reported by Zhao et al. [54]. This might be a result of solution conditions / properties. Low viscous solution shows relatively high mobility of polymer chains within polymer solution, results in more solution to come out from a spinneret at higher voltage. If this influence is dominant than that of stretching, higher voltage might result in a larger diameter. At higher range of applied voltage, beaded fibers

were found to be electrospun [45-47].

S-C distance is associated with an electric field strength and a jet traveling time which reflect solidification or stretching time for a solution jet. If an influence of jet traveling time is dominant, wet / interconnected fiber membranes are produced with a decreased S-C distance due to insufficient solidification time for a solution jet [53], while an increase in S-C distance results in electrospinning of smaller diameter of fibers due to relatively longer time to stretch a solution jet [54-56]. On the other hand, if an influence of an electric field strength is dominant, beaded fibers are electrospun at too short S-C distance due to an instable jet initiation [41,46], while fibers with larger diameter are electrospun at long S-C distance due to weak an electric field strength [52]. Zhao et al. also found that no fibers exhibited at too long S-C distance [54].

The amount of solution to come out from a spinneret is determined by *feed rate*. Hence, with other parameters held constant, higher feed rate results in larger diameter, although there is a limit to an increase in fiber diameter [57]. Feed rate also affects solidification time for a solution jet. Higher feed rate-induced a solution jet takes more time to solidify, results in wet / interconnected fiber membranes [58].

Higher *solution temperature* was found to result in electrospinning of more uniform fibers [45] and a smaller diameter of fibers [59]. However, the trends would be dependent of polymer and solvent characteristics (T_g, boiling point, etc.).

Ambient Conditions

Compared to the past studies of processing conditions and ambient conditions, only a small number of studies have been done for ambient conditions . This might be due to difficulties in the current setup to control ambient condition.

Humidity was found to affect surface feature of fibers electrospun from polymer dissolved in volatile solvents (Figure 2-11 [41,60]). Caper et al. also reported that porous surface of fibers are electrospun at higher humidity level and the size of pores is dependent of humidity level [61].

The individual parameters were well analyzed for each polymer and some parameters were found to affect the morphology of electrospun fiber. However, a comprehensive study to control the morphology has not been done yet, and there are difficulties in producing an ultra-fine polymer fibers via electrospinning.

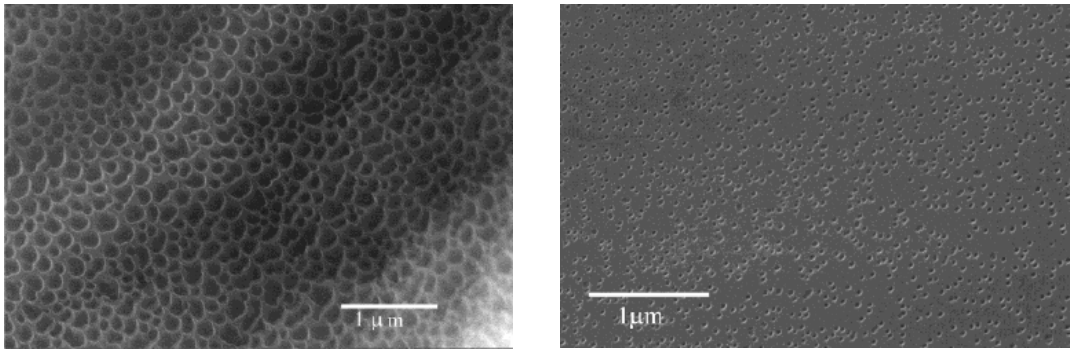

(a) (b)

Figure 2-11. FESEM images of PS fibers electrospun from THF (35 wt % PS/THF) at different relative humidities: (a) 50% relative humidity, (b) 30% relative Humidity [46].

.

Unique Shape of Nanofibers

According to past studies, electrospinning has been found to be versatile processing to produce various fiber morphologys of nanofibers, which is highly dependent of solution, processing and ambient conditions. As mentioned in previous sections, *beaded fibers* can be electrospun under certain conditions as shown in Figure 2-12. *Porous nanofibers* have been reported by Bognitzki, Megelski et al. (Figure 2-11, [41,60]). The process of the porous features seems to be similar to that found in as-cast polymer film. Bognitzki has reported that formation of porous fibers is a function of the solvent vapor pressure and lower

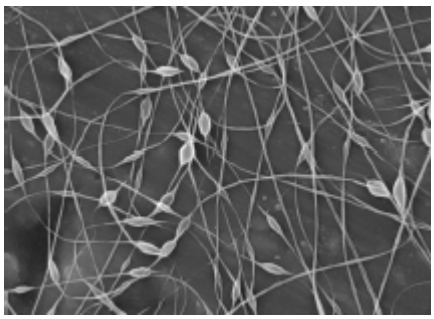

Figure 2-12. Beaded PEO fibers [47].

vapor pressure tends to suppress the formation of porous features. Impact of wet fibers on a collector results in *flattened ribbon-like fibers* (Figure 2-13, [62]). Instability of an initial solution jet has been found to induce branched fibers as shown in Figure 2-14 [62]. Co-axial spinning method has been conducted to electrospin core / sheath structured fibers or hollow fibers [63,64].

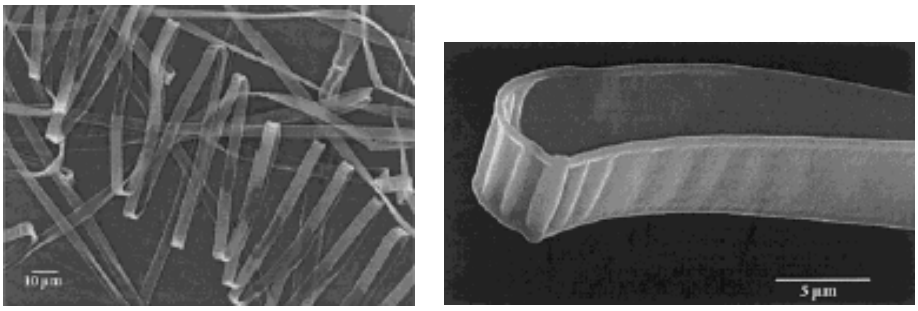

(a) (b)

Figure 2-13. (a) Poly(ester imide) ribbons fibers, (b) a wrinkled bend [67].

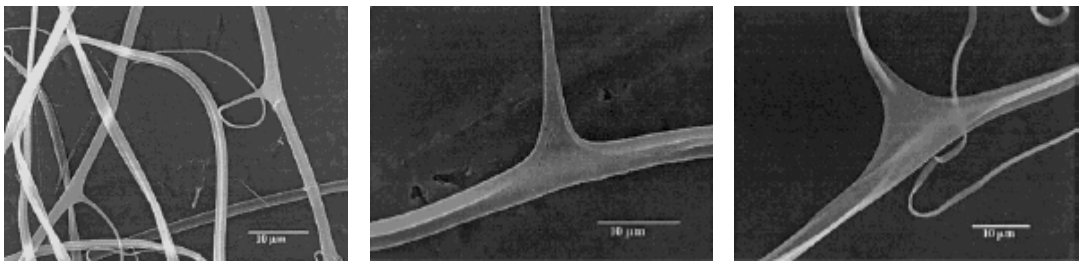

(a) (b) (c)

Figure 2-14. SEM images of branched (a) HEMA fibers, (b) PS fibers and (c) Poly(ester imide) [67].

Patterning of Electrospun Nanofibers

In electrospinning process, fiber orientation is dependent of an electric field which is

highly affected by collectors shape. The random fiber mat / membrane is fabricated using a plate collector which is used in the electrospinning as standard. Other architectures such as fiber bundle (1-D architecture) and mat with aligned fibers (2-D architecture) are produced using a rotatable disc and rotatable drum / frame, respectively.

A rotating drum collector is widely used to obtain aligned fibers [65,66]. Electrospun fibers are formed into alignment when a rotation speed of the drum collector is higher than a jet flying speed. There have been several attempts to improve alignment quality by modifying an electric field. Sundaray et al. have used a sharp pin applied negative potential in the rotating hollow drum (Figure 2-15 [67]). The created electric field is converged at the tip of sharp pin and consequently a solution jet is guided to direct the sharp pin, results in formation of relatively better aligned fibers. Katta et al. have introduce a method to collect aligned nanofibers using a rotating wire drum collector (Figure

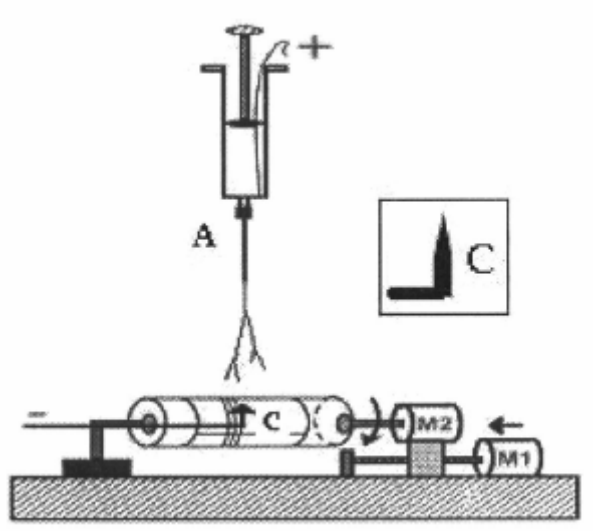

Figure 2-15. A rotating hollow drum collector with a sharp pin [72].

2-16, [68]) by developing a method using parallel conductive plates [69-71]. Two parallel conductive plates placed below a spinneret results in creating an electric field which is split into two fractions pointing towards edges of the gap along the electrodes. Electrospinning in the resultant electric field induce nanofibers aligned across the gap between the electrodes. In order to control alignment direction on a rotating drum collector, knife-edged aluminum bars have been used [72]. As shown in Figure 2-17, electrospun fibers are aligned in a diagonal direction instead of along the circumferential of the tube.

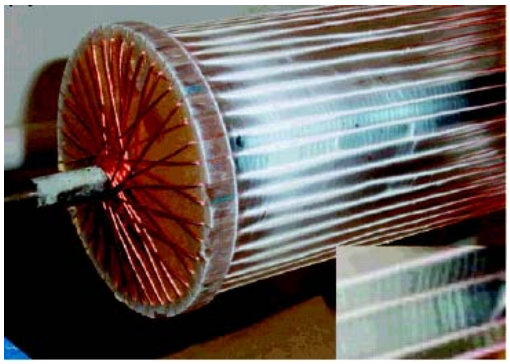

Figure 2-16. A rotating wire drum collector [73].

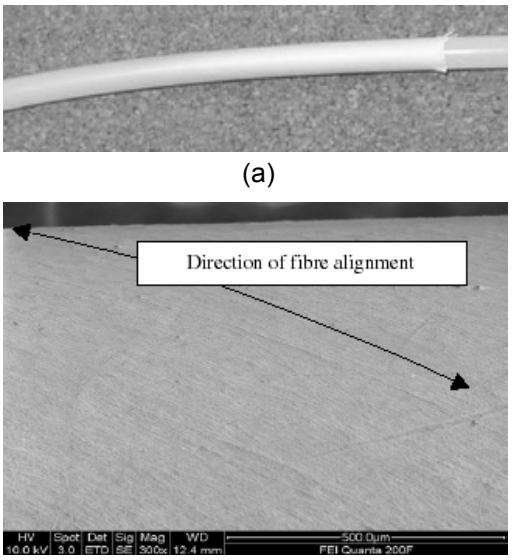

(a)

(b)

Figure 2-17. A knife-edged bar-induced diagonally aligned fibers on the tube (a) microphotograph at lower magnification, (b) SEM photo at higher magnification [77].

2-3-3. Processing-Molecular Structure Relationship

Many morphology studies have been conducted with electrospun biodegradable polymer nanofibers due to the interests in tissue engineering. However, a relatively small number of molecular structure studies have been done. Molecular structure of electrospun fibers have been conducted mainly using XRD and DSC. According to past studies, lower crystallization kinetics have been found in electrospinning process. Lee et al. has reported that electrospun Poly(caprolactone) (PCL) fibers showed lower crystallinity than that of as-cast film [49]. Final molecular structure seems to be as a function of a type of polymer. Among solution conditions / properties-related parameters, effects of molecular weight of polymer and polymer concentration on molecular structure of electrospun fibers have been investigated. High molecular weight of Poly(vinylalcohol) (PVA) nanofibers have been found to exhibit higher crystallinity than low molecular weight of PVA nanofibers [52]. Zong et al. have found that Poly(glycolide-*co*-lactide) (PLGA) nanofibers electrospun from solution with 15 wt% in polymer concentration exhibited crystalline structure, while PLGA nanofibers electrospun from 7.5 and 10 wt% solutions exhibited no crystalline structure [73]. As one of processing condition-related parameters, Zhao et al. have studied applied voltage effects on molecular structure of electrospun Ethyl-cyanoethyl cellulose (E-CE)C fibers [54]. Crystallinity of the electrospun

(E-CE)C fibers increased with increased voltage. Fennessey et al. have reported effects of take-up velocity of a rotating drum collector on molecular structure of Poly(acrylonitrile) nanofibers [74]. In the study, molecular orientation was found in the nanofibers electrospun at higher take-up velocity.

Considering the small number of molecular structure studies, a question still remains, that is, can a specific molecular arrangement or highly ordered structure be formed in polymer nanofibers via electrospinning process? In order to get the answer, more research works are needed to investigate the processing-structure relationship in the electrospinning.

2-3-4. Structure-Property Relationship

Mechanical properties of electrospun fibers from biodegradable polymers have been studied mainly with randomly oriented nanofiber sheets, PCL [49], and poly(glycolide-lactide) [73]. Although most the tensile tests have been performed using the electrospun random mats, the method is not suitable for characterizing the nanofiber property, because fiber orientation is changed during the tensile test, i.e. the tensile properties of the random nanofiber sheets is affected by friction between fibers as well as fiber property. The tensile tests using PAN nanofiber yarns have

been conducted [74]. In the study, nanofiber sheets were twisted and used as tensile test specimens. The effects of twist angles on tensile properties were well discussed, but the method may not be suitable for discussing tensile properties of the electrospun nanofibers. Bending test of electrospun PLLA single nanofibers was conducted using AFM-based nanoindentation [75]. Although this method is suitable for investigating bending modulus of nanofibers, it is impossible to discuss their strength and strain at break because only short shifting of an AFM cantilever tip is available.

Due to insufficient characterization, structure-properties relationship in electrospun fibers is not clear yet. One of the possible reasons why the tensile test with a single nanofiber has not been conducted is difficulties in the method to collect an electrospun single nanofiber. In order to study, structure-property relationship of electrospun fibers, new characterization method must be developed.

CHAPTER III

FIBER MORPHOLOGY OF ELECTROSPUN FIBERS AND THEIR ARCHITECTURE

3-1. Introduction

It has been found that fiber morphology (diameter and uniformity) of the electrospun polymer fibers are dependent on many electrospinning process-related parameters. These parameters can be divided into three groups as shown in Table 3-1. Numerous reports studying the effects of these parameters (solution consitions / properties [42,49], processing conditions [42,45,76], ambient conditions [45]) have been

Table 3-1. Parameters related electrospinning process.

Solution conditions / properties	Polymer concentration *
	Viscosity *
	Elasticity
	Molecular weight of polymer *
	Electrical conductivity *
	Dielectric constant *
	Surface tension
	Boiling point *
	Vapour pressure *
	Temperature *
Processing conditions	Applied voltage *
	Distance from needle to collector
	Volume feed rate *
	Needle inner diameter
	Take-up velocity *
Ambient conditions	Temperature
	Humidity *
	Atmospheric pressure

* Processing parameters tested in this study

reported and each of the parameters has been found to affect the morphology of the electrospun fibers. Under certain condition, not only uniform fibers but bead-like fibers can be produced by electrospinning. Till date, many polymers have been successfully electrospun into nanofibers and electrospun polymer nanofibers with diameter as small as 5 nm have been reported in the literature [77]. However, the detailed approach for the achievement was not presented clearly and information given from past processing studies is inadequate to support the electrospinning of ultra-fine nanometer scale polymer fibers. There is still a difficulty in electrospinning such ultra-fine nanometer scale polymer fibers. A more systematic parametric study is hence required. In this chapter, the effects of electrospinning parameters (the solution conditions / properties, processing conditions and ambient conditions) were studied to produce ultra-fine polymer fibers without beads.

On the contrary, patterning of electrospun nanofibers is also one of the challenges in electrospinning. Because a spinning jet ejected from a spinneret follows a spiral-shaped path during electrospinning process, and results in randomly oriented fibers. Well-aligned fibers and 3-D architecture with aligned fibers have potential applications in tissue engineering, filtration and composites. In tissue engineering, there are attempts to artificially produce tissue by seeding cells on scaffolds which

have similar structure as natural one. In fact, some human tissues such as inner and outer layers of blood vessels, tendon, cornea, nerve, etc. are replicated by culturing cells on aligned biodegradable polymer nanofibers. A high porous membrane, which is a good candidate as a filter media, might be enhanced by layered aligned fibers where fibers are aligned in different direction in each layer. A porosity of layered aligned fibers should be dependent on a pitch of aligned fiber. Layered membranes with aligned fibers can be used as reinforcement for composite materials. Aligned nanofibers can be processed into chopped nanofibers which can be applied to composite materials as reinforcement. Hence, once a technique to produce well-aligned nanofibers in the form of 2-D and 3-D architectures is developed, it may uncover new potentials of electrospun nanofibers. In this chapter, electrospinning of well-aligned nanofibers / 3-D architecture was investigated by using a rotating disc collector.

3-2. Experimental

3-2-1. Design of Electrospinning Setup

Figure 3-1 shows electrospinning setup used in this study. The setup consists of a high voltage supplier, a syringe pump, a syringe, tube with a fine conductive needle and different types of conductive collectors such as a plate collector and a disc

collector. As additional setup, an environmental chamber and a ribbon heater were designed. The chamber was connected with a gas supplier. Humidity level can be controlled by purging nitrogen gas / dried air. A ribbon heater, which can cover whole wall of syringe, was used to control solution temperature. Different types of collectors were used to spin nanofibers with different fiber orientation. A plate and disc collectors were used to spin randomly oriented fibers and fiber bundles, respectively. For spinning of aligned and single nanofibers, a disc collector was developed (Figure 3-2). Circumferential edge was covered with tubular shaped-covering, which can be used to mount any substrates in order to collect electrospun nanofibers.

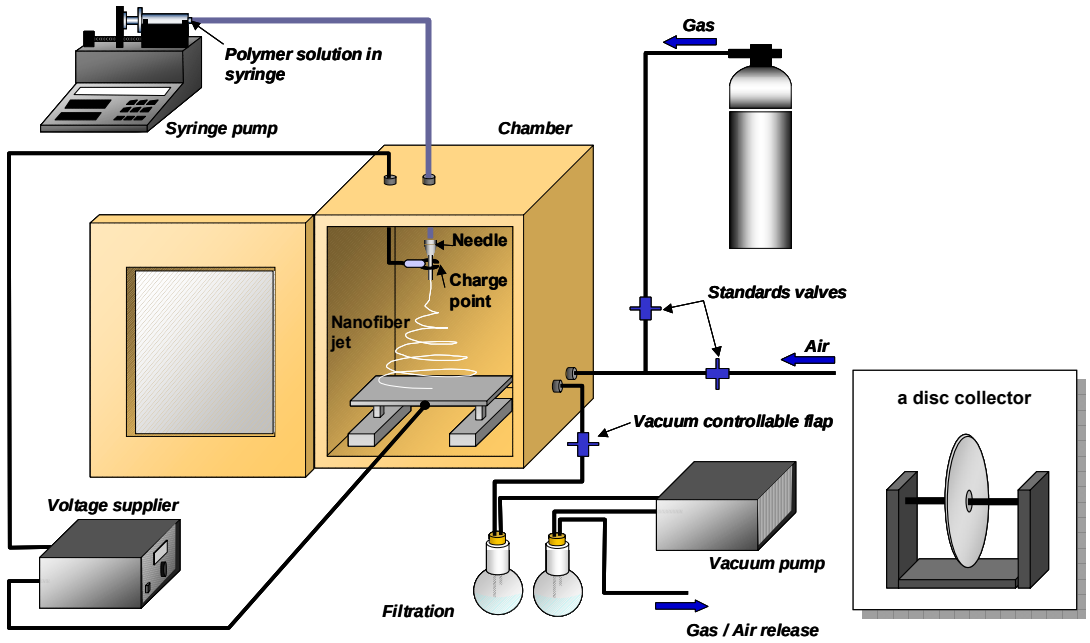

Figure 3-1. Schematic drawing of electrospinning setup.

Substrates can be fixed using double-side tape. The disc collector was also developed to collect electrospun single nanofibers. The collector design and a method to collect single nanofibers will be described in detail in Chap. 4.

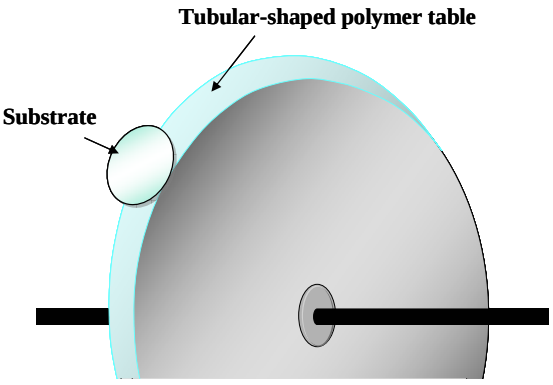

Figure 3-2. Disc collector developed for electrospinning of aligned fibers.

3-2-2. Material Selection

Several biodegradable polymers such as Poly($_L$-lactid-co-caprolactone) (70/30 wt%) (P(LLA-r-CL)) random co-polymer with molecular weight (Mw) of 150,000 g/mol, and Poly($_L$-lactid acid) (PLLA) with Mw of 100,000 and 300,000 g/mol, and Poly(caprolactone) (PCL) with Mn of 80,000 g/mol were used in this study. These polymers were dissolved in either dichloromethane (DCM) or chroloform ($CHCl_3$). To change the resultant solution properties, N, N-dimethylformamide (DMF) or pyridine was added. The solvent properties were summarized in Table 3-2.

All electrospun fibers were stored in vacuum for at least 24 hours to ensure that the solvents were completely vaporized.

Table 3-2. Solvent properties.

Solvents	Mixture ratio of solvents (wt%)	Electrical conductivity (μS)	Dielectric constant	Vapour pressure (at 20 °C) (kPa)	Boiling point (°C)	Viscosity (mPa-s)
DCM	-	0.0 (at 22.4°C)	9.1	47.4 *	40 *	0.45
DCM/DMF	70/30	1.7 (at 17.4°C)	-	-	-	0.64
DMF	-	2.3 (at 17.3°C)	36.7	0.492 *	153 *	0.92 *
DCM/Pyridine	80/20	7.2 (at 22.3°C)	-	-	-	-
	60/40	15.7 (-)	-	-	-	-
	50/50	13.1 (at 22.2°C)	-	-	-	0.65
	40/60	13.8 (at 22.1°C)	-	-	-	-
	20/80	13.2 (at 22.2°C)	-	-	-	-
Pyridine	-	4.4 (at 22.8°C)	12.5	2.0 *	115 *	0.95 *
$CHCl_3$	-	0.1 (21.1)	4.8	21.2	61.2	0.58
$CHCl_3$/Pyridine	60/40	-	-	-	-	-

* obtained from ref. [79-81]

3-2-3. Control of Humidity Level

Relative humidity was controlled through vacuuming and the release of either nitrogen gas or moist air into the chamber through the valves, depending on which humidity is desired. Since the properties of nitrogen gas follow closely to that of air and the gas makes up close to 80% of the air content, the project uses nitrogen as a substitution for dry air. The pressure within the chamber was maintained at the same level as room pressure, at around 0.1 MPa after the release of nitrogen gas into it was completed.

3-2-4. Conductivity Meter and Rheometer

The electrical conductivities of the solvents were measured using a conductivity

meter (TPS 901-C, Conductivity-TDS meter, Horida). The viscosities of the polymer solution used in the experiments was obtained using a strain controlled rheometer (ARES 100 Force Rebalanced Transducer (FRT), Rheometric Scientific).

3-2-5. Scanning Electron Microscopy (SEM) and Transmission Electron Microscopy (TEM)

In order to determine the morphology and orientation of the electrospun fibers, the nanofibers were observed under scanning electron microscope (SEM; JSM-5800LV, JEOL), filed-emission scanning electron microscope (Quanta FE-SEM, FEI) and transmission electron microscopy (TEM; JEM-2010F FasTEM, JEOL). The samples for SEM were coated with Au or Pt and observed at an accelerating voltage in the range of 10 to 15 kV.

3-3. Results and Discussion

3-3-1. Fiber Morphology

(1) Solution Conditions / Properties Effects

Polymer concentration

Polymer concentration effects on the morphology of electrospun fibers were studied using PLLA solutions at different polymer concentrations. The details of solvent

conditions were summarized in Table 3-3. Electrospinning results (Figure 3-3) showed that the diameter of the electrospun fibers dramatically decreased with decreasing polymer concentration. When the polymer concentration was too low (i.e.

Table 3-3. PLLA polymer solutions used for processing studies.

Polymer	Polymer concentration (wt%)	DCM/Pyridine Solvent mixture ratio (wt%)
PLLA	1.25	40 / 60
(Mw; 300K)	1.75	40 / 60
	2.5	50 / 50
	3.5	50 / 50
	4.0	50 / 50
PLLA	7.5	60 / 40
(Mw; 100K)	12.5	60 / 40

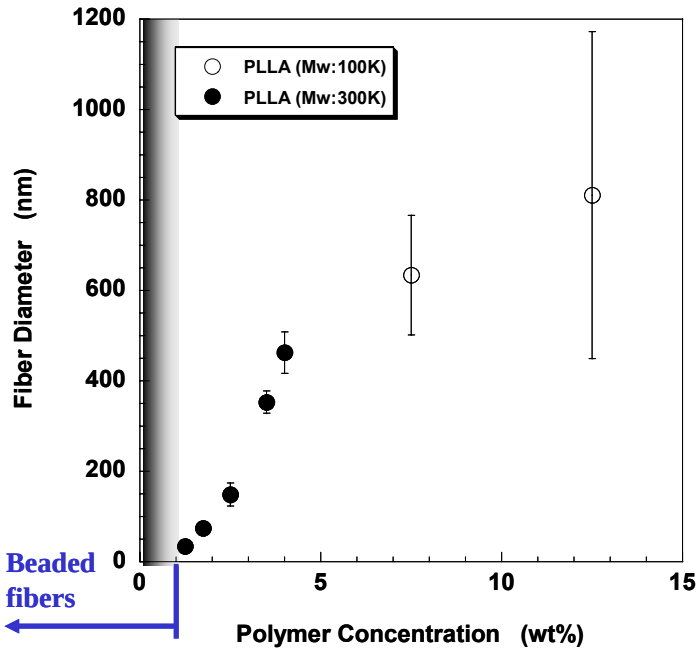

Figure 3-3. Polymer concentration effects on the diameter of the electrospun PLLA fibers.

less than 1 wt% of PLLA), beaded fibers were observed. Hence, despite the ability to shrink the size of the fibers by decreasing the polymer concentration, it was compromised by the change of the fiber uniformity. Surface tension effects could be dominant with decreased polymer concentration since polymer chain entanglements are reduced. It is considered that the formation of the beaded fibers is due to the initial jet instability which is led by solution with low surface tension. [45].

Molecular weight

PLLA with different molecular weights were used in this study: Mw of 100, 000 and 300, 000 g/mol. Each of the polymer was dissolved in the pure DCM to determine the minimum concentration to electrospin fibers without beads. Experimental results (Figure 3-4) showed that beads were formed more easily with low molecular weight of PLLA (LM-PLLA). Beads were first observed from LM-PLLA solution at a minimum concentration of 9 wt%, and the diameter of the beaded fibers was 400 ± 50 nm. While with similar diameter, high molecular weight of PLLA (HM-PLLA) solution, at 4.5 wt% in a concentration, was able to produce beads free uniform fibers. In addition, when HM-PLLA was electrospun at a lower polymer concentration of 3.5 wt%, finer uniform nanofibers with diameter of 322 nm were successfully produced.

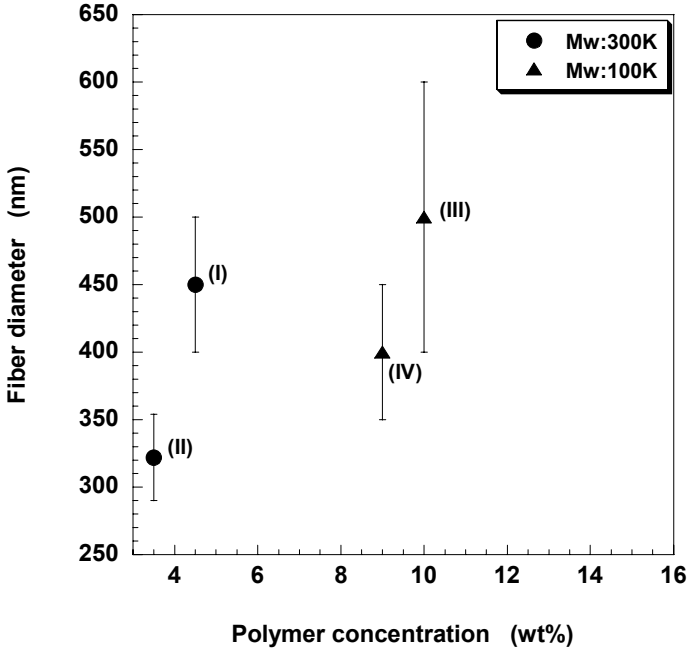

(a)

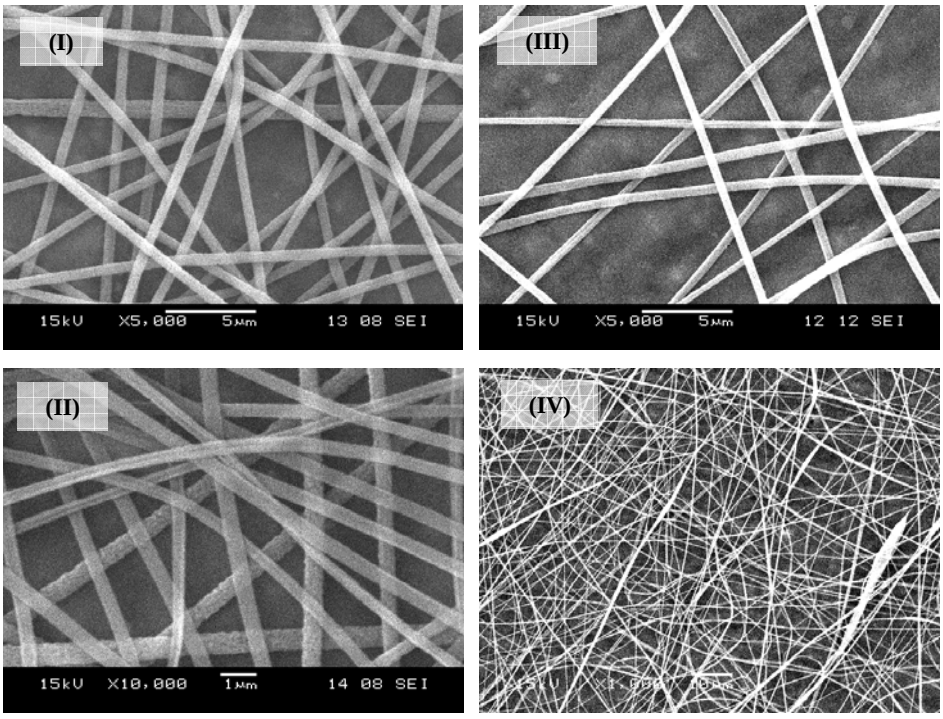

(b)

Figure 3-4. Molecular weight effects on the morphology of the electrospun PLLA fibers.

Molecular weight of the polymer affects solution viscosity, and surface tension. Hence, solution viscosity of HM-PLLA solution might be high enough to electrospin uniform fibers even when polymer concentration is low. In summary, polymer molecular weight played an important role in determining the minimum polymer concentration that is to electrospin fine polymer fibers.

Solvent properties

Table 3-4 shows P(LLA-r-CL) solutions used to study the effects of solvent properties on the morphology of electrospun nanofibers. The polymer was dissolved into DCM, and either DMF or pyridine was added into the resultant solution to change the solution properties (Table 3-2). The P(LLA-r-CL) fibers electrospun from Solution 3 showed the smallest diameter, while the fibers from Solution 1 showed the largest diameter. The decreased fiber diameter might be associated with the electrical conductivity of the solvents. Figure 3-5 shows the P(LLA-r-CL) fiber diameter as a function of the solvent electrical conductivity. There was a significant drop in the diameter of the electrospun polymer fibers when the electrical conductivity of the solutions was increased. Beaded fibers were produced with increasing electrical conductivity (i.e. over than 50 wt% of Pyridine). Beads formation might be interpreted by the poor solubility of polymer into pyridine.

P(LLA-r-CL) may precipitate when excess pyridine is added to a solution of the polymer in DCM. The resultant solution causes formation of beaded fibers / particles. Another possibility for beads formation may be the interaction between water molecules and pyridine molecules in a solution jet. Pyridine shows relatively high absorbability of water molecules which may be absorbed into a pyridine-based solution during electrospinning. Higher absorbance of water molecules decreases

Table 3-4. P(LLA-r-CL) solutions used to study electrical conductivity effects.

	Polymer	Polymer concentration (wt%)	Solvents	Mixture ratio of solvents (wt%)	Fiber diameter (nm)
Solution 1	P(LLA-r-CL)	10	DCM	–	310 ± 150
Solution 2			DCM / DMF	70 / 30	245 ± 139
Solution 3			DCM / Pyridine	50 / 50	109 ± 36

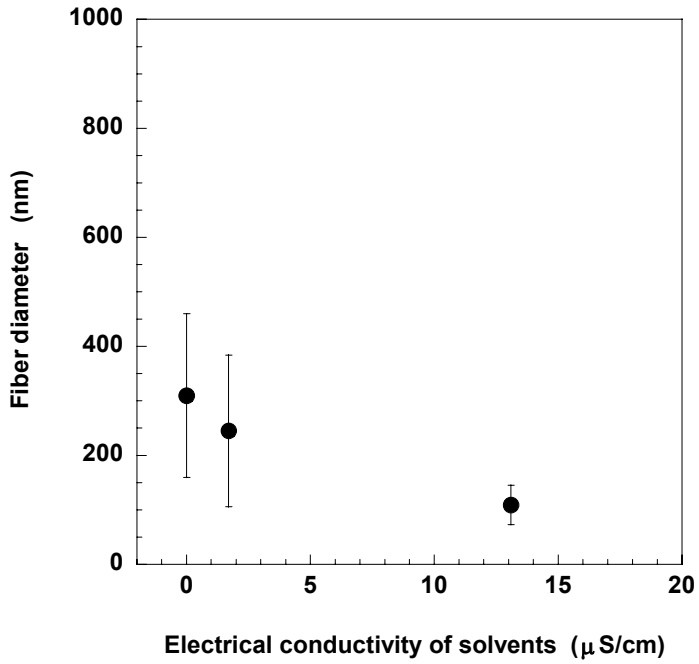

Figure 3-5. Solution conductivity effects on the diameter of the electrospun P(LLA-r-CL) fibers.

surface tension of a solution jet, leading to beaded fibers. Beads were also observed from solution 1 and this should be due to low viscosity of the solution. The beads can be removed if high molecular weight polymer is used. Despite solution 3 showing the highest viscosity, electrospun polymer nanofibers with the smallest fiber diameter were obtained. Therefore, the drop in the size of the fibers was proven to be due to the increased electrical conductivity.

Generally, the electrical conductivity of the solution affects the charges accumulated on the jet surface. The repulsion force between the neighboring charges may encourage the drawing of the jet. The electrospinning of smaller diameter of fibers is due to greater drawing of the jet.

Solution temperature

7.5 wt% of PLLA with molecular weight of 300K was dissolved in DCM / pyridine mixture (60/40wt%) to prepare a polymer solution. The PLLA solution was heated up at 40^{o}C and 70^{o}C, which are slightly lower and higher than glass transition temperature (T_g) of PLLA. As shown in Figure 3-6, fibers with the largest diameter were electrospun from solution heated up to 40 ^{o}C. The temperature is the same with the boiling point of DCM, which might encourage solidification of the jet. The faster

solidification suppresses the drawability of the jet. At solution temperature of 70 ^{o}C, electrospun fibers showed smaller fiber diameter than that of fibers spun at 40 ^{o}C. This is likely due to the mobility of PLLA molecules since the solution temperature is higher than T_g of PLLA (60 ^{o}C). The jet with high mobility of molecular chains might be highly stretched during electrospinning and formed into the fibers with smaller diameter.

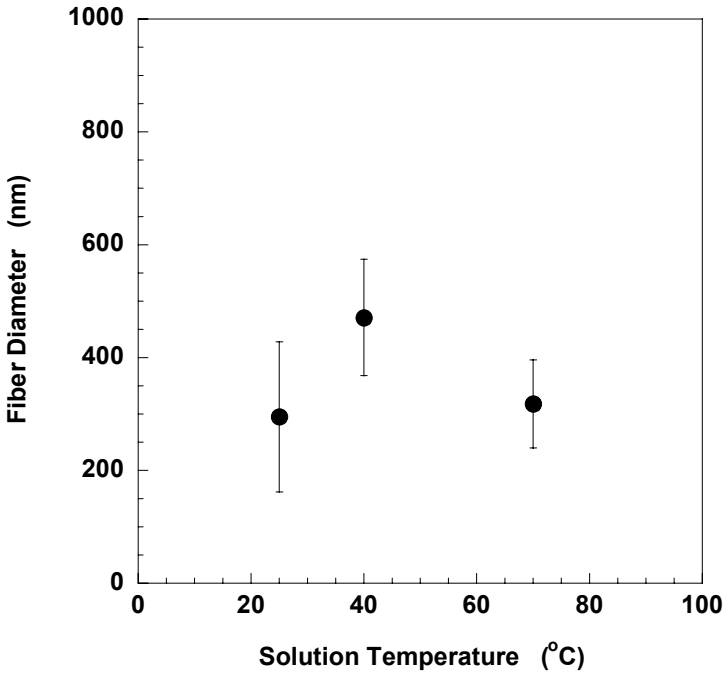

Figure 3-6. Solution temperature effects on the diameter of the electrospun PLLA fibers.

(2) Processing Conditions Effects

Effects of processing condition-related parameters such as applied voltage, volume feed rate and take-up velocity were investigated.

Applied Voltage

Figure 3-7 clearly illustrates the trend observed using P(LLA-r-CL) and HM-PLLA with various polymer concentrations. For P(LLA-r-CL) solution, 12.5 wt% of P(LLA-r-CL) was dissolved in $CHCl_3$ / pyridine mixture (60/40 wt%). For HM-PLLA solution, the same HM-PLLA solutions as that used in polymer concentration studies were used. It was observed that the electrospun fibers with slightly larger diameter were produced from higher polymer concentration of solutions at higher voltage. This phenomenon could be caused by larger amount of polymer solution that was drawn out from a spinneret at any one time, under a higher voltage, which hence resulted in electrospun fibers with larger diameter. This trend was also presented by other researchers [45]. However, with increasing voltage, electrospun nanofibers with smaller diameter was also observed [78]. This may be due to higher electric charges on the jet surface, resulting in larger repulsion force between neighboring charges to draw the jet. This voltage effect was found to diminish when the polymer concentration was low.

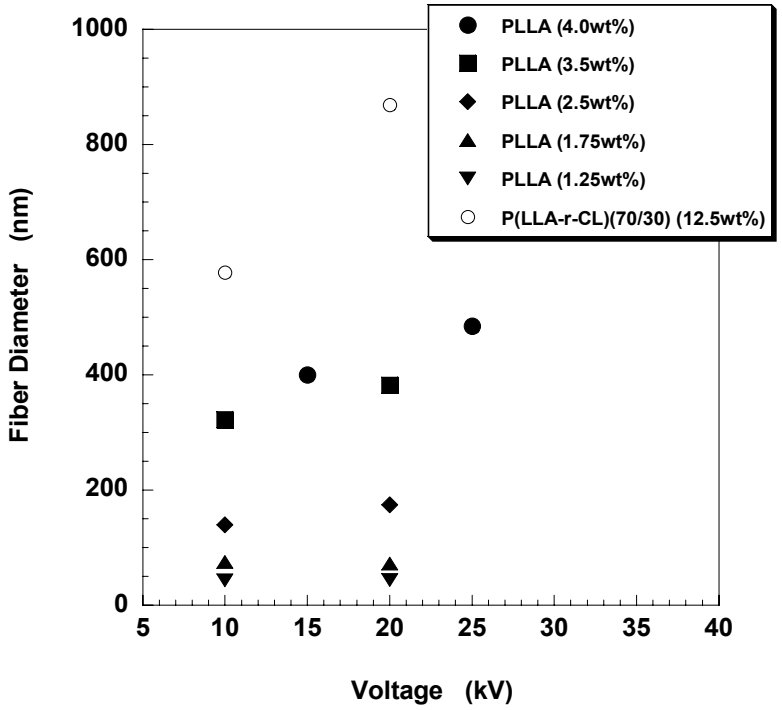

Figure 3-7. Applied voltage effects on the diameter of the PLLA (*Mw*: 300K) fibers electrospun from solutions with different polymer concentration.

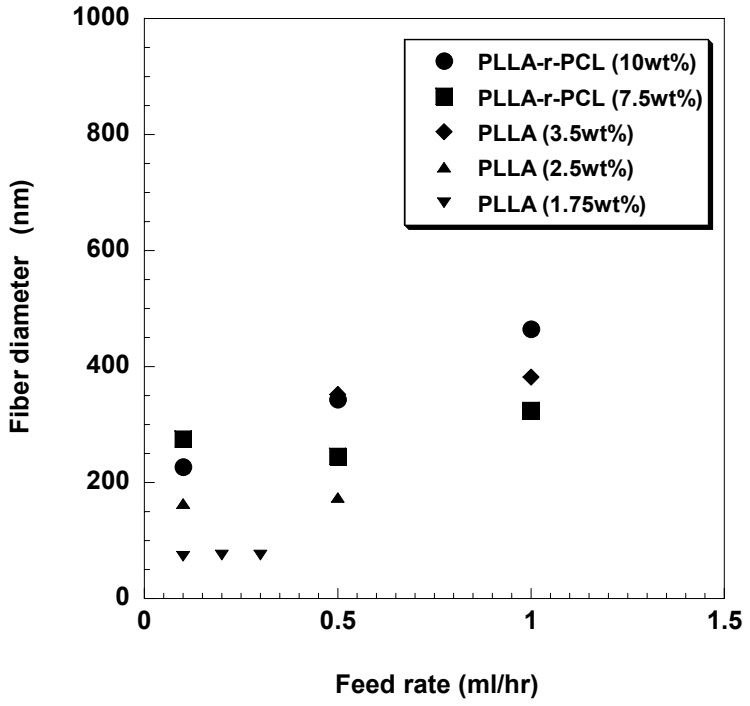

Figure 3-8. Volume feed rate effects on the diameter of the PLLA (*Mw*: 300K) fibers electrospun from solutions with different polymer concentration.

Volume Feed Rate

A similar trend to that found in voltage effect studies was observed on the effect of volume feed rate on the morphology of electrospun P(LLA-r-CL) and PLLA fibers. P(LLA-r-CL) was dissolved in DCM with 50 phr of pyridine. PLLA fibers were electrospun from the same solutions used in polymer concentration studies. Figure 3-8 shows that the diameter of the electrospun P(LLA-r-CL) and HM-PLLA fibers was slightly increased as higher steady volume feed rate was applied to push the polymer solution out through the needle. The influence due to the volume feed rate also diminished when the polymer concentration is low.

Take-up Velocity

Take-up velocity effects was investigated using PCL, P(LLA-r-CL) and HM-PLLA. As illustrated in Figure 3-9, diameter of electrospun HM-PLLA fibers decreased with higher take-up velocity. For electrospun PCL and P(LLA-r-CL) fibers, diameter is almost independent of the take-up velocity which might not be high enough to draw those fibers.

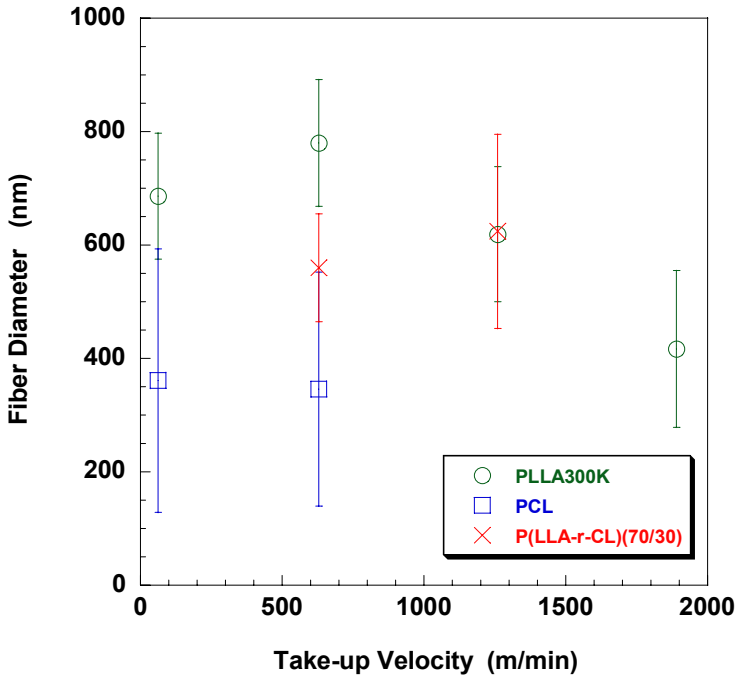

Figure 3-9. Electrospun fiber diameter as a function of take-up velocity.

(3) Ambient Conditions Effect

Experiments to study ambient conditions effects were conducted using an electrospinning setup with an environmental chamber in where HW-PLLA solutions with different polymer concentration was electrospun at different humidity levels. Relatively large diameter of nanofibers (> 500 nm) were electrospun from solution with 4.5 wt% in polymer concentration. For relatively large diameter of fibers, its fiber morphology was dependent on humidity level. Electrospinning between 48 and 83 % in humidity yielded circular and beads-free nanofibers (Figure 3-10(b)). Figure 3-11 shows diameter of electrospun circular / beads-free fibers as a function of humidity level. Relatively small diameter and highly uniform fibers, indicated by the

smallest standard deviation, were produced at around 68 % of humidity. At relative humidity above 72 %, fiber diameters are observed to increase with increasing

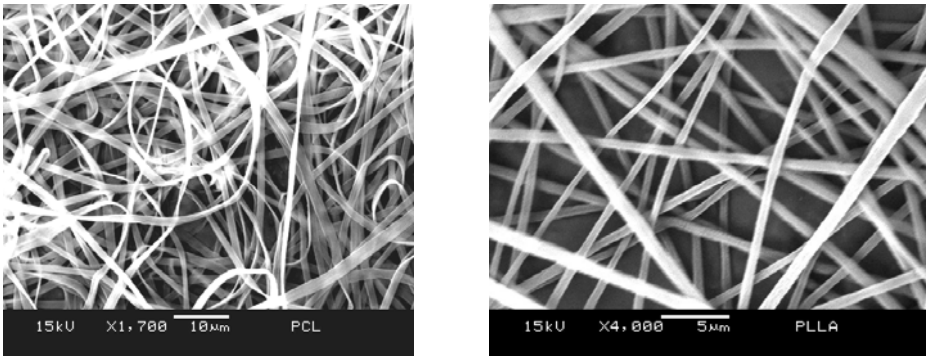

(a) (b)

Figure 3-10. SEM images of PLLA fibers electrospun at different humidity level; (a) flat fibers electrospun at blow humidity of 48 %, (b) uniform fibers electrospun between 48 % and 85 %.

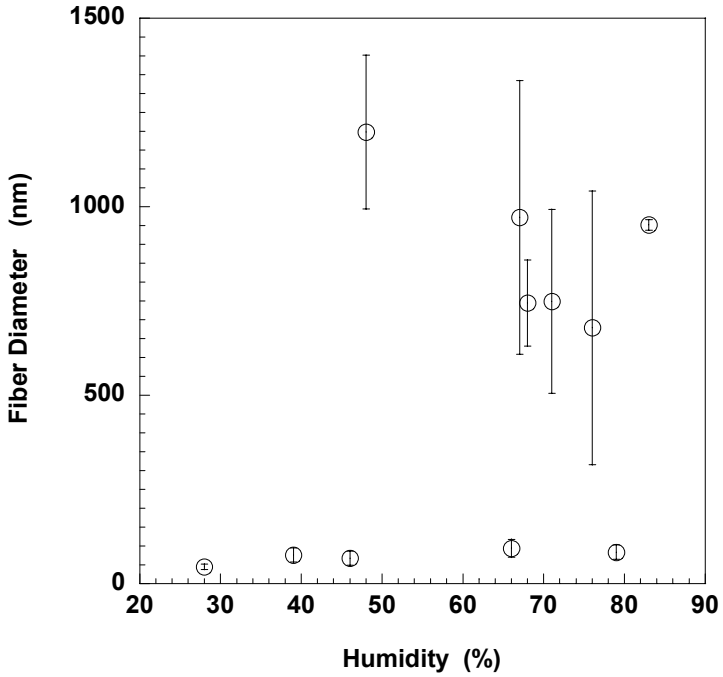

Figure 3-11. Diameter of electrospun uniform PLLA fibers as a function of humidity level.

humidity levels. Water molecules may be responsible for conducting charges away from the jet surface. Thus stretching of the jet would be minimized due to decreased repulsion force between the neighboring charges accumulated on the jet surface. On the other hand, at relative humidity less than 66%, an increase in fiber diameter was also observed. This may be explained by the “hardening and solidifying” of the jet due to rapid evaporation at lower relative humidity. This makes the elongation of the jet into thinner fiber difficult.

At different humidity level, electrospun fibers with different cross-sections were observed. At relative humidity greater than 85 %, beaded nanofibers were collected. On the contrary, when the process was carried out at relative humidity of less than 48%, flat fiber was observed (Figure 3-10(a)). Koombhongse et al. have also reported electrospinning flat fibers. It is reported that the occurrence of rapid solvent evaporation at the jet surface due to the volatile nature of the solvent resulted in the formation of a polymer skin over the solution core of the jet. The collapse of the tube like skin due to atmospheric pressure results in the formation of flat fibers. In this study, rapid solvent evaporation is likely the result of low humidity level [78], resulting in formation of flat fibers.

Relatively small scale of fibers (< 200nm) electrospun from solution with 1 wt% in polymer concentration showed different trends from that found from fibers with relatively large diameter. Fiber diameter was slightly decreased with decreasing humidity level. Unlike relatively large diameter of electrospun fibers, the smaller diameter of fibers had circular cross-section even at low humidity level of less than 48 %. Due to the relatively small size of fiber, the solution within the core is able to diffuse to the surface fast enough to replenish the evaporated solvent at the surface. The rapid diffusion of solvent from the core prevents the formation of polymer skin, by continuously replacing the evaporated solvent at the surface. Due to this phenomenon, the core solidifies before the surface and thus no flat fiber was observed.

Humidity level is variable with weather and time, i.e. humidity level dramatically changes between morning, daytime and night. If humidity level keeps varying during electrospinning, standard deviation of electrospun fibers will be larger, hence less uniformity. In addition, even though solution and processing parameters are held constant, morphology of electrospun fibers will be different unless humidity level is maintained at the same level. Thus, humidity level is an important parameter for uniformity and reproducibility of electrospun nanofibers.

According to parameter studies presented above, polymer concentration, its molecular weight and solvent properties were found to play a significant role in controlling the morphology of the electrospun nanofibers. Other parameters such as the voltage, feed rate and take-up velocity were less effective. Therefore, it can be noted that the morphology of the electrospun nanofibers is primary affected by polymer concentration, its molecular weight and solvent properties, followed by voltage, feed rate and take-up velocity.

Humidity was found to be an important parameter for fiber uniformity and reproducibility of electrospun fibers. Therefore, humidity level must be maintained to improve reproducibility.

(4) Processing Map

According to processing parameter studies, it was found that the jet shrink its size / diameter via solvent evaporation and drawing process. Namely all the parameters can be categorized from the viewpoint of effects on the fiber morphology. All the processing parameters were divided into two groups; i.e. one with parameters which changes the mass of polymer in the jet, and the other with parameters which changes the jet drawing ratio during electrospinning. Based on this concept, the effects of

processing parameter studies in this chapter were summarized in a processing map (Figure 3-12). Polymer concentration, applied voltage and volume feed rate were considered to affect the mass of polymer so that fiber diameter was decreased when the values of these parameters were decreased. It is noteworthy that the minimum polymer concentration to electrospin fine fibers was determined by the molecular weight of polymer. On the other hand, it was considered that solvent properties and applied voltage affect the charges accumulated on the jet, namely the repulsion force-induced jet drawing. Solvent properties include viscosity, electrical

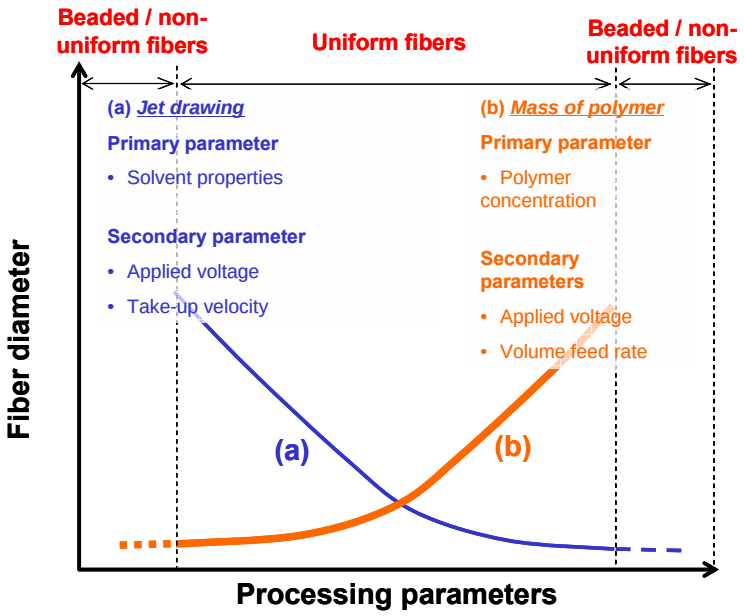

Figure 3-12. Processing map obtained based on the systematic parameter study: (a) jet drawability (affected by solvent properties, applied voltage, take-up velocity), (b) mass of polymer (affected by polymer concentration, applied voltage, volume feed rate).

conductivity, dielectric constant, boiling point and so on. Take-up velocity directly affects the jet drawing ratio. Hence fiber diameter decreases with increasing applied voltage, take-up velocity and adequate solvent properties (low viscosity, high electrical conductivity / dielectric constant and high boiling point). For both cases, non-uniformed / beaded fibers were found if the conditions were either too high or too low. In electrospinning process, there are several parameters which were not studied in this chapter and most of them affect the jet drawing. Figure 3-13 summarizes the parameters which are associated with the jet drawing. The jet drawing-related parameters are categorized in jet elasticity-, solidification time- and drawing force-related parameters. These parameters might show an important role in molecular structure development.

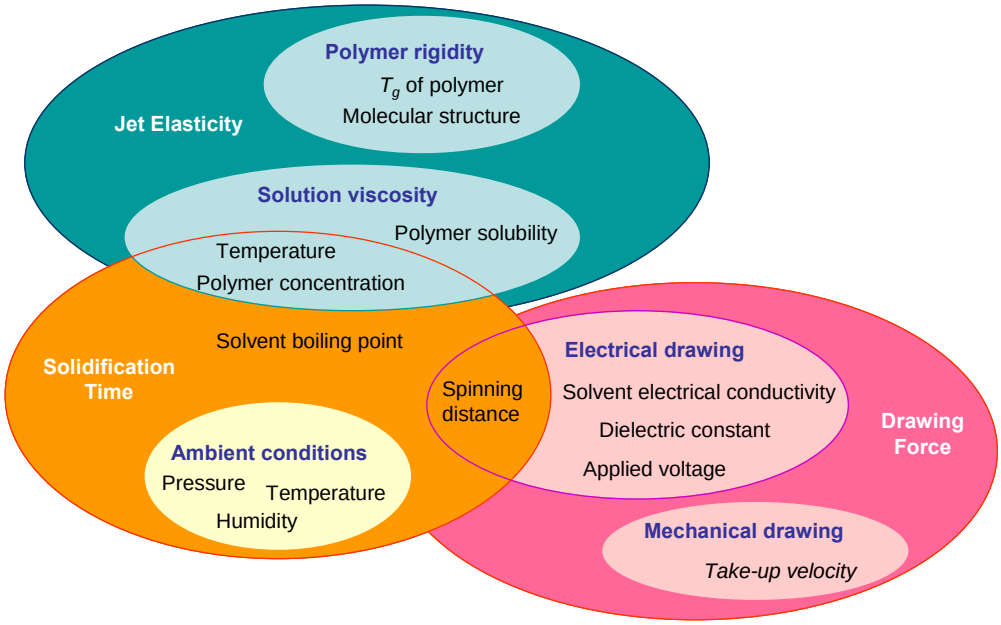

Figure 3-13. The jet drawing-related parameters.

(5) Electrospinning of Ultra-fine Polymer Fibers

With the target of electrospinning ultra-fine polymer fibers, all the parameters studied in this chapter were optimized in a systematic manner on the basis of the processing map shown in the previous section. As a start, HM-PLLA was selected and dissolved in solvents with high electrical conductivity. DCM was used as a main solvent to prepare the polymer solution, and pyridine was added at a high proportion to increase the overall conductivity of the solution, giving an overall proportion of DCM/pyridine ratio of 20/80 wt%. The minimum concentration of the polymer to produce uniform fibers was then determined at 1 wt%. Finally, when combined with the optimum processing parameters to electrospin this solution: i.e. smallest available metal needle of inner diameter of 0.21 mm; low volume feed rate of 0.1 ml/hr; applied voltage of 10kV and spinning distance of 100 mm, excellent results were achieved. Ultra-fine polymer fibers as small as 9 nm in diameter was observed under TEM (Figure 3-14). The average diameter of these fibers was 19 nm ± 6 nm.

3-3-2. Fibers Patterning

(1) Effects of Table Material

To spin aligned nanofibers, electrospun solution jet was deposited on cover-slips placed on the circumferential edge of a disc collector. Cover-slips must be firmly

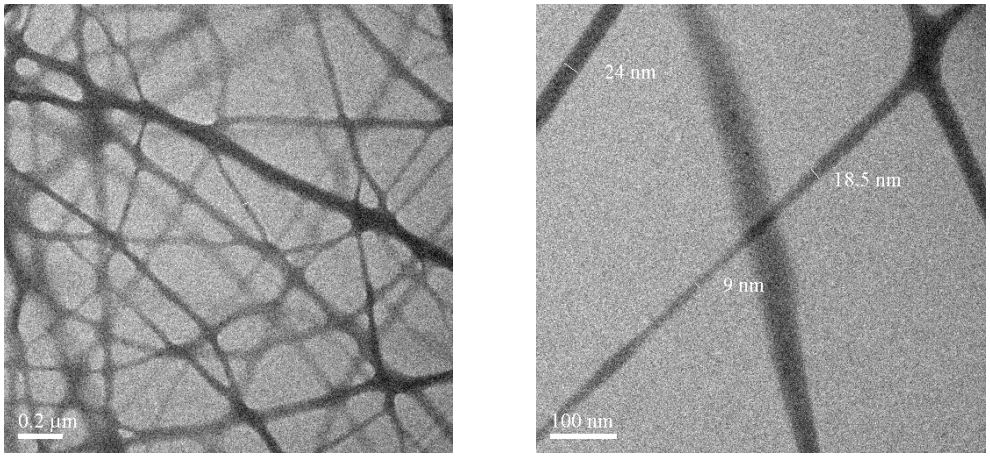

(a) (b)

Figure 3-14. TEM image of ultra-fine PLLA fibers: (a) at lower magnification, (b) at higher magnification.

attached so that it will not be detached from the disc collector by the rotation of the disc. In view of this, the table to mount the cover-slips was required to be fixed onto the circumferential edge of a disc collector and the table should not interrupt the guiding of the solution jet to the edge of the disc. In this section, table material effects on quality of 2-D alignment were investigated using non-conductive and conductive tables, i.e. a tubular-shaped polymer table and a square-shaped metal table (Figure 3-15). Figure 3-16 is the optical microscope images of PCL aligned fibers electrospun using tables of different material. PCL nanofibers collected using non-conductive table were well aligned, while PCL nanofibers collected using conductive table was relatively random in terms of fiber orientation. Electrostatic field during electrospinning converged to the sharp edge of the disc collector so that the edge of the disc collector was able to guide the solution jet onto itself. The edge

effect can be maintained using non-conductive table, but seems to be interrupted by using a conductive table. Material of the table must be carefully selected to electrospin well-aligned nanofibers.

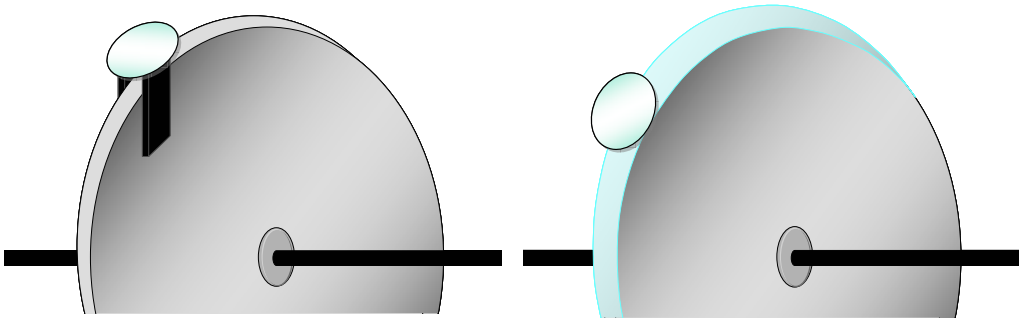

Figure 3-15. Disc collectors developed for electrospinning of aligned fibers: (a) conductive square-shaped table, (b) non-conductive tubular-shaped table fixed on the edge of a disc collector.

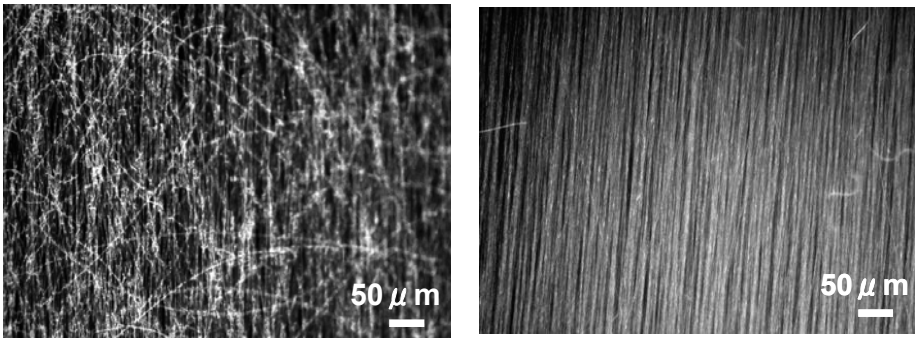

Figure 3-16. Fiber orientation as a function of table materials: PCL fibers electrospun on tables made from (a) conductive materials, (b) non-conductive material.

(2) Effects of Take-up Velocity

Figure 3-17 shows SEM images of HM-PLLA fibers electrospun at different take-up velocity. PLLA fibers electrospun at 63 m/min were randomly oriented. On the other hand, PLLA fibers electrospun at above 630 m/min was well aligned. Therefore, the take-up velocity of 630 m/min may be faster than the spinning rate of the jet, hence, the fibers might undergo drawing process during electrospinning. It is interpreted by the finding that the fiber diameter decreased at higher take-up velocity (see in section 3-3-3).

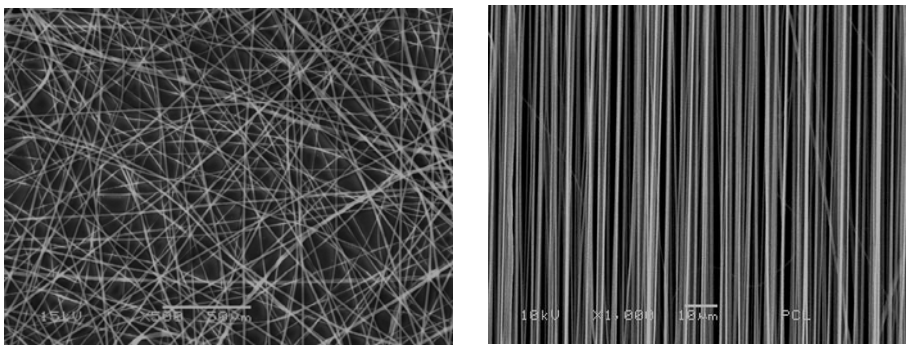

(a) (b)

Figure 3-17. Fiber orientation as a function of take-up velocity: PLLA fibers electrospun at (a) 63 m/min, (b) 630 m/min.

Based on the results mentioned above, optimized processing conditions for spinning aligned nanofibers are as follows;

- non-conductive table, which does not interrupt the efficiency of a disc collector, must be used for mounting any substrates

- take-up velocity must be higher than the spinning rate, i.e. take-up velocity above 630 m/min was required according to the author's experiment.

(3) Electrospinning of 3-D architecture with aligned nanofibers

On the basis of the experimental results mentioned in previous sections, electrospinning of 3-D architecture with aligned nanofibers was attempted. PCL nanofibers were electrospun on cover-slips mounted on tubular-shaped table fixed on circumferential edge of a disc collector, after which cover-slips were rotated at + 45 ^{o} against the direction of the disc edge and PCL nanofibers were re-electrospun, followed by re-electrospinning of PCL nanofibers on the same cover-slips rotated at – 45 ^{o}. As a result, 3-D architecture with aligned nanofibers, where each layer of aligned fibers in different direction (0^{o}, + 45^{o} and – 45^{o}), was successfully electrospun (Figure 3-18).

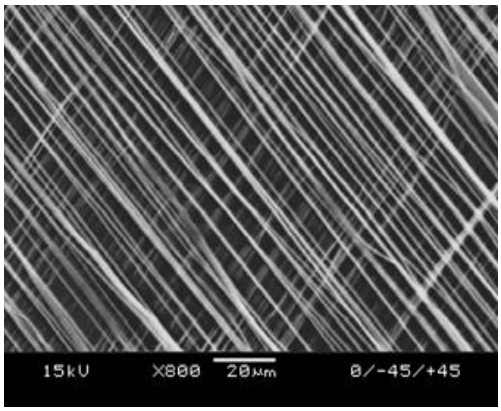

Figure 3-18. SEM image of 3-D architecture with PCL aligned nanofibers directed at 0^{o}, -45^{o} and 45^{o}.

3-5. Summary

Effects of processing parameters (solution conditions / properties, processing conditions and ambient conditions) on morphology of electrospun nanofibers (fiber diameter and uniformity) were investigated in this chapter. As the results, it was found that mass of polymer in the jet and the jet drawing ratio determines the electrospun fiber morphology. Fiber diameter is decreased with a decrease in mass of polymer in the jet or an increase in the jet drawing ratio. Their tendencies to change the fiber morphology were summarized in the processing map where the main processing parameters were classified. The fiber morphology is highly contributed by the polymer concentration, its molecular weight and the solvent properties.

In addition to the above dominant parameters, there are many parameters which are related with electrospinning process. Most of them affect the jet drawing ratio and which are categorized in jet elasticity-, solidification time- and drawing force-related parameters. Based on the systematic parametric study, polymer nanofibers as small as 9 nm in diameter had been successfully produced.

Additionally, electrospinning of 2-D / 3-D architecture with aligned nanofibers was attempted by developing a disc collector. The 2-D and 3-D architecture with

electrospun aligned fibers were successfully electrospun onto cover-slips mounted on tubular-shaped polymer table which covered the edge of a disc collector. The studies in this chapter has shown the possibility and ease of controlling the fiber morphology and architecture of the electrospun polymer fibers.

CHAPTER IV

STRUCTURE AND PROPERTIES OF AS-SPUN FIBERS

4-1. Introduction

Molecular structure analysis of electrospun polymer nanofibers have been mainly conducted with biodegradable polymers [46,49,60,82-86]. Past studies revealed that crystallization kinetics of electrospun nanofibers is low (see in Chap. 2). Electrospun PCL nanofibers were found to develop crystalline structure but its crystallinity is lower than casting film [49]. It was also reported that crystallization appearance on electrospun nanofibers is affected by the type of polymer structure. The low crystallization kinetics of electrospun nanofibers is closely related to the rapid solidification manner of spinning jets. However, the discussion to enhance crystalline structure of electrospun polymer nanofibers has not been sufficient from the viewpoint of processing parameters.

In Chap. 3, ultra-fine PLLA nanofiber with 9 nm diameter could be successfully achieved by the systematic study of electrospinning parameters. It was clear that the solvent properties and polymer concentration play an important role to decrease the fiber diameter [87]. The more reduction of fiber diameter under certain solvent

properties, the larger drawing force is applied to the electrically charged jets. Hence, during the reduction of fiber diameter, molecular structure of electrospun nanofibers may be transformed. Similarly, take-up velocity of a fiber collector should be taken into account as melt-spun polymer fibers clearly showed the interaction between their molecular structure and the take-up velocity [11,14,28,88-92].

Therefore, in this chapter, molecular structure of electrospun nanofibers has been discussed from the viewpoint of three electrospinning parameters, i.e., solvent properties, polymer concentration and take-up velocity. As model, two homopolymers with different glass transition temperature (T_g) and their block and random copolymers were used. As described in chap 2, molecular structure development of polymers is highly dependent on temperature. From this viewpoint, PLLA, PCL and their copolymer have been chosen. T_g of PLLA is around 60 ^{o}C, while that of ductile PCL is around - 60 ^{o}C which is lower than room or spinning temperatures. The comparative studies between the homopolymers and copolymers might show a way to control the molecular structure of electrospun fibers by material design. Finally, in order to understand the feedback of molecular structure into the whole nanofiber property, tensile property of single nanofibers was discussed.

4-2. Experimental

4-2-1. Materials

Semi-crystalline biodegradable polymer of poly($_L$-lactide) (PLLA), poly(caploractone) (PCL) and their copolymers of poly($_L$-lactide-*co*-caploractone) random copolymer (P(LLA-r-CL)), poly(L-lactide-*co*-caploractone) block copolymer (P(LLA-b-CL)) were used in this chapter. The details of these polymers were shown in Table 4-1. These polymers were dissolved into either acetone or dichloromethane (DCM) or chloroform ($CHCl_3$) were used to dissolve prepare polymer solutions. To change polymer solution properties, pyridine or methanol were added into the solution. The properties of the solvents used in the molecular structure studies are listed in Table 4-2.

Table 4-1. Materials used in molecular structure studies.

	Polymer	Molecular weigth (g/mol)	Unit ratio (wt%)
Homopolymer	PLLA	100,000	-
		300,000	-
	PCL	80,000	-
Block copolymer	P(LLA-b-CL)	440,000	75/25
Random copolymer	P(LLA-r-CL)	150,000	70/30

Table 4-2. Solvent properties.

Solvents	Mixture ratio (wt%)	Electrical conductivity (μS)	Dielectric constant	Vapour pressure (at 20 °C) (kPa)	Boiling point (°C)	Viscosity (mPa-s)
DCM	-	0.0 (at 22.4°C)	9.1	47.4 *	40 *	0.45
DCM/Pyridine	60/40	15.7 (-)	-	-	-	-
	50/50	13.1 (at 22.2°C)	-	-	-	0.65
Pyridine	-	4.4 (at 22.8°C)	12.5	2.0 *	115 *	0.95 *
DCM/Methanol	80/20	321 (-)	-	-	-	-
Methanol	-	2.05 (at 22.5°C)	32.6 *	12.3 *	64.6 *	0.55 *
$CHCl_3$	-	0.1 (21.1)	4.8	21.2	61.2	0.58
$CHCl_3$/Pyridine	60/40	-	-	-	-	-
$CHCl_3$/Methanol	80/20	-	-	-	-	-

* obtained from ref. [79-81]

4-2-2. Solvent-cast Film

As a reference for characterization, uniform thin films of each polymer were prepared from several polymer solutions (Table 4-3) by solvent-casting method. All of the polymer solutions were kept for overnight to dissolve the polymer completely. Approximately 5 to 10 mL of the solution was then cast into a glass petri dish with 14 cm diameter to obtain a thin layer of the solution. After solvent evaporation at 35 °C for 3 hours, a deposited thin polymer film on the petri dish was further dried for overnight under vacuum condition to remove the residual solvent.

Table 4-3. Polymer solutions used for solvent-casting.

Polymer	Unit ratio (wt%)	Molecular weigth (g/mol)	Polymer concentration (wt%)	Solvents
PLLA	–	100,000	4.5	DCM
	–	300,000	7.5	
PCL	–	80,000	10.0	$CHCl_3$
P(LLA-b-CL)	75/25	440,000	7.5	Acetone
P(LLA-r-CL)	70/30	150,000	12.5	$CHCl_3$

4-2-3. Annealing

Nanofibers with fixed weight of 1.0 mg were collected on coverslip with 15mm in diameter. The collected fiber sample was annealed at 90 ^{o}C for 10 hours in a heating oven. In the process, the heating oven was switched on after sample was deposited inside the oven and switched off once 10 hours passed. The door of oven was kept open to cool the temperature down after the oven was switched off.

4-2-4. X-ray Diffraction (XRD)

The molecular structure of electrospun nanofibers was investigated by XRD (Lab-X, XRD-6000, Shimazu) with Cu Kα source. A 2D wide-angle x-ray diffraction (WAXD) pattern was obtained by a Bruker x-ray diffractometer with nickel-filtered Cu Kα1 radiation. Electrospun nanofibers were collected on cover-slips with 13 mm in diameter, at fixed sample weight of 1 mg.

4-2-5. Differential Scanning Calorimetry (DSC)

The thermal behavior of electrospun fibers was characterized by DSC (Pyris 6, Perkin Elmer) in the temperature range from 20 to 200 ^{o}C for PLLA, - 80 to 80 ^{o}C for PCL and 0 to 200 ^{o}C for P(LLA-b-CL) and P(LLA-r-CL) at heating rate of 10 ^{o}C/min. All sample weight was held constant at 5 mg. ΔH_c (peak area at cold

crystallization temperature) and ΔH_m (peak area at melting temperature) were measured from the DSC results. ΔH was calculated using the following equation.

Eq. $\Delta H = \Delta H_m - \Delta H_c$

4-2-6. Tensile Test of Electrospun Nanofiber Membranes

Tensile test of electrospun nanofibrous membranes was conducted by Instron 5848 microtester with 30 mm/min stroke rate. A tensile specimen had the rectangular dimension (width: 10mm, length: 60 mm, thickness: around 0.03mm, gauge length: 40mm) and the loading was applied to the longitudinal direction of a specimen until its break. Tensile stress was calculated by the cross-sectional area of the tensile specimen (not the total area of the fibers). From stress-strain curves, tensile deformation manner of nanofibrous membranes was determined by three strain points, i.e., strains before (point A) and after (point B) an onset of nonlinearity in the curves and at the final fracture or maximum extension (point C). In each strain point, the deformation manner of a membrane was observed under scanning electron microscope (SEM; JSM-5800LV, JEOL) and fiber orientation angles against the loading direction (defined as 0^o) were measured using photos taken by optical microscope (BX51M, Olympus).

4-2-7. Tensile Test of Electrospun Single Nanofiber

A disc collector with gaps at its circumferential edge was used to collect an electrospun single nanofiber (Figure 4-1). The procedure for collecting single nanofibers is as follows. Firstly, a short time of electrospinning was conducted using the rotating disc collector (Figure 4-2(a)). As a result, a few fibers make a bridge between the gaps of the disc collector (Figure 4-2(b)). Those fibers were picked up onto the paper frame by passing the frame through the gap of the disc collector. The electrospun single nanofiber can be last (Figure 4-2(d)) by removing non-required nanofibers from the resultant nanofibers on the paper frame (Figure 4-2(c)). Nanofibers on the paper frame can be viewed by strong light reflection. An electrospun single nanofiber on the paper frame with a 20 mm gauge length was used as tensile specimen. Tensile test was performed by nano tensile testing system (Nano Bionix, MTS). The used load range is up to 500mN and resolution was 50nN level. Strain rate was 25 %/min.strain rate. The fracture feature of the broken fiber was observed under FE-SEM.

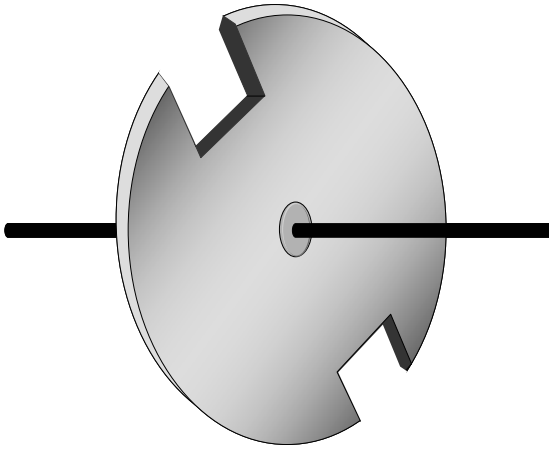

Figure4-1. Disc collector for single nanofibers.

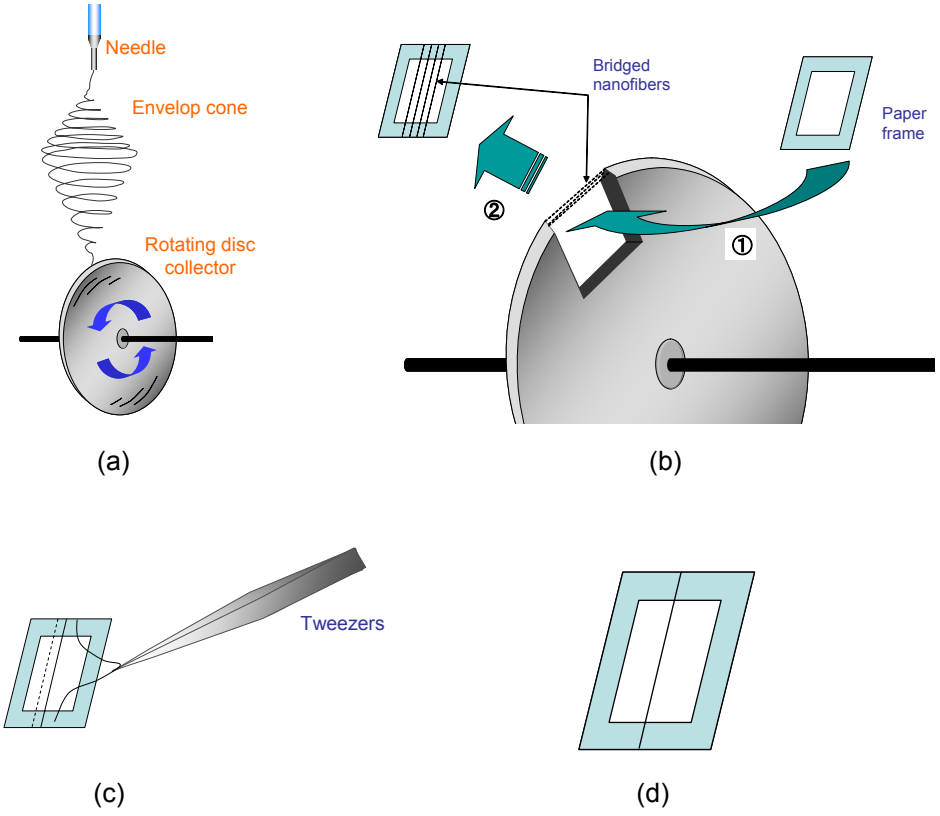

Figure 4-2. Procedures to prepare single nanofiber sample: (a) short time electrospinning, (b) pick aligned nanofibers onto a paper frame, (c) removing non-required nanofibers and (d) single nanofiber sample.

4-3. Results

4-3-1. Evaluation of Tensile Test Method using Nanofiber Membranes

In order to investigate structure-property relationship of electrospun fibers, characterization method was firstly consolidated with P(LLA-b-CL) samples. Solution and processing conditions for the electrospinning of P(LLA-b-CL) are shown in Table 4-4. As shown in Figure 4-3, deposited P(LLA-b-CL) electrospun nanofibers possessed uniform fiber morphology. Figure 4-4 (a) shows the XRD profiles of P(LLA-b-CL) in the forms of as-received pellet, cast film and electrospun nanofibers. For as-received copolymer pellet, a sharp peak and a low intensity peak were found at 17 ^{o} and 19 ^{o}, respectively. This profile is similar to XRD profile of PLLA homopolymer cast film [95]. Indistinct peak was also found at 22 ^{o}. For as-spun P(LLA-b-CL) nanofibers, a broad peak with high intensity was found at around 22 ^{o} which corresponds to the PCL crystal phase. However, sharp peak was absent around 17 ^{o} which should be seen for PLLA crystallization phase. Cast P(LLA-b-CL) film showed a sharp peak at 17 ^{o} and low intensity and broad peak at 22 ^{o}.

Table 4-4. Solution and processing conditions for electrospinning of P(LLA-b-CL).

solution conditions			spinning parameters				
polymer	solvent	polymer concentration (wt%)	applied voltage (kV)	distance (mm)	feed rate (ml/hr)	inside needle diameter (mm)	diameter (nm)
P(LLA-b-CL) (75/25wt%)	Acetone	5	18	150	1.0	0.21	962 ± 200

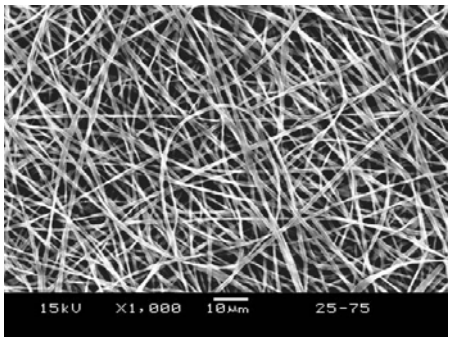

Figure 4-3. SEM images of electrospun P(LLA-b-CL) fibers.

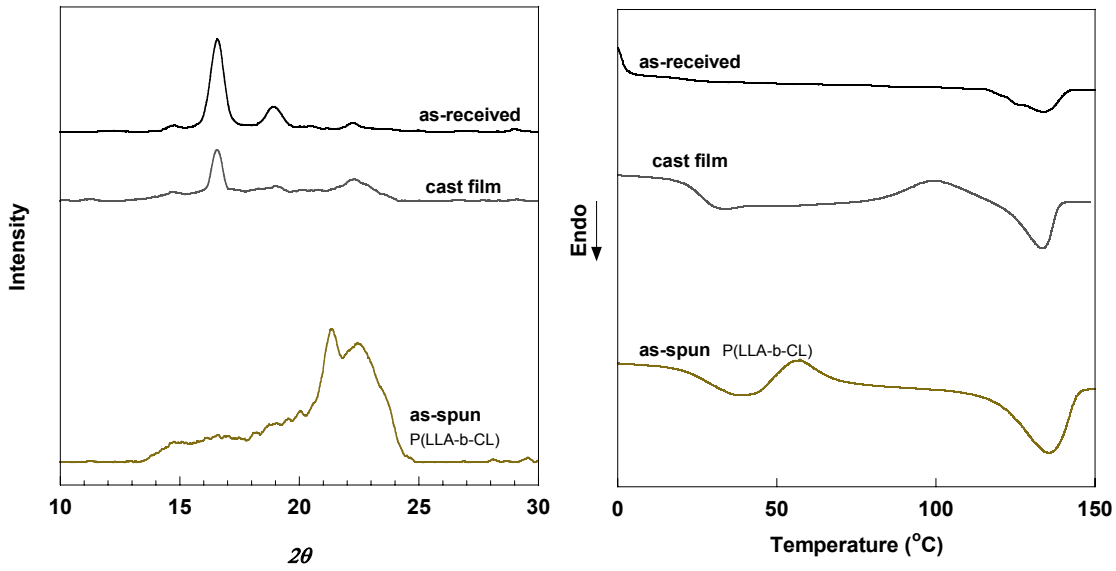

Figure 4-4. (a) XRD diagram and (b) DSC thermogram of electrospun P(LLA-b-CL) fibers.

As shown in DSC profiles (see in Figure 4-4 (b)), as-received copolymer showed the melting point at 133.5 ^{o}C which is same as the electrospun fibers and the cast film. With respect to exothermic peak, electrospun fibers exhibited it at 57.3 ^{o}C, which is recognized as the cold crystallization temperature. For the cast film, there was also an exothermic peak at 99.6 ^{o}C, whose intensity is higher than electrospun fibers.

However, as-received copolymer did not show the exothermic peak which suggests highly crystallized structure. It implies that the molecular chains in the electrospun fibers were not crystallized as as-received copolymer.

Figure 4-5 shows typical stress-strain curves of P(LLA-b-CL) membranes deformed under tensile loading. The membrane showed onset of nonlinearity around strain of 4.5 % in the initial stress – strain curve. The slope of the curve decreased after the nonlinear point. Tensile properties obtained from the stress – strain curves are listed in Table 4-5. Figure 4-6 shows the fiber orientation angle of nanofibrous membranes at three defined strain points. There is the trend that some fibers oriented to the loading direction before the nonlinear point (point A) and a much larger number of fibers aligned to the loading

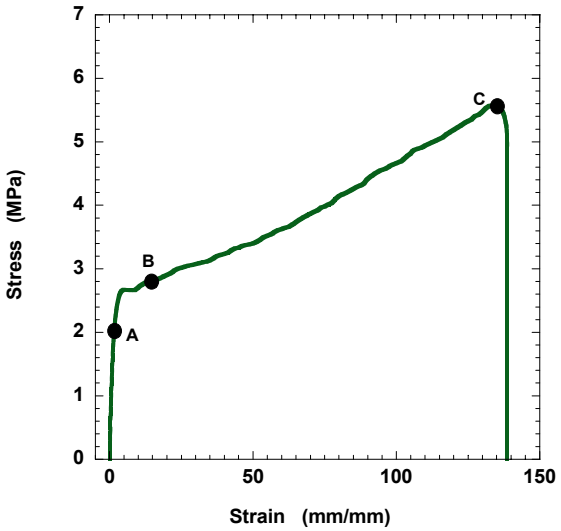

Figure 4-5. Typical stress-strain curves of electrospun P(LLA-b-CL) nanofiber membrane under tensile loading

Table 4-5. Tensile properties of electrospun P(LLA-b-CL) nanofiber membrane.

Polymer	Mw (g/mol)	Fiber diameter (nm)	Tensile modulus (MPa)	Tensile strength (Mpa)	Strain at break (%)
P(LLA-b-CL) (75/25wt%)	440,000	962 ± 200	156 ± 65	5.0 ± 1.0	127 ± 22

direction at point B. However, the slope of a stress – strain curve dropped at point B rather than point A. This is attributed to the damage of stretched fibers. SEM image of P(LLA-b-CL) membrane stretched up to point-C is shown in Figure 4-7. It is seen that most of fibers oriented along the loading direction and some number of broken fibers were observed. As P(LLA-b-CL) fibers possess a higher portion of - LLA unit sequence, the fiber deformation manner is reflected by rigid PLLA homopolymer characteristic. The fiber orientation observed at point-B and -C should be due to the fiber breakage.

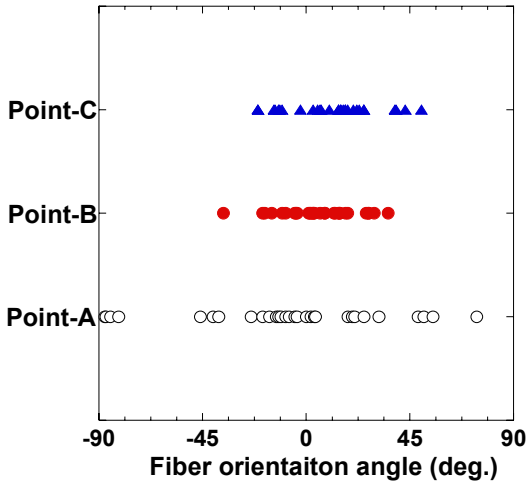

Figure 4-6. Fiber orientation angles in the P(LLA-b-CL) membranes during the tensile deformation.

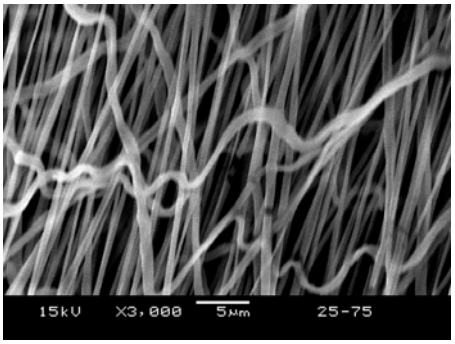

Figure 4-7. SEM micrograph of an electrospun P(LLA-b-CL) (75/25wt%) membrane during the tensile deformation (at point C).

To conclude this section, it is noted that the tensile method using fiber membranes is useful to discuss mechanical properties of the membranes, but not individual fibers. Because fiber orientation which strongly affects tensile properties of nanofibrous membranes changes during tensile test. It is also difficult to count the number of nanofibers in a membrane or measure the cross sectional area of nanofibrous membranes. The tensile test using single nanofiber should be more direct evaluation method to understand the structure-mechanical property relationship of electrospun nanofibers [96].

In the following sections, effects of processing parameters on molecular structure and tensile properties of electrospun PLLA nanofibers were investigated to find dominant parameters that control its molecular structure. To study structure – properties relationship of the fibers, tensile tests using electrospun PLLA single nanofibers were carried out.

4-3-2. As-spun PLLA Nanofibers

Polymer Concentration Effect

As shown in Table 4-6 and Figure 4-8, uniform PLLA nanofibers were electrospun from 7.5wt% and 12.5 wt% PLLA solutions. The smaller diameter of electrospun

Table 4-6. Solution and processing conditions applied to study polymer concentration effects on PLLA fibers.

solution conditions			spinning parameters				
polymer	solvents	polymer concentration (wt%)	applied voltage (kV)	distance (mm)	feed rate (ml/hr)	inside needle diameter (mm)	diameter (nm)
PLLA with Mw of 100,000	DCM/Pyridine (60/40wt%)	***7.5***	10	100	0.5	0.21	*634 ± 132*
	DCM/Pyridine (60/40wt%)	***12.5***					*811 ± 362*

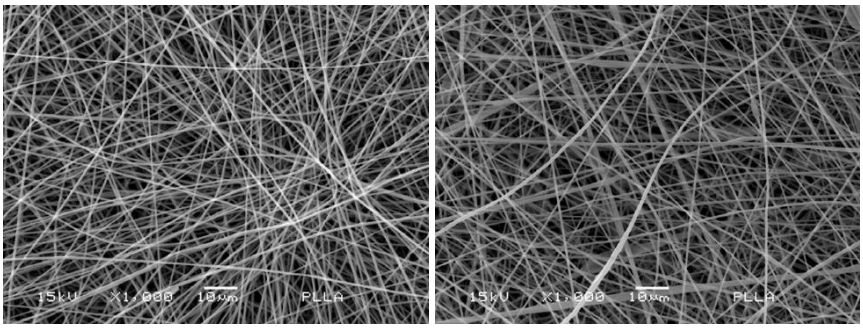

(a) (b)

Figure 4-8. SEM images of PLLA fibers electrospun from solutions with different polymer concentration of: (a) 7.5 wt% and (b) 12.5 wt%.

PLLA nanofibers was found at lower polymer concentration. The decreased fiber diameter is due to the less polymer amount per volume of spinning jets (see in Chap. 3). As shown in XRD results (see in Figure 4-9(a)), as-received PLLA pellet and cast PLLA film possessed two main diffraction peaks corresponding to PLLA crystalline phase [95], while those peaks were absent in electrospun PLLA nanofibers. The absence of clear diffraction peaks implies that extensive crystallization did not occur for PLLA nanofibers. Annealing was applied to the electrospun PLLA nanofibers to further discuss the difference in molecular structure of the nanofibers from 7.5 and 12.5 wt% solutions. Annealing process induces molecular structure development of

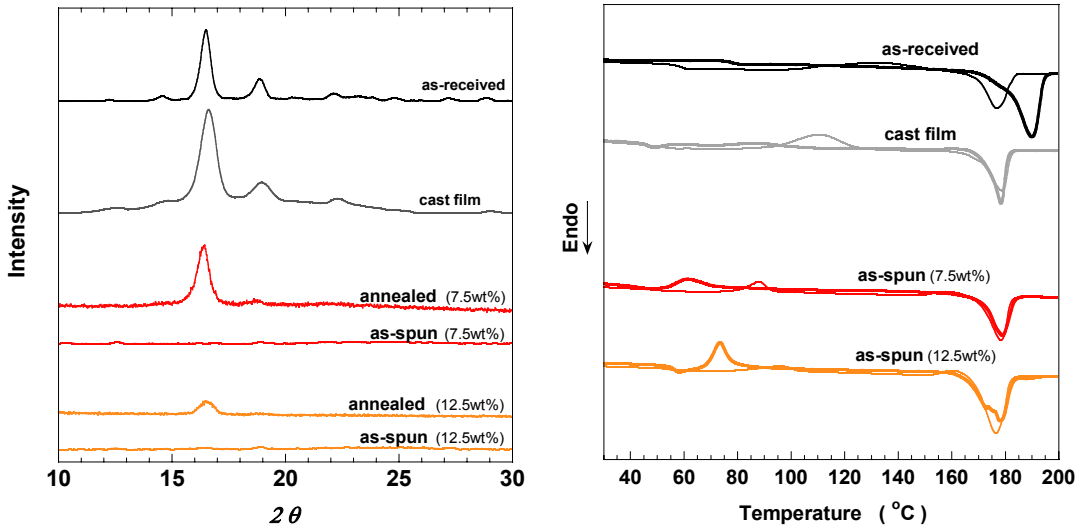

Figure 4-9. Polymer concentration effects: (a) XRD diagram and (b) DSC thermogram of PLLA fibers electrospun from 7.5 wt% and 12.5 wt% solutions.

Table 4-7. The corresponding thermal properties of PLLA fibers as a function of polymer concentration.

samples	*Tc* (°C)	*ΔHc (J/g)*	*Tm* (°C)	*ΔHm (J/g)*	*ΔH (J/g)*
as-received			188	65	65
cast film	85	4	177	49	45
as-spun (7.5wt%)	58	13	176	60	47
as-spun (12.5wt%)	72	21	178	71	50

the polymer. It is noted that the peak intensity of as-spun nanofibers followed by annealing (annealed fibers) were higher than that from as-spun fibers, and the peak intensity increased with the decreased polymer concentration.

Figure 4-9 (b) shows DSC profiles of electrospun PLLA nanofibers. The solid curve and the dashed curve correspond to the thermal properties of electrospun fibers at the first and second run, respectively. For the first run, it was found that PLLA

nanofibers with 7.5wt% polymer concentration indicated the lower cold crystallization temperature (T_c) and crystallization exothermic peak, as shown in Table 4-7. The cold crystallization with decreased T_c can be explained by the decrease of conformation entropy of the chain. The preferential molecular orientation for crystallization decreases the conformation entropy. This implies that ordered structure exists in electrospun fibers at lower polymer concentration.

For the second run, the T_c peak was shifted to the higher temperature as compared to the first run because ordered structure presented in the first run disappeared at the second run. It is noteworthy that electrospun PLLA nanofibers showed the heat of fusion (ΔH=47 for 7.5wt% and ΔH=50 J/g for 12.5wt%) although those samples did not show diffraction XRD peaks. Hence, crystalline structure (i.e., crystallite) formed in electrospun PLLA nanofibers might be too small to detect by XRD.

As summary, electrospun PLLA nanofibers possess the ordered structure at lower polymer concentration. Electrospinning jets with lower polymer concentration results in slower solidification process so that the jet might be kept at semi-solid state for a long time. As presented in chap3, the jet shrink its size via the drawing and solvent evaporation. Compared to the solid jet, the semi-solid jet has a higher

chance to be deformed via the electrical drawing. Therefore, the electrical drawing might facilitate internal structure development of electrospun fibers.

Effects of Solvent Properties

PLLA was dissolved into the solvent mixtures of DCM/Pyridine and DCM/Methanol (Table 4-8). As shown in Figure 4-10, uniform electrospun PLLA fibers were observed in both two different solvent mixtures. The smaller fiber diameter was obtained from DCM/Pyridine-based solution rather than DCM/Methanol-based solution. This is due to the highly drawn spinning jet (in Chap. 3). It was reported

Table 4-8. Solution and processing conditions applied to study effects of solvents properties on PLLA fibers.

solution conditions / properties				spinning parameters				
polymer	solvents	solvents conductivity (μS)	polymer concentration (wt%)	applied voltage (kV)	distance (mm)	feed rate (ml/hr)	inside needle diameter (mm)	diameter (nm)
PLLA with Mw of 100,000	DCM/***Pyridine*** * (60/***40wt%***)	15.7	7.5	10	100	0.5	0.21	*634 ± 132*
	DCM/***Methanol*** * (80/***20wt%***)	321.0						*2075 ± 444*

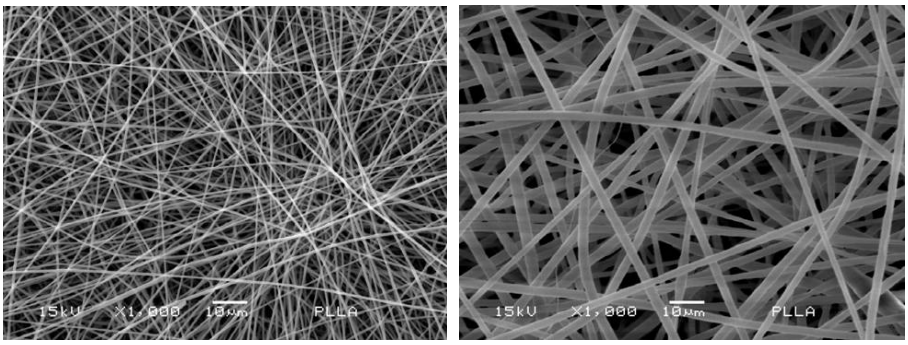

(a) (b)

Figure 4-10. SEM images of PLLA fibers electrospun from solutions consisting of: (a) DCM/Pyridine(60/40wt%) and (b) DCM/Methanol (80/20wt%).

that electrical conductivity of pyridine is higher than that of methanol and higher conductivity reduces diameter of electrospun fibers. Although DCM/Methanol mixture has higher electrical conductivity than DCM/Pyridine mixture (321 μS for DCM/Methanol and 15.7 μS for DCM/Pyridine), it has lower boiling point (65 ^{o}C) and higher vapor pressure (12.3), which might encourage the faster solidification of spinning jet during electrospinning. Nanofibers can be easily deformed in semi-solid condition rather than in solid condition. If solution jet slowly solidifies, a solution jet would be able to keep in semi-solid condition for a longer time. Hence, a slower solidification due to higher boiling point and low vapor pressure increases time to draw a spinning jet during electrospinning. Thus, the high volatile nature of methanol might diminish drawing of the solution jet.

As shown in the XRD diagram (Figure 4-11 (a)), as-received PLLA pellets and cast PLLA film exhibited two main diffraction peaks at 17^{o} and 19^{o}, while the corresponding peaks were absent in both types of electrospun fibers. It is noteworthy that annealed fibers showed the peak at 17^{o} and higher peak intensity was found in nanofibers electrospun from DCM/Pyridine-based solution.

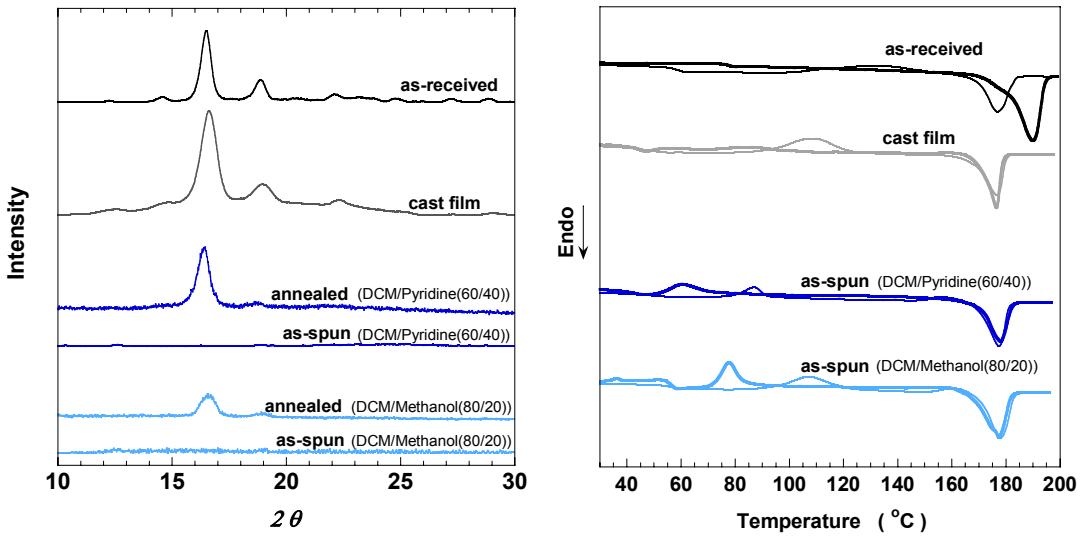

Figure 4-11. Effects of solvents properties: (a) XRD diagram and (b) DSC thermogram of PLLA fibers electrospun from 7.5 wt% solutions with DCM/Pyridine(60/40 wt%) and DCM/Methanol(80/20 wt%).

Table 4-9. The corresponding thermal properties of PLLA fibers as a function of solvents properties.

samples	*Tc* (°C)	*⊿Hc (J/g)*	*Tm* (°C)	*⊿Hm (J/g)*	*⊿H (J/g)*
as-received			188	65	65
cast film	85	4	177	49	45
as-supn (DCM/Pyridine(60/40wt%))	58	13	176	60	47
as-spun (DCM/Methanol(80/20wt%))	77	27	177	73	46

The DSC thermogram (Figure 4-11 (b)) shows that T_c was associated with type of solvents. In the first run, T_c peak position at a lower temperature and the smaller crystallization exothermic peak was found in the fibers spun from DCM/Pyridine-based solution (Table 4-9). In the second run, the T_c peak positions for electrospun fibers was found at higher temperature compared to the first run, this is consistent with the findings from as-spun fibers from solutions with different polymer concentration. ΔH is almost equivalent between electrospun PLLA fibers

spun from DCM/Pyridine-based and DCM/Methanol-based solutions (Table 4-9). According to structure analyses, it is concluded that molecular structure as well as fiber morphology is highly dependent on solvent properties.

Solution Temperature Effect

Solution temperature effects on molecular structure were investigated using electrospun fibers from solutions at room temperature, 40^{o} and 70^{o} (Table 4-10). SEM image (Figure 4-12) shows that beaded fibers were electrospun from solution heated up to 70 ^{o}C. The beads formation is due to the insufficient surface tension (see in Chap. 3).

Table 4-10. Solution and processing conditions applied to study solution temperature effects on PLLA fibers.

solution conditions				spinning parameters				
polymer	solvents	polymer concentration (wt%)	solution temperature (^{o}C)	applied voltage (kV)	distance (mm)	feed rate (ml/hr)	inside needle diameter (mm)	diameter (nm)
PLLA with Mw of 100,000	DCM/Pyridine (60/40wt%)	7.5	***room temp***	10	100	0.5	0.21	*295±133*
			40					*471±103*
			70					*318 ± 78*

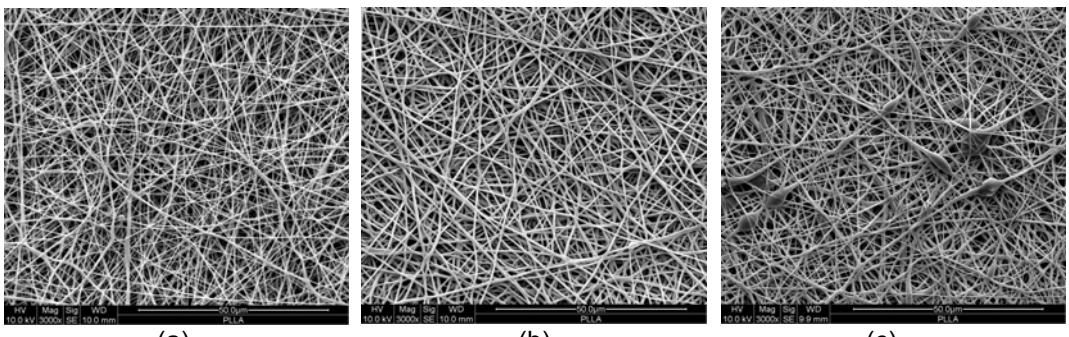

(a) (b) (c)

Figure 4-12. SEM images of PLLA fibers electrospun from solutions at: (a) room temperature, and (b) 40^{o}C and (c) 70^{o}C.

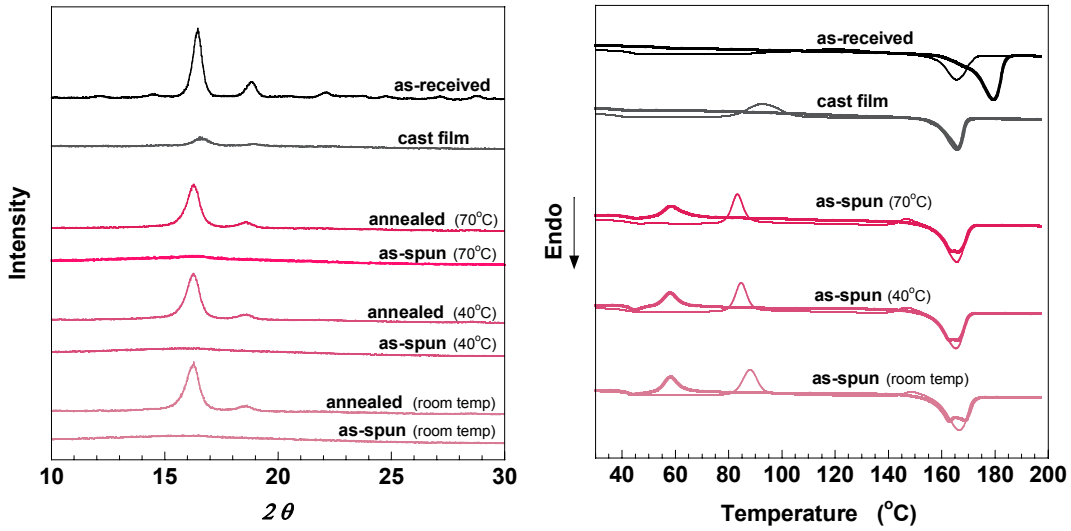

Figure 4-13. Solution temperature effects: (a) XRD diagram and (b) DSC thermogram of PLLA fibers electrospun from solutions at room temperature, and 40°C and 70°C.

Table 4-11. The corresponding thermal properties of PLLA fibers as a function of solution temperature.

samples	*Tc* (°C)	*ΔHc (J/g)*	*Tm* (°C)	*ΔHm (J/g)*	*ΔH (J/g)*
as-received			188	65	65
cast			166	54	54
as-supn (70°C)	58	13	166	67	54
as-spun (40°C)	58	23	165	70	47
as-spun (room temp.)	58	20	167	73	53

As the results of XRD analysis (Figure 4-13 (a)), no diffraction peaks were observed from as-spun fibers even when the solution temperature changed. From annealed fibers, almost similar intensity of the peaks was observed. Figure 4-13 (b) shows the DSC profile of the electrospun PLLA fibers. Table 4-11 summarizes the corresponding thermal properties. Thermal analysis revealed that cold crystallization of all the electrospun fibers occurred at the same temperature of 58 °C. As described

in chap 2, temperature is one of the important parameters which strongly affect crystallization kinetics of polymers. However, the experimental results suggest that changing the solution temperature is not a major factor to develop crystalline structure of electrospun polymer fibers. In this study, fibers were electrospun at room temperature. There might be a significant drop in the solution temperature when the polymer solution was ejected from the tip of a spinneret since the spinning jet diameter is very small. The decreased temperature might diminish structure development of the electrospun fibers.

Take-up Velocity Effects

Take-up velocity effects on molecular structure were studied using PLLA fibers with different rotation speeds of a disc collector (see in Table 4-12). As shown in SEM images (Figure 4-14), aligned fibers were observed at take-up velocity of 630 m/min and above. In the speed range between 630 to 1,890 m/min, increased take-up velocity reduced the fiber diameter from 780 nm into 417 nm. It was found that the smaller diameter is due to highly drawn spinning jet at higher take-up velocity (see in Chap. 3). The XRD diagram in Figure 4-15 (a) shows that PLLA nanofibers collected higher than 630 m/min rotation speed exhibited a broad and small diffraction peak at 16^{o}, while nanofibers collected at 63 m/min speed exhibited no

peak. The intensity of the peaks was almost independent of the take-up velocity. For DSC analysis shown in Figure 4-15(b) and Table 4-13, it was shown that increased take-up velocity resulted in the lower temperature shifting of a T_c peak and a decrease in the crystallization exothermic peak. ΔH value of electrospun nanofibers slightly increased with increasing take-up velocity but saturated after 1,260m/min.

Table 4-12. Solution and processing conditions applied to study take-up velocity effects on PLLA fibers.

solution conditions			spinning parameters					
polymer	solvents	polymer concentration (wt%)	applied voltage (kV)	disc rotation speed (m/min)	distance (mm)	feed rate (ml/hr)	inside needle diameter (mm)	diameter (nm)
PLLA with Mw of 300,000	DCM/Pyridine (50/50wt%)	4.5	15	***63***	150	0.5	0.21	*686 ± 111*
				630				*780 ± 112*
				1260				*619 ± 119*
				1890				*417 ± 138*

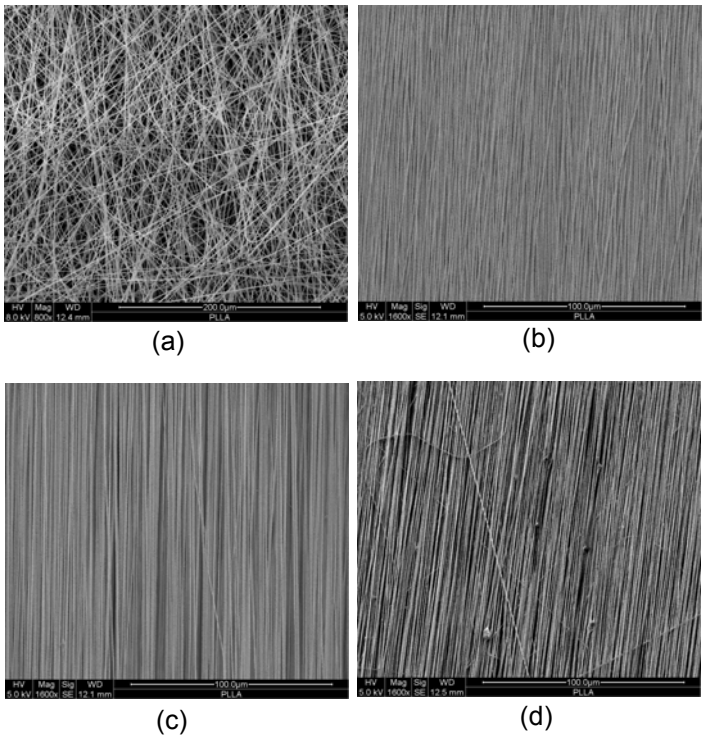

Figure 4-14. SEM images of PLLA fibers electrospun at different take-up velocity of: (a) 63 m/min, (b) 630 m/min, (c) 1,260 m/min and (d) 1,890 m/min.

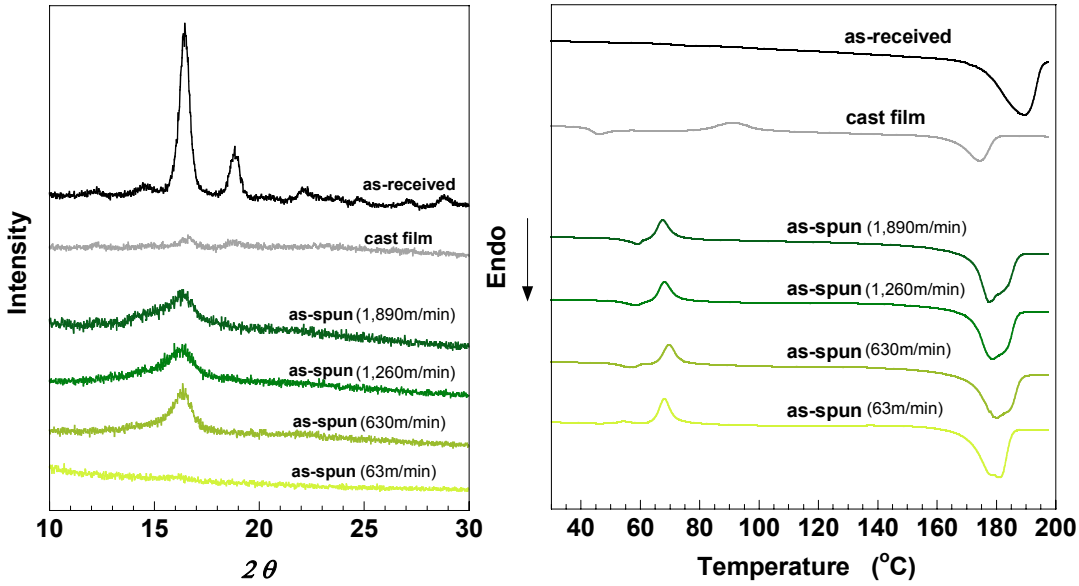

Figure 4-15. Take-up velocity effects: (a) XRD diagram and (b) DSC thermogram of PLLA fibers electrospun at 63 m/min, 630 m/min, 1,260 m/min and 1,890 m/min.

Table 4-13. The corresponding thermal properties of PLLA fibers as a function of take-up velocity.

samples	*Tc* (°C)	*ΔHc (J/g)*	*Tm* (°C)	*ΔHm (J/g)*	*ΔH (J/g)*
as-received			190	84	84
cast film	91	10	175	28	17
as-spun (1890m/min)	67	7	177	72	65
as-spun (1260m/min)	68	9	178	74	65
as-spun (630m/min)	70	12	179	74	62
as-spun (63m/min)	68	16	177	69	53

These XRD and DSC results suggest that the take-up velocity higher than 1,260m/min did not contribute to further develop molecular structure of PLLA nanofibers. However, up to 1,260m/min rotation speed, take-up velocity contributed to form the crystalline structure indeed. The above finding is consistent with the experimental result on electrospun polyacrylonitrile (PAN) fibers [97]. The

crystalline structure found in electrospun PLLA fibers was further studied using WAXD. As shown in WAXD patterns (see in Figure 4-16), crystalline orientation of electrospun PLLA nanofibers was enhanced by the faster take-up velocity. This experimental result is similar to the finding on PLLA micronfibers melt-spun at different take-up velocities [91]. The diffraction pattern obtained from the electrospun nanofibers is due to the existence of α-phase crystal as reported by Hoogsten et al.[98].

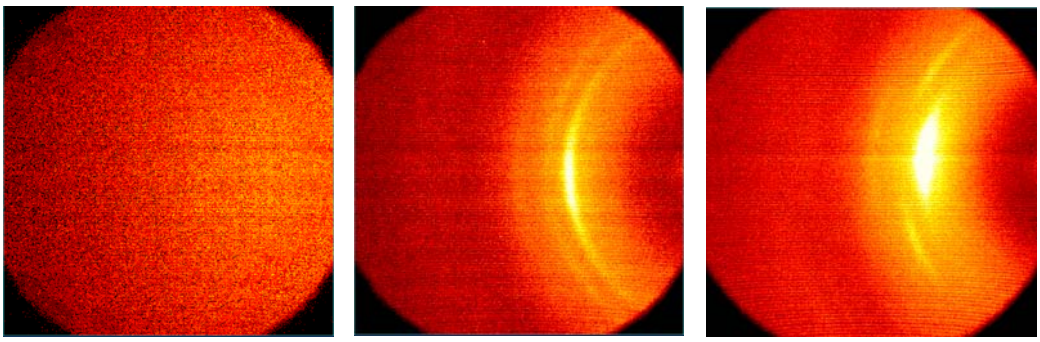

(a) (b) (c)

Figure 4-16. WAXD pattern of PLLA fibers electrospun at: (a) 63 m/min, (b) 630 m/min and (c) 1,890 m/min.

Here, the concern is whether the crystalline structure in electrospun PLLA nanofibers reflects to their mechanical response. Typical tensile stress–strain curves of a PLLA single nanofiber are shown in Figure 4-17 and the detailed values of tensile properties are summarized in Table 4-14. It was found that tensile modulus and strength dramatically increased at higher take-up velocity. Figure 4-18 shows

SEM micrographs of fractured single nanofibers after the tensile test. The single nanofiber electrospun at 63 m/min showed a spearhead-like fracture feature at the break point, which is attributed to large deformation under tensile loading. However, the single nanofiber electrospun at 630m/min did not show the ductile fracture manner. The difference of such fracture manner should be attributed to the

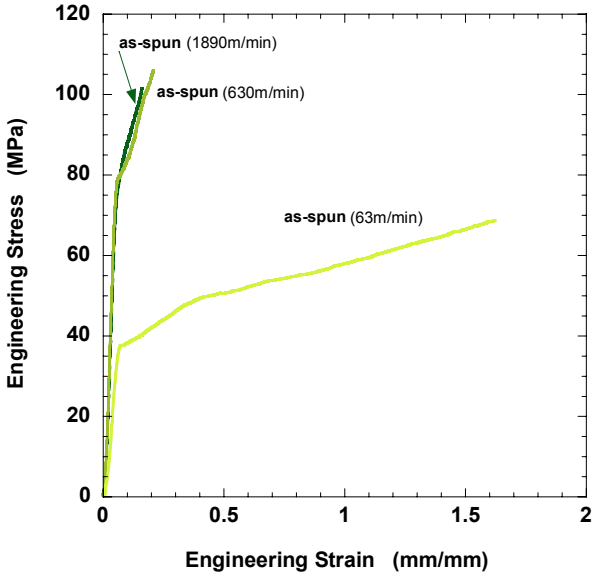

Figure 4-17. Tensile stress-stain curves of PLLA single nanofibers electrospun at take-up velocity of 63, 630 and 1,890 m/min.

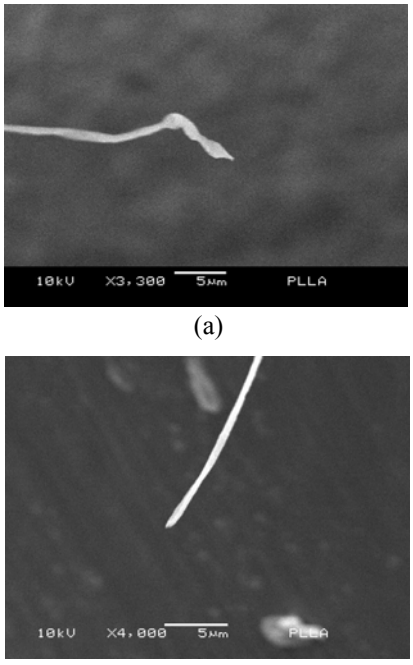

(a)

(b)

Figure 4-18. SEM micrographs of fractured PLLA single nanofibers after tensile tests: (a) 63 m/min and (b) 630 m/min.

Table 4-14. Tensile properties of electrospun PLLA single nanofibers.

Samples	Mw (g/mol)	Take-up velocity (m/min)	Fiber diameter (nm)	Tensile modulus (GPa)	Tensile strength (MPa)	Strain at break
Electrospun fibers	300,000	63	890 ± 190	1.0 ± 1.6	89 ± 40	1.54 ± 0.12
		630	506 ± 81	2.2 ± 0.3	94 ± 33	0.22 ± 0.04
		1890	775 ± 145	1.8 ± 0.5	104 ± 50	0.15 ± 0.05
Melt-spun fibers [16]	212,450	600	34,000	3.9	192	2.2

molecular structure developed in each nanofiber sample. XRD and DSC results revealed that PLLA nanofibers possessed the crystalline structure. Hence, brittle tensile fracture behavior was seen for the nanofibers collected at faster take-up velocity. According to XRD analysis, it was also found that crystalline structures were oriented along fiber axis. This finding suggests that molecules around crystals are also oriented along fiber axis. Those molecular orientation as well as crystalline structure could contribute higher tensile modulus and strength of fibers spun at higher take-up velocity. On the other hand, there is not a significant difference in tensile properties between the PLLA fibers electrospun at 630 and 1,890 m/min. This phenomenon well corresponds to the result of structure analysis.

Tensile properties of the electrospun PLLA nanofibers were compared with that of melt-spun PLLA micronfibers. Tensile properties shown by these electrospun fibers were lower than that of fibers melt-spun at 600 m/min [99]. In electrospinning process, nanofibers are spun via fast solidification process which might suppress structure development of electrospun nanofibers. The low tensile properties of the electrospun PLLA nanofibers should be due to the suppressed structure development.

To conclude this section, it was found that molecular structure of electrospun fibers was dependent on electrospinning parameters. To change molecular structure in amorphous region, solvents properties and polymer concentration played important roles. On the other hand, take-up velocity is the important parameter to develop crystalline structure oriented in the electrospun PLLA fibers. As found from tensile tests using single nanofibers, the crystalline structure induced high tensile modulus, strength but low strain at break. However, it is noted that the take-up velocity effects on structure development of the electrospun PLLA nanofibers were diminished when take-up velocity is higher than 630 m/min. This finding suggests that it may be difficult to form further molecular structure of electrospun PLLA nanofibers by changing only processing-related parameters.

4-3-3. As-spun PCL Nanofibers

In this section, effects of representative parameters to which affected the order of amorphous structure and the formation of crystalline structure of electrospun PLLA fibers were investigated using different kind of polymer, PCL with T_g of – 60 ^{o}C. T_g of polymers is strongly associated with structural formation so that electrospun PCL fibers may show different structure development from electrospun PLLA fibers. As the representative parameters, solvents properties and take-up velocity in the range

from 63 to 630 m/min were selected.

Effect of Solvent Properties

In this section, electrospun PCL nanofibers were prepared by the solvents of $CHCl_3$/Pyridine (60/40 wt%) and $CHCl_3$/Methanol (80/20 wt%) (see in Table 4-15). As shown in SEM image (Figure 4-19), uniform fibers were electrospun from $CHCl_3$/Methanol-based solution, whereas beaded fibers were electrospun from $CHCl_3$/Pyridine-based solution. The solubility of PCL in pyridine was poor and which might leads to concentration fluctuations, namely the formation of beaded fibers.

Table 4-15. Solution and processing conditions applied to study effects of solvents properties on PCL fibers.

solution conditions / properties				spinning parameters				
polymer	solvents	solvents conductivity (μS)	polymer concentration (wt%)	applied voltage (kV)	distance (mm)	feed rate (ml/hr)	inside needle diameter (mm)	diameter (nm)
PCL with Mn of 80,000	$CHCl_3$/***Pyridine*** (60/***40wt%***)	0.7	10	15	100	0.5	0.21	*315 ± 263 (straight portions)* *1982 ± 629* *(beads/thick portions)*
	$CHCl_3$/***Methanol*** (80/***20wt%***)	1.4						*730 ± 325*

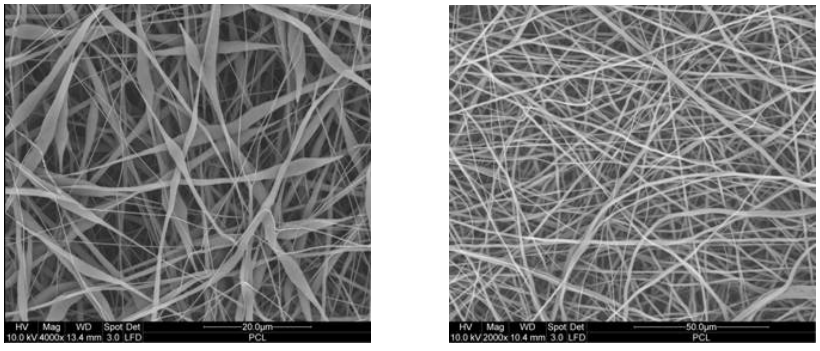

(a) (b)

Figure 4-19. SEM images of PCL fibers electrospun from solutions consisting of: (a) $CHCl_3$/Pyridine(60/40wt%) and (b) $CHCl_3$/Methanol(80/20wt%).

As shown in XRD diagram (Figure 4-20 (a)), PCL nanofibers electrospun from both types of solvent exhibited the two main diffraction peaks corresponding to that of PCL crystal phase [95]. The peak intensities were almost the same in both as-spun PCL fibers from $CHCl_3$/Pyridine-based and $CHCl_3$/Methanol-based solutions.

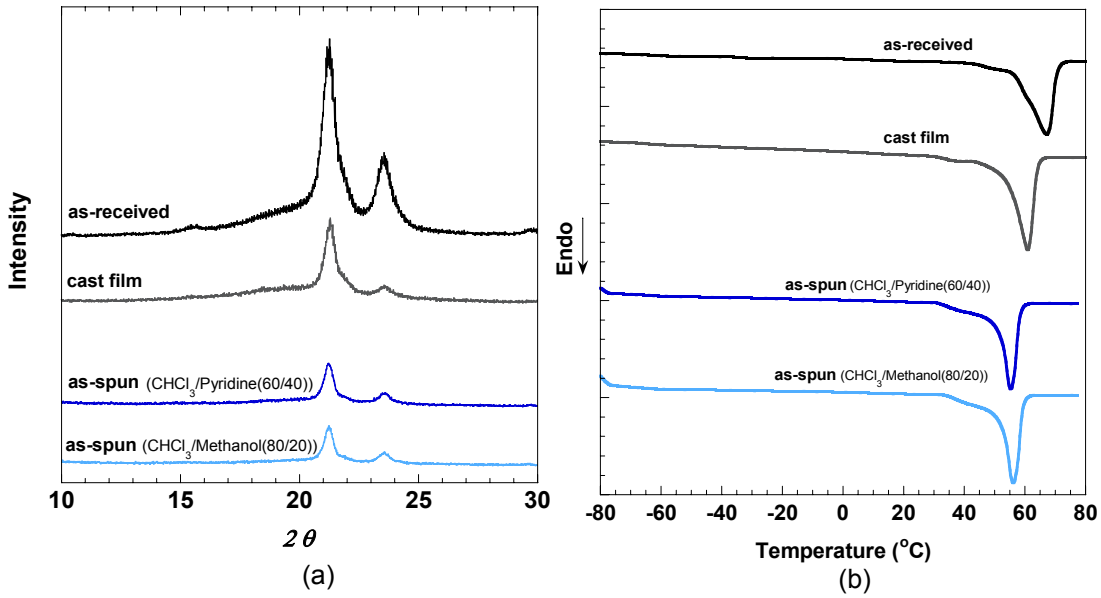

Figure 4-20. Effects of solvents properties: (a) XRD diagram and (b) DSC thermogram of PCL fibers electrospun from 10 wt% solutions in $CHCl_3$/Pyridine(60/40 wt%) and $CHCl_3$/Methanol(80/20 wt%).

Table 4-16. The corresponding thermal properties of PCL fibers as a function of solvents properties.

samples	ΔHc (J/g)	Tm (°C)	ΔHm (J/g)	ΔH (J/g)
as-received	-	68	90	90
cast film	-	61	82	82
as-spun (CF/Pyridine (60/40wt%))	-	56	71	71
as-spun (CF/Methanol (80/20wt%))	-	56	76	76

Figure 4-20 (b) shows the DSC profiles of the PCL nanofibers. T_c peaks were not observed from both PCL fibers electrospun from $CHCl_3$/Pyridine-based and

$CHCl_3$/Methanol-based solutions. There is no significant difference in ΔH of as-spun PCL fibers from $CHCl_3$/Pyridine-based and $CHCl_3$/Methanol-based solutions (Table 4-16). Crystalline structure that might be crystal lamellae developed in the electrospun PCL fibers. The structure development was independent of solvents properties. These results are inconsistent with that shown in the electrospun PLLA fibers.

Take-up Velocity Effects

PCL fibers were prepared at different take-up velocity of 63 and 630 m/min (Table 4-17). As shown in SEM images (Figure 4-21), uniform PCL fibers were electrospun at both take-up velocity. The fiber diameter was not changed even when the take-up velocity was increased. This finding suggests that the as-spun nanofibers might not be drawn enough during electrospinning even at the faster take-up velocity.

Table 4-17. Solution and processing conditions applied to study take-up velocity effects on PCL fibers.

solution conditions			spinning parameters					
polymer	solvents	polymer concentration (wt%)	applied voltage (kV)	take-up velocity (m/min)	distance (mm)	feed rate (ml/hr)	inside needle diameter (mm)	diameter (nm)
PCL with Mn of 80,000	DCM/Pyridine (50/50 wt%)	12	15	***63***	150	0.5	0.21	361 ± 232
				630				346 ± 206

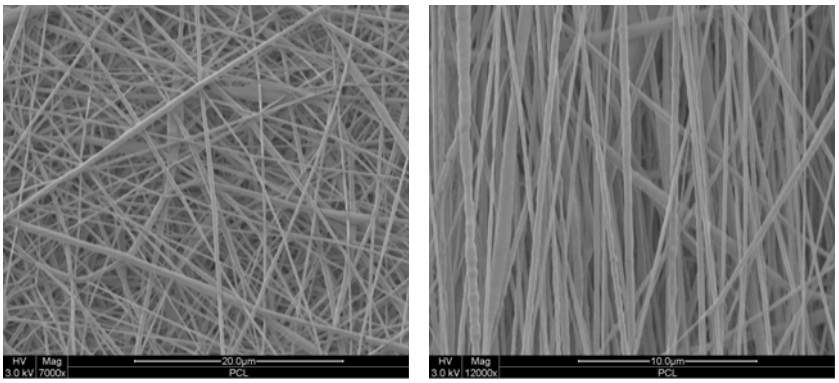

(a) (b)

Figure 4-21. SEM images of PCL fibers electrospun at: (a) 63 m/min and (b) 630 m/min.

As the results of XRD diagram in Figure 4-22 (a), both PCL fibers electrospun at 63 and 630 m/min in take-up velocity exhibited the two diffraction peaks corresponding to crystal phase. The peaks intensity of the as-spun PCL fibers was independent of the take-up velocities. Figure 4-22 (b), and Table 4-18 shows DSC results of PCL fibers. T_c peaks were not observed from the electrospun fibers. ΔH of the PCL nanofibers was independent of the take-up velocities.

According to the structure analyses of electrospun PCL fibers, it is concluded that crystalline structure that might be crystal lamellae was formed in electrospun PCL fibers, however, the structure development was not a function of parameters like solvents properties and take-up velocity in the range from 63 to 630 m/min. These findings are inconsistent with that shown by the electrospun PLLA fibers.

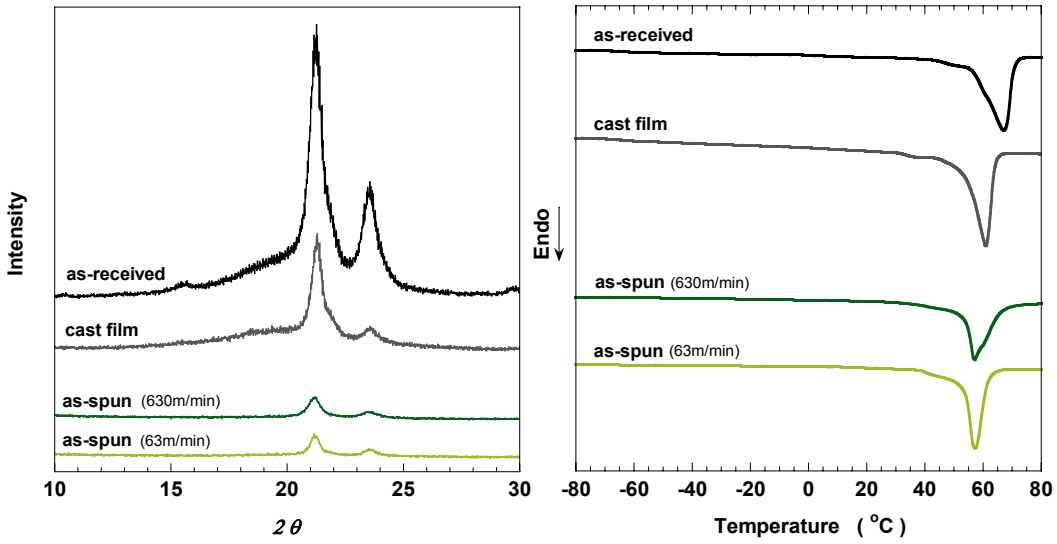

(a) (b)

Figure 4-22. Take-up velocity effects: (a) XRD diagram and (b) DSC thermogram of PCL fibers electrospun at 63 and 630 m/min.

Table 4-18. The corresponding thermal properties of PCL fibers as a function of take-up velocity.

samples	*⊿Hc (J/g)*	*Tm* (°C)	*⊿Hm (J/g)*	*⊿H (J/g)*
as-received	-	68	90	90
cast film	-	61	82	82
as-spun (630m/min)	-	57	62	62
as-spun (63m/min)	-	57	59	59

4-3-4. As-spun P(LLA-r-CL) Copolymer Nanofibers

Structure analyses shown in the previous section revealed a difference in structure development between PLLA and PCL nanofibers. This finding leads to the question that if each sequence of - LLA and – CL units are randomly combined, how the combined polymer develops its structure in electrospinning. To discuss the issue, the structure analysis was conducted using random copolymer of P(LLA-r-CL) with 70 % of - LLA units sequences. To discuss the structure development of the random

copolymer, the take-up velocity was selected as representative processing parameter to study.

Take-up Velocity Effects

Samples were prepared by electrospinning at different take-up velocities of 63 and 630 m/min (Table 4-19). As shown in SEM images (Figure 4-23), randomly oriented manner are changed into aligned manner at higher take-up velocity. Increased take-up velocity led to decrease the fiber diameter. This is due to a highly drawn spinning jet at higher take-up velocity (see in Chap. 3). As shown in XRD diagram in Figure 4-24, as-spun fibers at 630 m/min showed a small and wide diffraction peak at 17^{o}, while diffraction peaks were not observed in as-spun fibers at 63 m/min. These results suggest that crystalline structure attributed to PLLA crystal developed in electrospun P(LLA-r-CL) fibers at higher take-up velocity. This trend is similar to the electrospun PLLA fibers, but inconsistent with the PCL and P(LLA-b-CL) nanofibers which exhibited the diffraction peaks corresponding to PCL crystalline phase even when the fibers were spun at take-up velocities of 0 and 63 m/min.

Table 4-19. Solution and processing conditions for electrospinning of P(LLA-r-CL) at different take-up velocity.

solution conditions			spinning parameters					
polymer	solvents	polymer concentration (wt%)	applied voltage (kV)	take-up velocity (m/min)	distance (mm)	feed rate (ml/hr)	inside needle diameter (mm)	diameter (nm)
P(LLA-r-CL) (70/30wt%)	$CHCl_3$/Pyridine (60/40wt%)	12.5	15	***63***	150	0.5	0.21	1783 ± 388
				630				694 ± 313

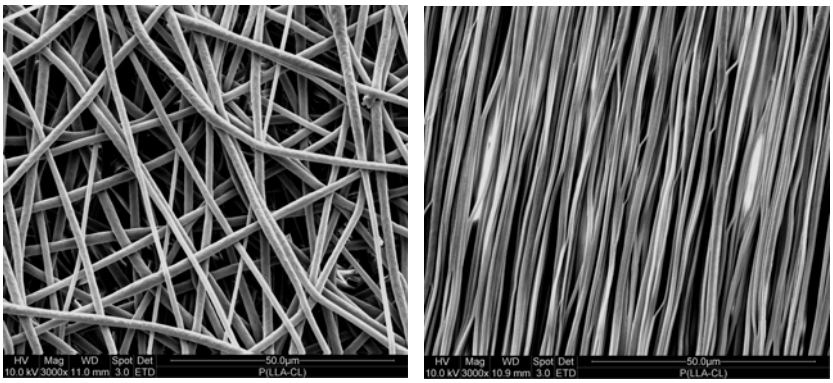

(a) (b)

Figure 4-23. SEM images of P(LLA-r-CL) fibers electrospun at: (a) 63 m/min and (b) 630 m/min.

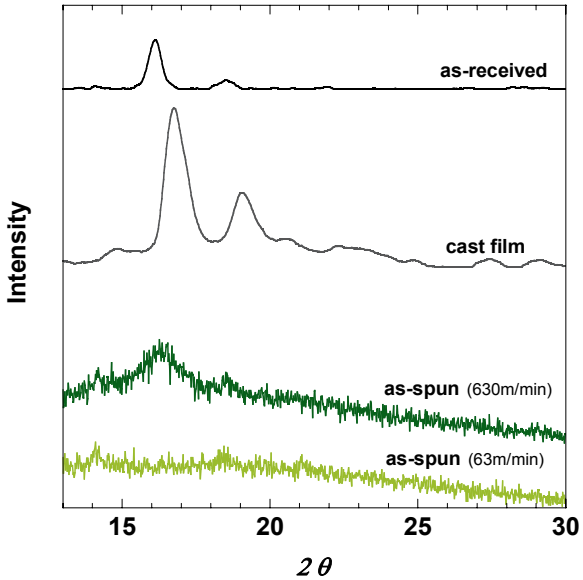

Figure 4-24. XRD diagram of electrospun P(LLA-r-CL) fibers at 63 and 630 m/min.

4-4. Discussion

According to structure analysis of electrospun fibers, different structure formation was shown among rigid (PLLA), ductile (PCL), semi-ductile (P(LLA-b-CL) and P(LLA-r-CL)) polymers. The results of structure analyses were summarized in Table 4-20. The molecular structure formed in electrospun fibers appeared to be a result of the jet drawing. The drawing might be conducted electrically or mechanically as presented in Chap 3. Polymer concentration and solvent properties contribute to the electrical drawing and the take-up velocity is associated with the mechanical drawing. For rigid polymer like PLLA, the electrical drawing has an important role in enhancing the order structure in amorphous region. The mechanical drawing highly contributes to the development of crystalline structure. On the other hand, crystal formation of ductile polymer like PCL seems to be a result of the electrical drawing, although its crystallinity was not a function of the electrical and mechanical drawing.

To analyze the difference between rigid and ductile polymer nanofibers, the structural formation by the electrical drawing was discussed from the viewpoint of crystallization rate and molecular mobility. As shown in Table 4-21, crystallization time of PCL is shorter than that of PLLA [100,101]. T_g of PCL is lower than room or

Table 4-20. Summary of structure analysis of electrospun nanofibers.

Electrospinning-related parameters	Drawing process	Rigid polymer (PLLA)	Ductile polymer (PCL)	Semi-ductile polymer P(LLA-r-CL)
Polymer concentration	Electrical drawing	*7.5wt%* / *12.5wt%* (SEM) Fiber diameter: 634 ± 132nm / 811 ± 362nm (XRD) Crystallization peaks as-spun: NON / NON annealed: @ 17° > @ 17° (DSC) *Δ Hc (Tc)*: 13J/g (58°C) < 21J/g (72°C) *Δ H*: 47J/g / 50J/g ***Ordered structure in amorphous region @ LOW polymer concentration***		
Solvent properties	Electrical drawing	*DCM/Pyridine (60/40wt%)* / *DCM/Methanol (80/20wt%)* (SEM) Fiber diameter: 634 ± 132nm / 2075 ± 444nm (XRD) Crystallization peaks as-spun: NON / NON annealed: @ 17° > @ 17° (DSC) *Δ Hc (Tc)*: 13J/g (58°C) < 27J/g (77°C) *Δ H*: 47J/g / 46J/g ***Ordered structure in amorphous region w/ DCM/Pyridine(60/40wt%)***	*CF/Pyridine (60/40wt%)* / *CF/Methanol (80/20wt%)* (SEM) Fiber diameter: 315 ± 263nm (beads; 1982) / 730 ± 325nm (XRD) Crystallization peaks: @ 21 & 23.5° = @ 21 & 23.5° (DSC) *Δ Hc (Tc)*: NON / NON *Δ H*: 71J/g = 76J/g ***Crystalline → Crystalline (No change)***	
Take-up velocity	Mechanical drawing	*63m/min* / *630m/min* / *1,260m/min* / *1,890m/min* (SEM) Fiber diameter: 686 ± 111nm / 780 ± 112nm / 619 ± 119nm / 417 ± 138nm (XRD) Crystallization peaks: @ 17° = @ 17° = @ 17° = @ 17° (DSC) *Δ Hc (Tc)*: 7J/g (67°C) < 9J/g (68°C) < 12J/g (70°C) < 16J/g (68°C) *Δ H*: 79J/g < 83J/g < 86J/g / 85J/g ***Ordered structure in amorphous region w/ HIGHER take-up velocity*** ***Amorphous @63m/min → Crystalline @630-1,890m/min***	*63m/min* / *630m/min* (SEM) Fiber diameter: 361 ± 232nm / 346 ± 206nm (XRD) Crystallization peaks: @ 21 & 23.5° = @ 21 & 23.5° (DSC) *Δ Hc (Tc)*: NON / NON *Δ H*: 59J/g = 62J/g ***Crystalline → Crystalline (No change)***	*63m/min* / *630m/min* (SEM) Fiber diameter: 1783 ± 388nm / 694 ± 313nm (XRD) Crystallization peaks: NON / @ 17° (DSC) *Δ Hc (Tc)*: – / – *Δ H*: – / – ***Amorphous @63m/min → Crystalline @630m/min***

spinning temperatures, while T_g of PLLA is higher than spinning temperature. Mobility of molecular chains would be high if its T_g is lower than spinning temperature. The high mobility of molecular chains would encourage faster crystallization. Therefore, its higher crystallization rate and higher molecular mobility induced ductile polymer (PCL) crystalline structure by the electrical drawing. There might not be enough time for rigid polymer (PLLA) with lower molecular mobility and lower crystallization rate.

The influence of the mechanical drawing on the structure development could be discussed from the viewpoint of the spinning jet drawing ratio. SEM images exhibited that fiber diameter was decreased in rigid polymer (PLLA) nanofibers but not changed in ductile polymer (PCL) nanofibers at higher take-up velocity. The take-up velocity up to 630 m/min seems to be not high enough to draw the spinning jet of ductile (PCL) polymer.

According to the structure analyses of electrospun semi-ductile polymer (P(LLA-b-CL)) fibers, the peaks attributed to ductile (- CL) units sequence presented in the XRD diagram even though the copolymer contained only 25 wt% of ductile (- CL) units. For rigid (- LLA) units sequences, amorphous structure was

confirmed by DSC analysis. The semi-ductile copolymer (P(LLA-b-CL)) used in this study is a block type in the entire range of the monomer mixture so that the rigid (- LLA) units and ductile (- CL) units sequence might behave similarly to rigid (PLLA) and ductile (PCL) homopolymers, respectively.

On the other hand, semi-ductile copolymer (P(LLA-r-CL)) electrospun at take-up velocity of 63 m/min revealed no crystalline peaks attributed to rigid (- LLA) units and ductile (- CL) units sequence. The structure formation of ductile (- CL) units sequence was different from that of ductile (PCL) homopolymers and ductile (- CL) units sequence in semi-ductile copolymer (P(LLA-b-CL)). In the electrospinning semi-ductile copolymer (P(LLA-r-CL)) jet, mobility of rigid (- LLA) units sequence showing high T_g would be lower than that of ductile (- CL) units sequence. Molecular arrangement of ductile (- CL) units sequence might be restricted by neighboring rigid (- LLA) units. This hinders crystallization of ductile (- CL) units sequence. It is noted that semi-ductile (P(LLA-r-CL)) copolymer nanofibers electrospun at 630 m/min showed the diffraction peak attributed to rigid (- LLA) units sequence but no peaks attributed to ductile (- CL) units sequence. Although crystalline structure attributed to ductile (- CL) units sequence was not developed due to its random sequences, crystalline structure attributed to rigid (- LLA) units

sequence was developed in electrospun semi-ductile (P(LLA-b-CL)) copolymer fibers as found in electrospun rigid polymer (PLLA) fibers.

To discuss the formation of crystalline structure of rigid (- LLA) units sequence, it would be important to consider structure development of ductile (- CL) units sequence. Crystalline formation or structure development of ductile (- CL) units sequence would be completed prior to that of rigid (- LLA) units sequence due to its higher crystallization rate, and even after the structure formation, ductile (- CL) units sequences show high mobility. According to structure analysis of electrospun ductile polymer (PCL) fibers, it seemed that there is no difference in structure development between as spun fibers at 63 and 630 m/min. The above findings suggest that ductile (- CL) units sequences did not disturb and it might support structure development of rigid (- LLA) units sequence. It is also important that semi-ductile (P(LLA-b-CL)) copolymer has high component ratio of rigid (- LLA) units sequence.

4-5. Summary

Structure formation / development in electrospun nanofibers were discussed using semi-crystalline rigid (PLLA), ductile (PCL) homopolymers and their block and random copolymers. XRD and DSC analysis were conducted to investigate

processing condition effects on the molecular structure.

For electrospun rigid polymer (PLLA) nanofibers, solvents properties and polymer concentration, which contribute to an electrical drawing of a jet, were found to affect molecular structure in amorphous region. Take-up velocity which is associated with the mechanical drawing of the jet was the dominant parameter to develop crystalline structure. As the results of WAXD analysis, the crystalline structure appeared to be lamella which was oriented along the fiber axis at higher take-up velocity.

On the other hand, crystalline structure was developed in electrospun ductile polymer (PCL) nanofibers via electrospinning process. However, the crystal formation was independent of processing parameters like solvent properties and take-up velocity. Ductile polymer (PCL) has short crystallization time and low T_g which is lower than spinning temperature. Crystal formation of electrospun polymer fibers should be highly dependent on its crystallization rate and molecular mobility.

It was found that structure development of rigid (- LLA) units and ductile (- CL) is different in their block and random copolymers. Crystalline structure attributed to rigid (- LLA) units was developed in random units sequence (P(LLA-r-CL))

copolymer, while ductile (- CL) units were transformed into crystalline structure in block units sequence (P(LLA-b-CL) copolymer. The structure formation of ductile or rigid units is also highly reflected by their crystallization rate and molecular mobility. The mobility of ductile (- CL) units is high in block sequence (P(LLA-b-CL)) copolymer, while the mobility is restricted in random sequence (P(LLA-r-CL) copolymer. It would be concluded that crystalline structure is developed by ductile units with high mobility and short crystallization rate in block sequence semi-ductile copolymer, whereas the ductile units support structure development of rigid units.

To understand structure-properties relationship, tensile tests using electrospun single nanofibers were conducted. As the results, crystallized PLLA nanofibers (as-spun at 630m/min) showed higher tensile modulus, strength but lower strain at break than that of amorphous PLLA nanofibers (as-spun at 63m/min).

CHAPTER V

STRUCTURE AND TENSILE PROPERTIES OF ELECTROSPUN FIBERS VIA POST-PROCESSING

5-1. Introduction

In the previous chapter, molecular structure and tensile properties of electrospun nanofibers has been discussed from the viewpoint of electrospinning parameters. Amorphous and crystalline structure might be formed in fibers electrospun from rigid polymer like PLLA. The molecular structure in amorphous region was a function of the parameters which affect the electrical jet drawing, such as polymer concentration and solvents properties. The formation of crystalline structure was dependent on the mechanical jet drawing ratio contributed by take-up velocity. However, it seems to be difficult to induce further structure development of the electrospun PLLA nanofibers through electrospinning process. Alternate processing may be required for the further structure development. According to past structure analyses, post-processing such as annealing and hot-drawing are effective to facilitate structure development of melts-spun or solution-spun fibers (see in Chap. 2). Through the post-processing, electrospun nanofibers may develop highly crystallized structure. Melt-spun and solution-spun PLLA micronfibers via

post-processing have been found to show α-, and β-crystal modification [34,35,103-105 (PSP93,52,81,83,84)] and β-crystal has higher contribution to mechanical properties than α-crystal. The crystal modification is associated with post-processing parameters, i.e., annealing temperature or time [106 (S-R2)], and hot-drawing temperature [36,33,107 (PSP82,105,51)] and hot-drawing ratio or extension ratio [36,31,33,107 (PSP82,96,105,51)]. It was reported that hot-drawing at high drawing ratio is required to increase crystallinity and develop β-phase crystal which is the results from molecular rearrangements of α-phase crystals via hot-drawing. These structure developments of polymer fibers might be affected by fiber scale / diameter. Hence, structure analysis of electrospun nanofibers via post-processing might lead to the recognition of a new concept in polymer science.

In this chapter, molecular structure of electrospun PLLA nanofibers has been discussed from the viewpoint of post-processing, i.e. annealing and hot-drawing. Additionally, the interaction between molecular structure and tensile properties was discussed based on the tensile test using electrospun single nanofiber.

5-2. Experimental

5-2-1. Material Selection

Semi-crystalline biodegradable polymer of Poly($_L$-lactide) (PLLA) with molecular weight (Mw) of 300,000 g/mol was dissolved in dichloromethane (DCM) and Pyridine mixture with 50 and 50 wt% ratio. Different scale nanofibers were prepared from PLLA solutions with different polymer concentrations at 1.5 and 4.5 wt%. Processing parameters were held constant at electrospinning from both solutions (Table 4-1). To change the drawability of nanofibers, samples with different molecular structure were prepared for hot-drawing by electrospinning with / without annealing. All the samples used in this chapter were listed in Table 4-2. The details of post-processing were described in the following sections.

5-2-2. Post-processing

Annealing

Samples were prepared from PLLA fibers electrospun at different take-up velocities of 63, 630, 1,260 and 1,890 m/min. Those nanofibers were collected on coverslip with 15 mm in a diameter, at fixed weight of 1.0 mg. Annealing was applied at 90 ^oC for 10 hours in a heating oven. All samples were scanned by XRD before and after annealing process to understand their molecular structure.

Hot-drawing

Hot-drawing was applied to fiber bundles electrospun at different take-up velocities

Table 5-1. Solution and processing conditions applied to study hot-drawing effects on PLLA fibers.

Solution conditions			Spinning parameters				
Polymer	Solvents	Polymer concentration (wt%)	Applied voltage (kV)	Take-up velocity (m/min)	Distance (mm)	Feed rate (ml/hr)	Inside needle diameter (mm)
PLLA with Mw of 300,000	DCM/PRD (50/50wt%)	4.5	25	***63*** ***630***	150	0.5	0.21

Table 5-2. PLLA nanofiber samples used for post-processing studies.

Sample name	Polymer	Polymer concentration	Sample condition	Processing parameter	Post-processing	Initial Fiber diameter	Fiber diameter
Sample A-63	PLLA (Mw; 300K)	4.5wt%	as-spun & annealed	spun @ 63m/min	@ 90 °C x 10hrs	483 ± 184 nm →	448 ± 40 nm
Sample A-630				spun @ 630m/min		484 ± 186 nm →	504 ± 182 nm
Sample A-1260				spun @ 1,260m/min		449 ± 78 nm →	480 ± 48 nm
Sample A-1890				spun @ 1,890m/min		422 ± 129 nm →	353 ± 42 nm
Sample H-63 (114%)			as-spun & hot-drawn	spun @ 63m/min	@ 160°C x 114 %	567 nm →	390 nm
Sample H-63 (257%)					@ 160°C x 257 %		376 nm
Sample H-63 (1000%)					@ 160°C x 1,000 %		373 nm
Sample H-630 (114%)				spun @ 630m/min	@ 160°C x 114 %	502 nm →	333 nm
Sample H-630 (257%)					@ 160°C x 257 %		336 nm
Sample H-630 (1000%)					@ 160°C x 1,000 %		223 nm
Sample AH-630 (114%)			as-spun & annaled & hot-drawn	spun @ 630m/min	@ 90 °C x 10hrs → @ 160°C x 114 %	542 nm →	688 nm → 421 nm
Sample AH-630 (257%)					@ 90 °C x 10hrs → @ 160°C x 257 %		688 nm → 312 nm
Sample AH-630 (1000%)					@ 90 °C x 10hrs → @ 160°C x 1,000 %		688 nm → 295 nm

of 63 and 630 m/min, and that spun at 630 m/min followed by annealing. According to structure analyses, it was found that low take-up velocity of 63 m/min induced amorphous structure, whereas high take-up velocity of 630 m/min induced crystalline structure (see in Chap. 4). Crystalline structure of electrospun fibers at 630 m/min further developed via annealing.

The procedures to prepare fiber bundle samples are as follows. The fiber bundles were spun using a disc collector. The collected fiber bundles were peeled off from the edge of disc collector. Hot-drawing was conducted using Instron 5848 microtester with a heating chamber at 160 ^{o}C in a drawing temperature and 5 mm/min in a testing speed. The samples with a gage length of 35 mm were drawn up to 40 mm and 90 mm, corresponding to 114 % and 214 % in an extension ratio.

The microtester has a limitation in the stroke length. Due to the stroke limitation, the maximum extension for the sample with a gage length of 35 mm is up to 90 mm. In order to apply higher drawing extension ratio to samples, samples with a gage length of 5 mm was also prepared. In hot-drawing process, this sample was drawn to 50 mm, corresponding to 1,000 % in the extension ratio. Hot-drawing ratio (λ) was calculated by initial fiber diameter / final diameter after hot-drawing.

The structure analysis of the resultant fiber bundles via post-processing was conducted using XRD and DSC. For XRD analysis, samples were prepared as follows. After hot-drawing, fiber bundle was folded back at around 5 mm in a length on a glass plate to make the sample thick enough for XRD scanning. Since the number of fibers in each bundle sample is different, sample thickness is not constant in all samples.

5-2-3. Tensile Test of Electrospun Single Nanofibers

A disc collector with gaps at its circumferential edge was used to collect electrospun single nanofibers. The procedures to prepare single nanofibers are shown in Chap. 4. The tensile tests were performed at a strain rate of 25 %/min using a nano tensile testing system (Nano Bionix, MTS) with 500 mN load range, and 50 nN load resolution.

5-3. Results

5-3-1. Annealing Effects

As shown in SEM images (Figure 5-1), fiber diameter was not significantly changed before and after annealing. The XRD diagram in Figure 5-2 (a) revealed the

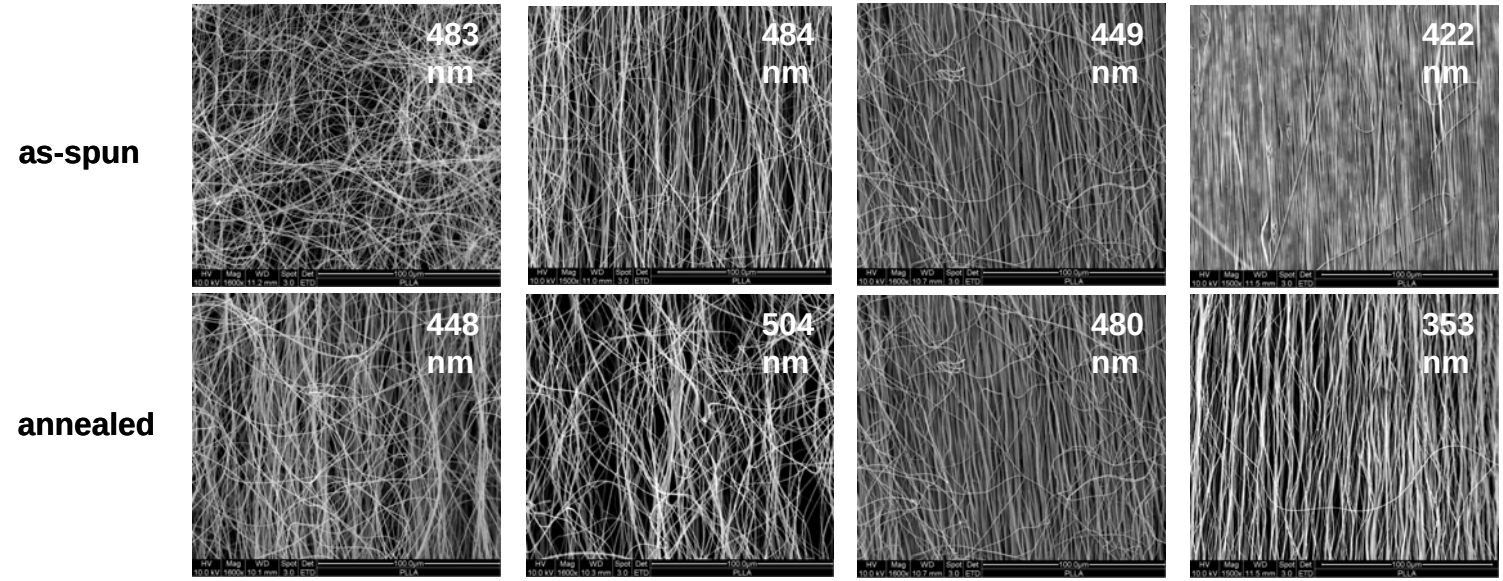

Figure 5-1. SEM images of as-spun, annealed fibers spun at 63, 630, 1,260 and 1,890 m/min.

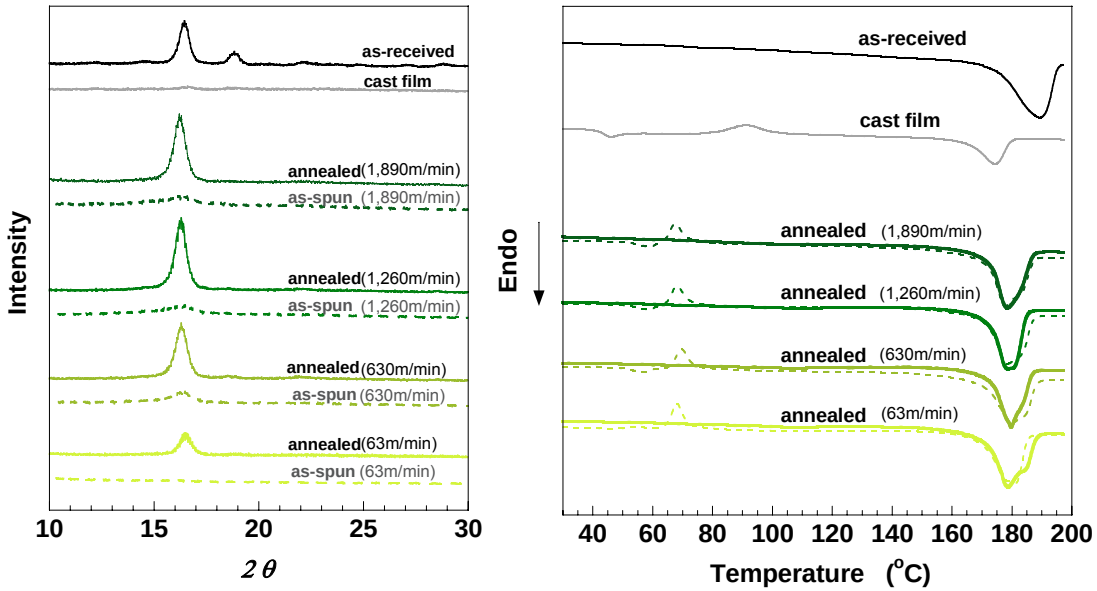

Figure 5-2. Annealing effects on PLLA fibers electrospun at different take-up velocity: (a) XRD diagram and (b) DSC thermogram.

Table 5-3. The corresponding thermal properties of annealed fibers.

Conditions	*Tc* (°C)	*ΔHc (J/g)*	*Tm* (°C)	*ΔHm (J/g)*	*ΔH (J/g)* annealed	as-spun
as-received			190	84	84	–
cast film	91	10	175	28	18	–
annealed (1890m/min)			179	76	76	← 66
annealed (1260m/min)			180	73	73	← 65
annealed (630m/min)			179	70	70	← 62
annealed (63m/min)			178	84	84	← 53

diffraction peaks at around 16° in all the annealed nanofibers. The peak intensity was almost independent of take-up velocities in the range from 630 to 1,890 m/min, while annealed fibers spun at 63 m/min (Sample A-63) showed lower intensity diffraction peak than that from fibers at 630 m/min and above. As shown in Figure 5-2 (b) and Table 5-3, no exothermic peak was found in all the annealed nanofibers from the DSC profiles. The heat of fusion (ΔH) of the annealed fibers was higher

than that of as-spun fibers and it was slightly increased at higher take-up velocity in the range from 630 to 1,890 m/min. The increased ΔH of annealed fibers was due to the crystalline structure developed by annealing. As presented in Chap. 4, higher take-up velocity induces the further mechanical drawing of the jet. The higher ΔH at higher take-up velocity is reflected by the crystalline structure developed via the higher mechanical drawing. It is noted that Sample A-63 showed a dramatic increase in ΔH. The results of XRD analysis suggest that amorphous structure in electrospun fibers at 63 m/min (Sample E-63) was preferential structure to form highly crystallized structure by annealing.

Tensile tests of the annealed PLLA single nanofibers were carried out to study structure – properties relationship. Electrospun fibers at 630 /min (Sample E-630) and 1,890 m/min (Sample E-1,890), followed by annealing were used as samples. As shown in Figure 5-3 and Table 5-4, both electrospun fibers at 630 /min, followed by annealing (Sample A-630) and electrospun fibers at 1,890 m/min, followed by annealing (Sample A-1,890) showed higher modulus, strength and higher strain at break than that of as-spun fibers. It is reported that tensile modulus and strength are reflected by crystallinity [24]. Higher modulus of annealed fibers is the result of crystalline structure developed via annealing process, in which molecular relaxation

from ordered manner into random manner occures in amorphous region. Large strain at break of annealed fibers is due to the random manner in amorphous region.

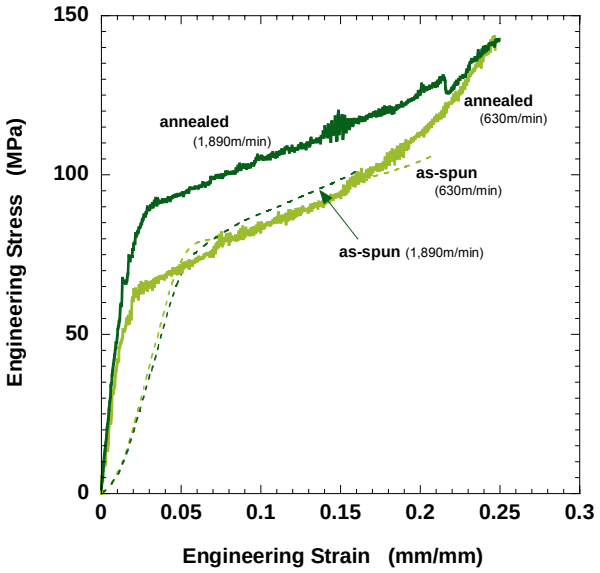

Figure 5-3. Tensile stress-stain curves of annealed PLLA single nanofibers electrospun at 630 and 1,890 m/min.

Table 5-4. Tensile properties of annealed PLLA single nanofibers.

Samples	Mw (g/mol)	Take-up velocity (m/min)	Fiber diameter (nm)	Tensile modulus (GPa)	Tensile strength (MPa)	Strain at break
Electrospun fibers	300,000	630	506 ± 81	2.2 ± 0.3	94 ± 33	0.22 ± 0.04
		1890	775 ± 145	1.8 ± 0.5	104 ± 50	0.15 ± 0.05
Annealed fibers	300,000	630	673 ± 157	4.3 ± 1.5	121 ± 59	0.25 ± 0.05
		1890	797 ± 108	5.3 ± 1.3	150 ± 41	0.26 ± 0.06
Melt-spun fibers [16]	212,450	600	34,000	3.9	192	2.2

5-3-2. Hot-drawing Effects

PLLA fiber bundle electrospun at 63 m/min

As shown in SEM images (Figure 5-4), nanofibers with smaller diameter were

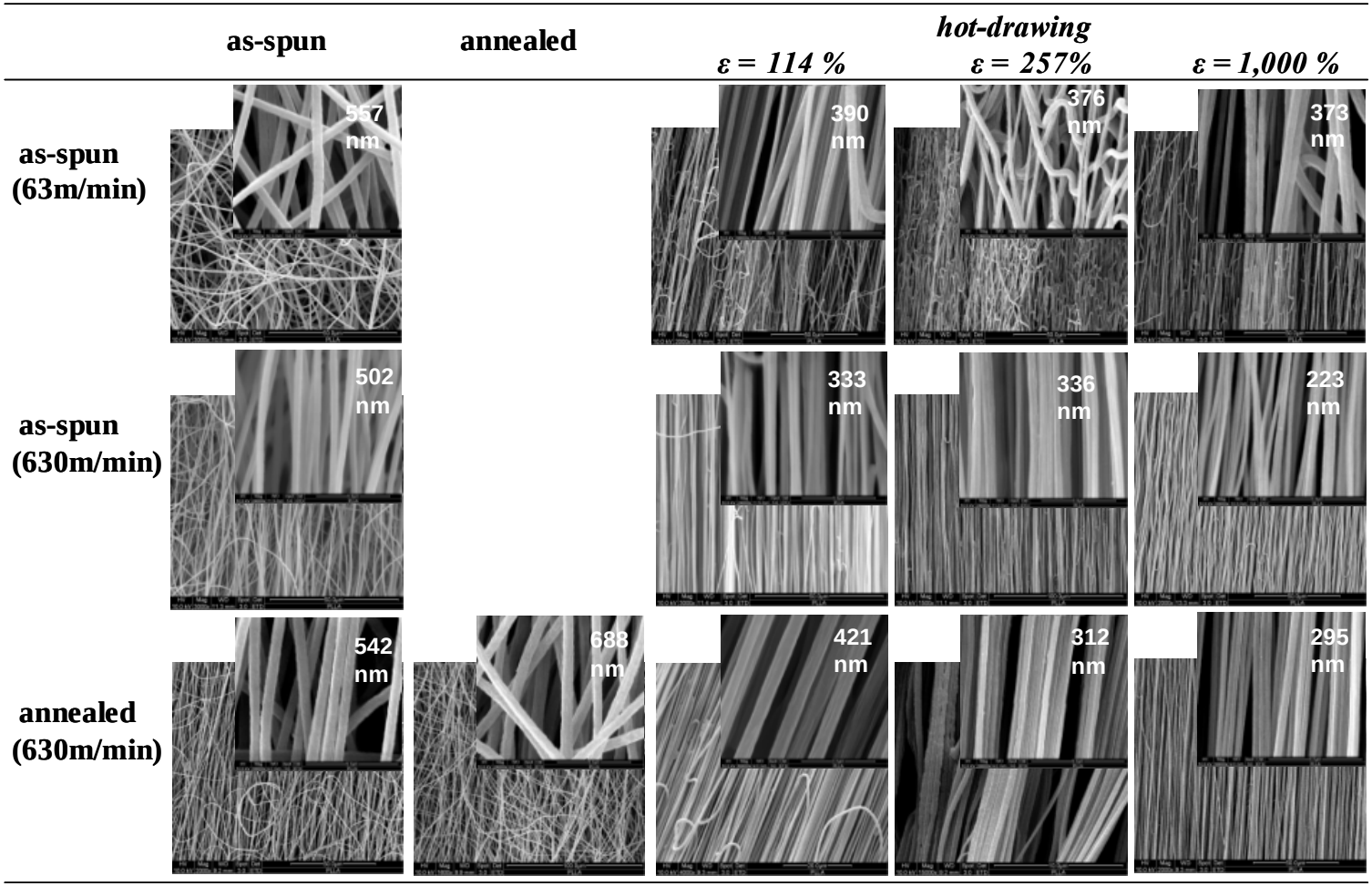

Figure 5-4. SEM images of as-spun, annealed and hot-drawn PLLA fiber bundles.

produced by hot-drawing at larger extension ratio and which are oriented along the loading direction. Due to the random fiber orientation, as-spun 63m/min was not highly drawn since the fiber drawing is initiated after its random manner is rearranged into aligned manner. XRD patterns in Figure 5-5 (a) revealed that hot-drawn 63 m/min possess the two main diffraction peaks at 16^{o} and 19^{o}, and small peaks at 13^{o}, 15^{o}, 22^{o} and 29^{o}. Some indistinct peaks were also found. The peak intensity was independent of hot-drawing ratio. The peak intensity in WAXD diagrams from Figure 5-5(a), -7(a), -8(a) and -9(a) might be as a function of sample thickness. The samples were prepared by folded fiber bundle back and fixed them onto a glass plate. As each fiber bundle contains different number of fibers, the resultant sample thickness was not held constant in all samples. This inconstant sample thickness causes the difficulty in discussing dependency of crystallization peak intensity on hot-drawing. Figure 5-5 (b) shows DSC profiles of electrospun fibers at 63 m/min, followed by hot-drawing. Exothermic peaks (cold crystallization peaks) were absent in all hot-drawn fibers, while as-spun fibers exhibited the cold crystallization peak at around 70 ^{o}C. As shown in Table 5-5, hot-drawn fibers showed higher ΔH than that of as-spun fibers. The ΔH was a function of extension ratio, and larger extension ratio increased ΔH. The ΔH of electrospun fibers at 63 m/min, followed by hot-drawing at 114 % in a extension ratio (Sample H-63

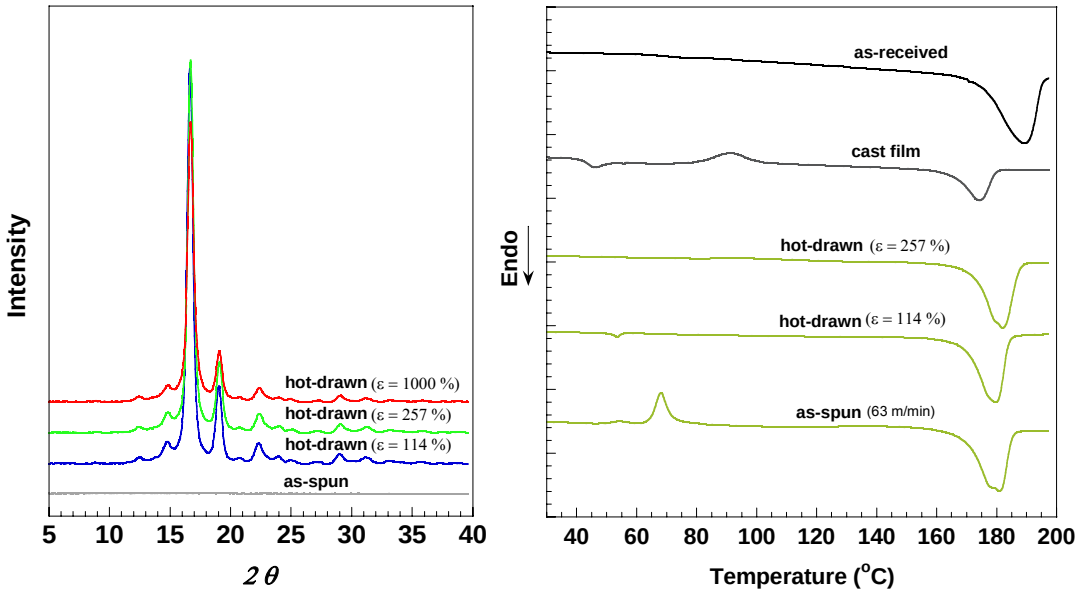

Figure 5-5. Hot-drawing effects on PLLA nanofibers spun at 63 m/min: (a) XRD diagram and (b) DSC thermogram.

Table 5-5. The corresponding thermal properties of PLLA fibers spun at 63 m/min, followed by hot-drawing.

Conditions	*Tc* (°C)	*ΔHc (J/g)*	*Tm* (°C)	*ΔHm (J/g)*	*ΔH (J/g)*
as-received			190	84	84
cast film	91	10	175	28	18
as-spun 63m/min	68	16	181	69	53
Hot-drawn (ε = 114 %)			180	61	61
Hot-drawn (ε = 257 %)			182	64	64

(114%)), or followed by hot-drawing at 257 % in a extension ratio (Sample H-63 (257%)) were close to that of Sample E-630, that is 62 J/g. In order to identify the crystalline structure of hot-drawn PLLA fibers, WAXD analysis was conducted. More distinct crystalline diffractions appeared on the equator by an increase in extension ratio, while as-spun fibers showed no diffraction (see in Figure 5-9). The

distinct diffractions imply crystalline orientation. The WAXD pattern is similar to that reported by Santis et. al. [34 (PSP93)]. The diffractions from (110) phase at 15^{o} and (200) phase at 16^{o} shown by hot-drawn PLLA nanofibers should corresponds to α-phase crystal. It is difficult to see the presence of β-phase from the WAXD pattern.

Figure 5-6 shows Stress - Strain curves of the hot-drawn PLLA single nanofibers. For PLLA single nanofiber spun at 63 m/min, hot-drawing was successfully conducted at extension ratio of 114 %, while all the fibers were broken via hot-drawing at higher extension ratio above 114 %. All PLLA single nanofibers spun at 630 m/min were broken during hot-drawing process even when the fibers were hot-drawn at small extension ratio. The breakage of the fibers might be due to hot-air blow into the heating chamber used for hot-drawing. As shown in Figure 5-6 and Table 5-6, hot-drawn

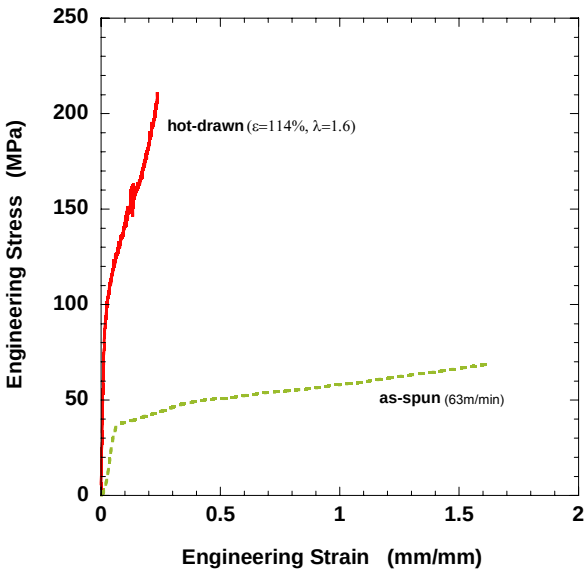

Figure 5-6. Tensile stress-stain curves of hot-drawn PLLA single nanofibers electrospun at take-up velocity of 63 m/min.

PLLA single nanofiber showed a dramatic increase in tensile modulus and strength compared to as-spun single nanofibers. In this study, Sample H-63 (114%) showed the best performance among the electrospun fibers with or without post-processing in terms of tensile properties. However, the tensile properties of the fibers were much lower than the strongest PLLA micron fibers produced by solution-spinning via hot-drawing [33 (PSP105)].

Table 5-6. Tensile properties of hot-drawn PLLA single nanofibers.

Samples	Mw (g/mol)	Take-up velocity (m/min)	Fiber diameter (nm)	Tensile modulus (GPa)	Tensile strength (MPa)	Strain at break
Electrospun fibers	300,000	63	890 ± 190	1.0 ± 1.6	89 ± 40	1.54 ± 0.12
		630	506 ± 81	2.2 ± 0.3	94 ± 33	0.22 ± 0.04
		1890	775 ± 145	1.8 ± 0.5	104 ± 50	0.15 ± 0.05
Annealed fibers	300,000	630	673 ± 157	4.3 ± 1.5	121 ± 59	0.25 ± 0.05
		1890	797 ± 108	5.3 ± 1.3	150 ± 41	0.26 ± 0.06
Hot-drawn fibers (λ= 1.6)		63	538 ± 91	6.6 ± 0.7	232 ± 31	0.26 ± 0.04
Melt-spun fibers [16]	212,450	600	34,000	3.9	192	2.2
Hot-drawn dry-spun fibers (λ= 10) [7]	330,000			9.2	870	
Hot-drawn dry-spun fibers (λ= 13) [3]	910,000				2300	

PLLA fibers electrospun at 630 m/min

XRD patterns as shown in Figure 5-7 (a) exhibited some small peaks in addition to the two main diffraction peaks at 16^{o} and 19^{o} in electrospun nanofibers at 630 m/min, followed by hot-drawing (Sample H-630). The pattern was similar to that seen in electrospun fibers at 63 m/min, followed by hot-drawing (Sample H-63). As the result of DSC analysis (Figure 5-7 (b) and Table 5-7), cold crystallization peaks

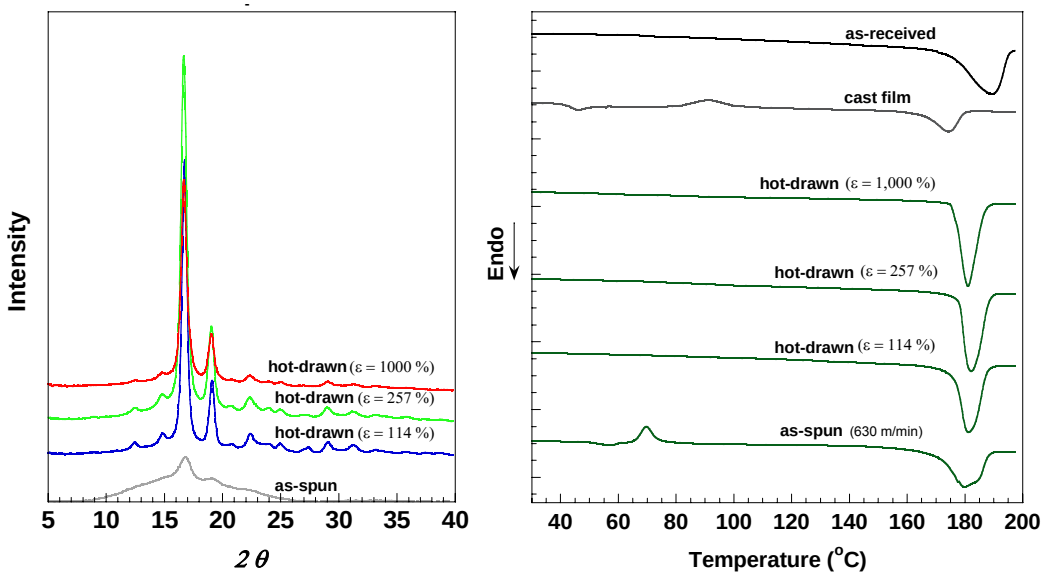

Figure 5-7. Hot-drawing effects on PLLA nanofibers spun at 630 m/min: (a) XRD diagram and (b) DSC thermogram.

Table 5-7. The corresponding thermal properties of PLLA fibers spun at 630 m/min, followed by hot-drawing.

Conditions	*Tc* (°C)	*ΔHc (J/g)*	*Tm* (°C)	*ΔHm (J/g)*	*ΔH (J/g)*
as-received			190	84	84
cast film	91	10	175	28	18
as-spun 630m/min	70	12	182	74	62
Hot-drawn (ε = 114 %)			181	85	85
Hot-drawn (ε = 257 %)			182	80	80
Hot-drawn (ε = 1,000 %)			181	74	74

were absent in all hot-drawn fibers. *ΔH* of Sample E-630 increased via hot-drawing process. The higher *ΔH* of hot-drawn fibers is due to crystalline structure formed by hot-drawing. It is noteworthy that the highest *ΔH* was shown by hot-drawn fibers at the smallest extension ratio of 114 %. An increase in hot-drawing ratio decreased the *ΔH* of hot-drawing fibers. According to WAXD analysis (Figure 5-9), all hot-drawn fibers exhibited the similar diffraction patterns as that shown by Sample H-63. The

diffraction pattern is attributed to α-phase crystal. It was also found that the crystalline diffractions were more distinct which was attributed to crystalline orientation at increased extension ratio.

Annealed PLLA nanofibers electrospun at 630 m/min, followed by hot-drawing

In the XRD diagram (Figure 5-8 (a)), the strong diffraction peaks at 16^{o} and 29^{o} were found in annealed fibers. XRD patterns of electrospun fibers at 630 m/min, followed by annealing and hot-drawing (Sample AH-630) were similar to that shown by Sample H-63 and H-630. DSC thermogram (Figure 5-8 (b)) exhibited no cold crystallization peak in annealed and hot-drawn PLLA fibers. The ΔH of the annealed fibers was decreased via hot-drawing at 114 % in extension ratio, but increased at 257 % (Table 5-8). WAXD patterns (Figure 5-9) suggest that crystalline structure in annealed and hot-drawn fibers would be α-phase crystal. It is noted that arc shaped-diffractions were shown by annealed fibers and it is attributed to isotropic crystalline structures. On the other hand, annealed & hot-drawn fibers showed more distinct crystalline diffractions at higher extension ratio. Sample AH-630 developed crystalline structure which was oriented along the fiber axis.

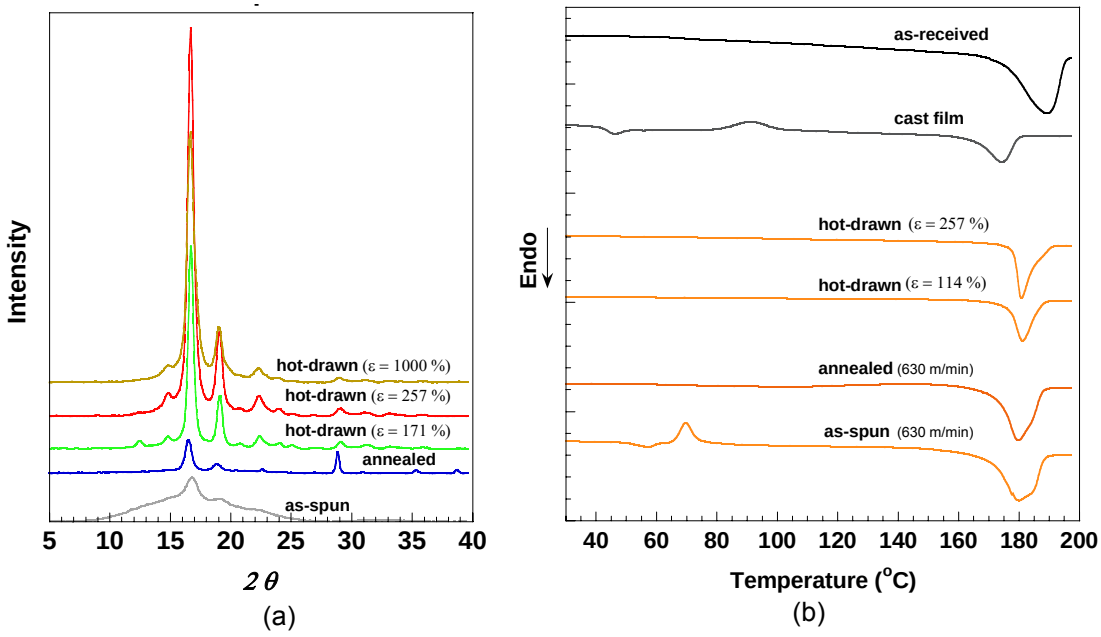

Figure 5-8. Hot-drawing effects on annealed PLLA nanofibers spun at 630 m/min: (a) XRD diagram and (b) DSC thermogram.

Table 5-8. The corresponding thermal properties of annealed PLLA fibers spun at 630 m/min, followed by hot-drawing.

Conditions	*Tc* (°C)	*ΔHc (J/g)*	*Tm* (°C)	*ΔHm (J/g)*	*ΔH (J/g)*
as-received			190	84	84
cast film	91	10	175	28	18
as-spun 630m/min	70	12	182	74	62
annealed			180	68	68
Hot-drawn (ε = 114 %)			181	61	61
Hot-drawn (ε = 257 %)			181	72	72

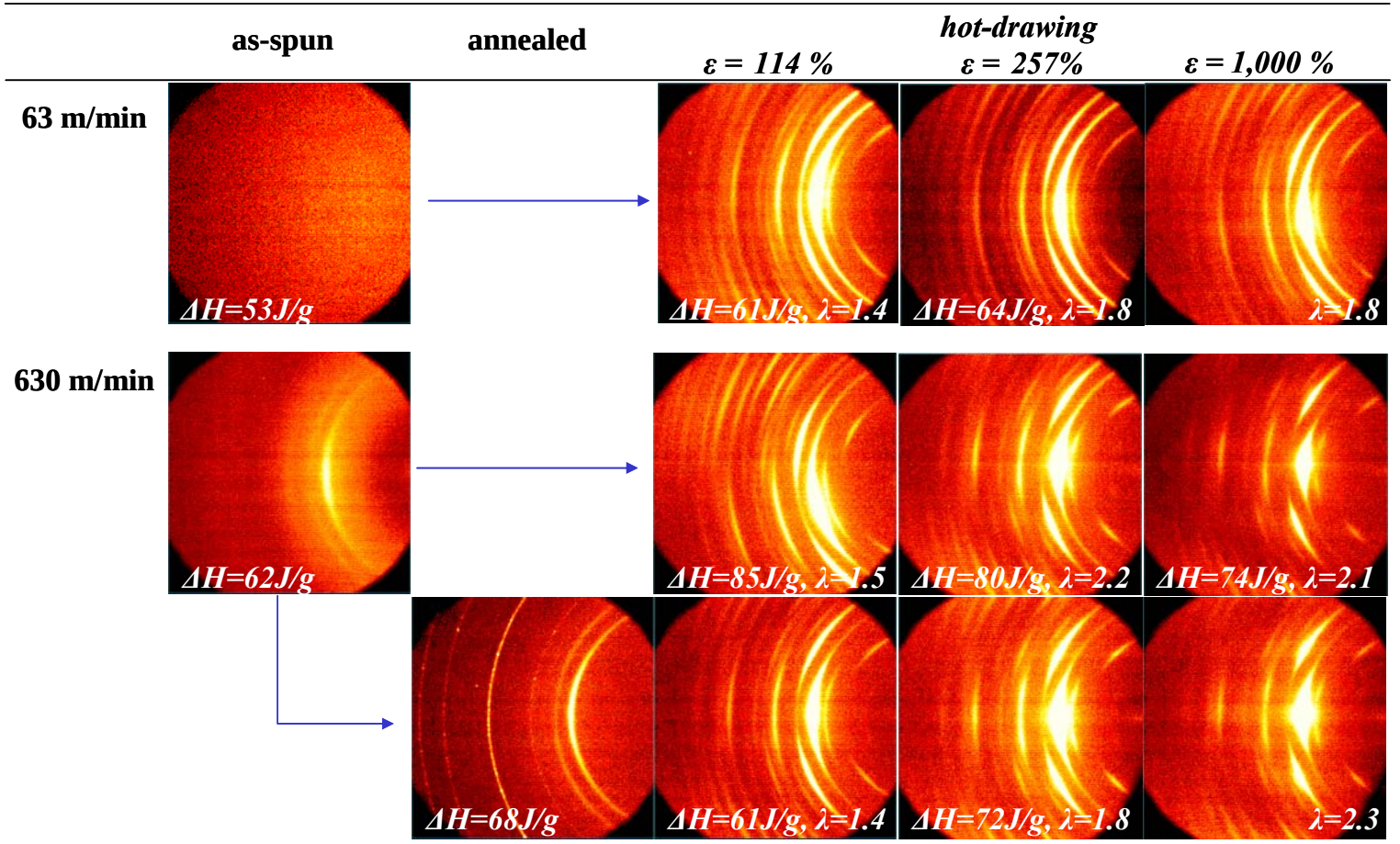

Figure 5-9. WAXD patterns of as-spun, annealed and hot-drawn PLLA fiber bundles.

5-4. Discussion

Based on the structure analysis in the previous section, it was found that post-processing such as annealing and hot-drawing facilitated to develop crystalline structure of electrospun nanofibers. Via annealing process, the maximum ΔH was shown by Sample E-63 which possesses amorphous structure determined by XRD. Via hot-drawing process, the maximum ΔH was shown by Sample E-630 which exhibited crystallized structure determined by XRD. Structural formation of polymer nanofibers via post-processing was discussed in the viewpoint of initial molecular structure (amorphous and crystalline). Figure 5-10 summarized the model of structural formation in electrospun nanofibers via post-processing.

Annealed nanofibers

It was indicated that amorphous nanofibers (Sample E-63) have a high potential for developing highly crystallized structure via annealing process. The resultant molecular structure by annealing was further considered based on the comparative studies on the results between XRD and DSC analysis.

As shown in XRD and DSC results, the peak intensity of Sample A-63 was lower than that of Sample A-630 to A-1,890 although ΔH of the Sample A-63 was higher

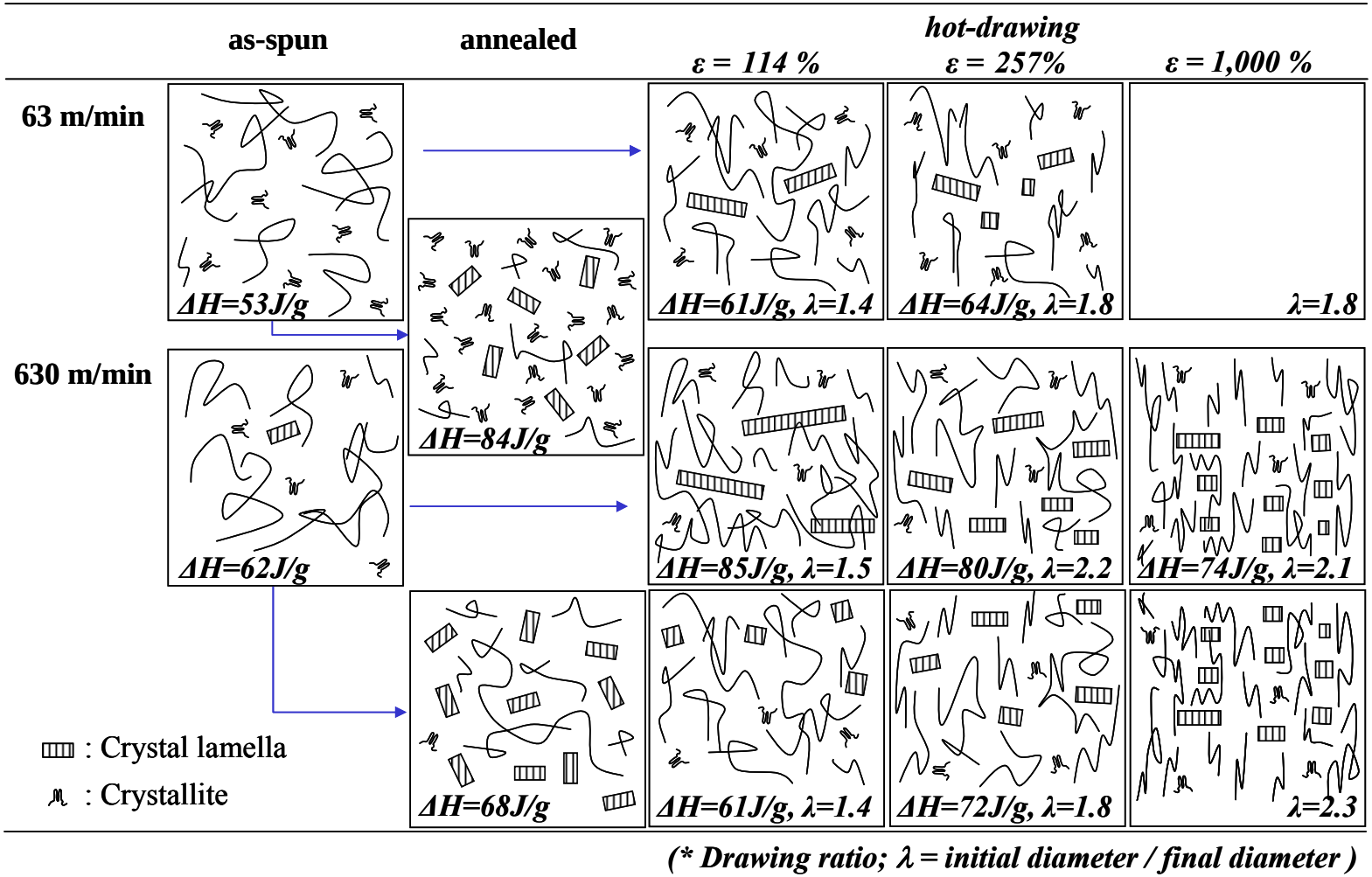

Figure 5-10. Structural model of electrospun PLLA nanofibers followed by hot-drawing.

than the others. These analysis results suggest that ΔH of Sample A-63 is contributed by crystalline structures which might be too small to be detected by XRD. It may be defined that crystalline structure detected by XRD and DSC are crystallites and lamella, respectively.

The structure development in amorphous nanofibers (Sample E-63) and crystallized nanofibers (Sample E-630 to E-1,890) might be highly dependent on entropy required for crystallization. In terms of crystal formation, entropy to develop crystallites should be lower than that for lamella growth. As another factor affecting entropy, molecular arrangements must be considered. Crystal lamella traps surrounding molecular chains in amorphous region and which would suppress the surrounding molecular rearrangement. As shown in WAXD analysis (see in Chap. 4), Sample E-630 to E-1,890 possess crystal lamella oriented along the fiber axis. On the other hand, isotropically oriented crystal lamella was developed in Sample A-630 via annealing process (Figure 5-9). Higher entropy would be required to rearrange crystalline orientation from aligned matter into isotropic manner. Based on the above issue, it is considered that Sample E-63 possess preferential structure for crystal formation compared to Sample E-630 to 1,890.

Hot-drawn nanofibers

Via hot-drawing process, crystallized nanofibers (Sample E-630) showed higher ΔH than that of amorphous (Sample E-63) and highly crystallized nanofibers (Sample A-630). The resultant ΔH would be highly associated with initial molecular structure formed in as-spun fibers.

WAXD analysis in Figure 5-9 indicated that crystallized nanofibers (Sample E-630) possess crystal lamella oriented along the fiber axis, while no crystal lamella and isotropically oriented crystal lamella were found in amorphous (Sample E-63) and highly crystallized nanofibers (Sample A-630), respectively. It was reported that the crystal grows radially outward parallel to the fiber axis under the drawing process [108]. The above issues suggest that entropy required for crystalline structure development in crystallized nanofibers (Sample E-630) is lower than that of amorphous (Sample E-63) and isotropically highly crystallized (Sample A-630) nanofibers. The hot-drawn crystallized nanofibers (Sample H-630) could have a high potential for highly crystallized structure formation via hot-drawing.

It is noted that in crystallized nanofibers (Sample E-630), the highest ΔH (85 J/g corresponding to 91 % crystallinity) was obtained at the drawing ratio of 1.5.

According to past studies, it is reported that high drawing ratio is required to highly develop crystalline structure. Fabbri et al. has reported that around 65 % of crystallinity (initially 37.5 %) was enhanced by PLLA fibers at 6.5 in a hot-drawing ratio [34]. There should be nanometer scale effects on the development of highly crystallized structure. Molecular interaction and shear force between molecular chains would be increased in the smaller dimension where molecular chains are packed, and they affect crystallization kinetics. Compared to micronfibers, nanofibers may have a potential for the development of highly crystallized structure at smaller hot-drawing ratio.

The results of structure analysis indicated that in crystallized nanofibers (Sample E-630), further structure development was saturated above the drawing ratio of 1.5. ΔH was decreased at higher drawing ratio. As shown in Figure 5-10, this may be due to lamella break-up. The crystal orientation found at higher drawing ratio was enhanced by the lamella break-up.

For highly crystallized nanofibers (annealed 630m/min), ΔH was decreased at the drawing ratio of 1.4 but increased at the drawing ratio of 1.8. As seen in WAXD patterns, crystallized nanofibers (Sample A-630) possess isotropically oriented

lamella. Namely, lamella break-up would occurred and resulted in decreased *ΔH*. At increased drawing ratio of 1.8, lamellae grew up and induced increased *ΔH*.

According to studies on structure-properties relationship in hot-drawn nanofibers, it was found that tensile properties of electrospun single nanofibers at 63m/min dramatically increase at drawing ratio of 1.6. It is noted that the tensile properties of the hot-drawn 630m/min were higher than that of electrospun single nanofibers at 630 m/min although *ΔH* was almost equivalent between the samples. The difference in their tensile properties could be discussed from the viewpoints of the methods of structure and properties analysis. PLLA nanofiber samples were prepared by different manner for structure analyses and tensile properties characterization. Electrospun 'single nanofibers' were applied to tensile tests whereas electrospun 'fiber bundles' were used for XRD and DSC characterizations. In the hot-drawing process, drawing load / extension would show higher contribution to the deformation of single nanofibers than the fiber bundles. Individual fibers of the bundle could not be deformed evenly. Namely, molecular feedback on structure development under hot-drawing may be different between single nanofibers and fiber bundles even under same hot-drawing conditions. This suggests that molecular structure of PLLA single nanofibers was further developed compared to that of the fiber bundle. The

further structure development highly contributes to increase tensile properties of hot-drawn single nanofibers.

Structure analysis of as-spun fibers with small diameter

The finding on structure analysis of hot-drawn nanofibers indicated that there should be nanometer scale effects on the development of highly crystallized molecular. The diameter of electrospun fiber samples were around 500 nm. To further discuss the nanometer scale effects, hot-drawing was applied to PLLA nanofibers with less than 100 nm in a fiber diameter. The sample conditions and electrospinning parameters were listed in Table 5-9 and -10.

SEM images in Figure 5-11 revealed that some nanofibers were broken by hot-drawing. This should be due to the small number of molecular chains in the sample. The fiber breakage might lead to the saturated drawing ratio at increased extension ratio. As the results of XRD analysis (Figure 5-12(a) and -13), similar diffraction patterns as that of hot-drawn large scale nanofibers were exhibited. Increased extension ratio induced highly crystallized structure which appeared to be lamella oriented along the fiber axis. The highly crystallized structure reflected to high ΔH determined by DSC analysis (Figure 5-12(b) and Table 5-11). ΔH was

Table 5-9. Solution and processing conditions applied to study nanometer scale effects on PLLA fibers.

Solution conditions			Spinning parameters				
Polymer	Solvents	Polymer concentration (wt%)	Applied voltage (kV)	Take-up velocity (m/min)	Distance (mm)	Feed rate (ml/hr)	Inside needle diameter (mm)
PLLA with Mw of 300,000	DCM/PRD (50/50wt%)	1.5	20	630	130	2.0	0.1

Table 5-10. PLLA nanofiber samples used for nanometer scale effects studies.

Polymer	Polymer concentration	Sample condition	Processing parameter	Post-processing	Initial Fiber diameter	Fiber diameter
PLLA (Mw; 300K)	1.5wt%	as-spun & annealed	spun @ 630m/min	@ 90 °C x 10hrs	101 nm →	97 nm
		as-spun & hot-drawn	spun @ 630m/min	@ 160°C x 114 % @ 160°C x 257 %	101 nm ⟶	71 nm 84 nm

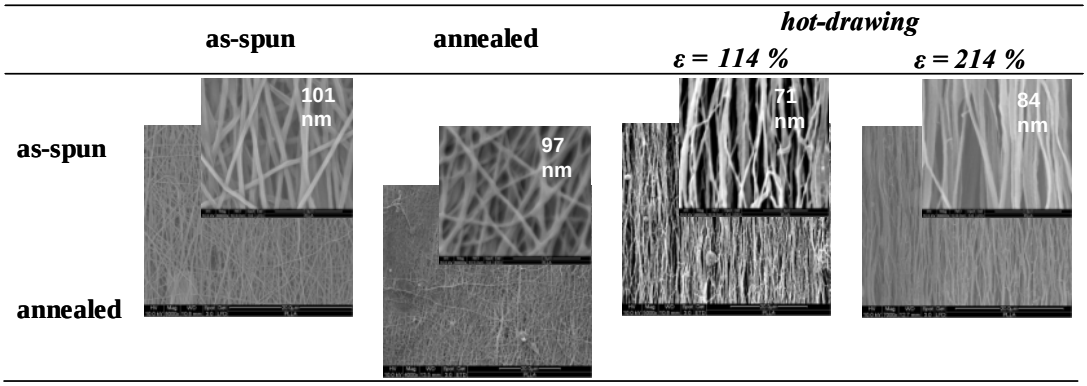

Figure 5-11. SEM images of as-spun, annealed and hot-drawn PLLA fiber bundles with small scale of diameter.

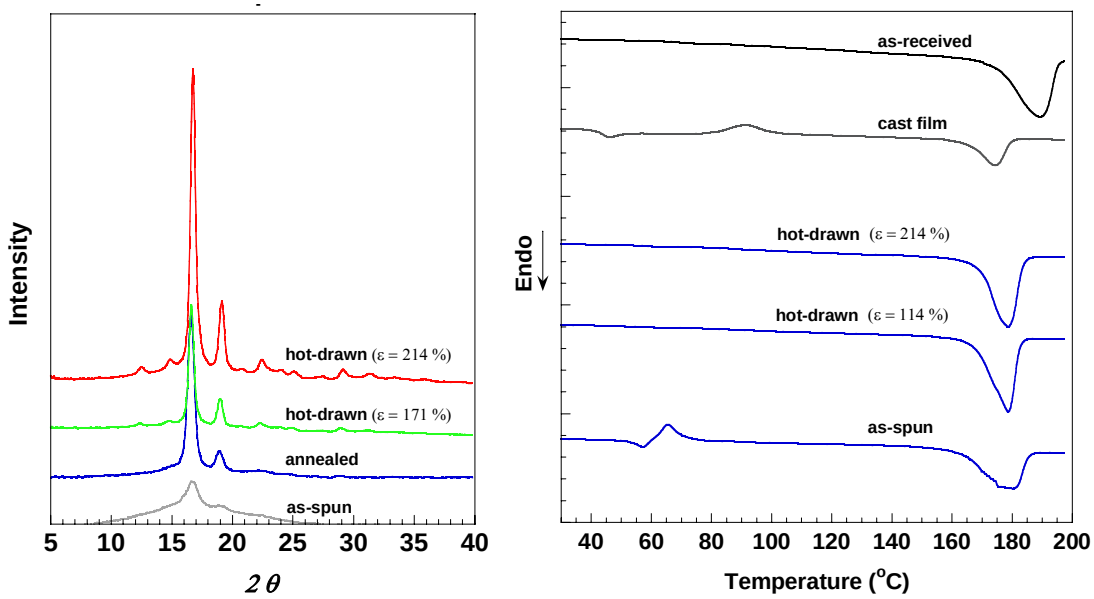

Figure 5-12. Hot-drawing effects on small scale PLLA nanofiber bundles spun at 630 m/min: (a) XRD diagram and (b) DSC thermogram.

Table 5-11. The corresponding thermal properties of small scale PLLA fibers spun at 630 m/min, followed by hot-drawing.

Conditions	*Tc (°C)*	*ΔHc (J/g)*	*Tm (°C)*	*ΔHm (J/g)*	*ΔH (J/g)*
as-received			190	84	90
cast film	91	10	175	28	18
as-spun	65	11	180	65	53
Hot-drawn (ε = 114 %)			179	75	75
Hot-drawn (ε = 214 %)			179	75	75

significantly increased at small drawing ratio of 1.4, although it was not as high as the maximum ΔH shown by hot-drawn large scale nanofibers. These experimental results strongly supported nanofibers potential for highly crystallized structure formation at small hot-drawing ratio.

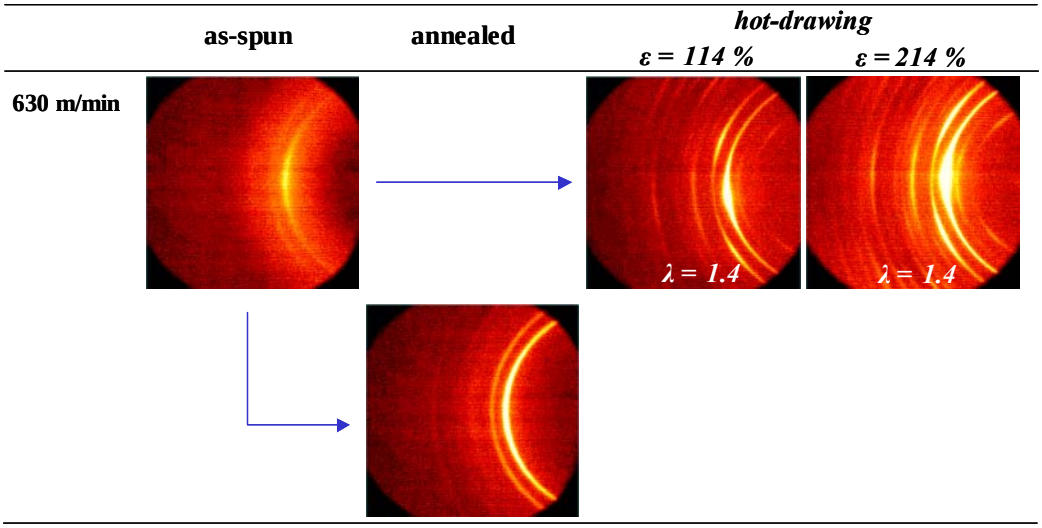

Figure 5-13. WAXD patterns of as-spun, annealed and hot-drawn PLLA fiber bundles with small scale of diameter.

5-5. Summary

Semi-crystalline PLLA polymer was electrospun into nanofibres. Post-processing was applied to electrospun PLLA nanofibers in order to discuss structure formation / development of the nanofibers. Structure-properties relationship was investigated by tensile test using single nanofibers.

XRD and DSC analysis indicated that initial molecular structure before post-processing is important to develop highly crystallized structure via post-processing. Via annealing process, amorphous fibers (as-spun at 63m/min) has a high potential for the development of highly crystallized structure which is corresponding to isotropic crystallites. On the other hand, crystallized fibers (as-spun at 630m/min) have a preferential structure to facilitate crystallization via hot-drawing. The crystalline structure in hot-drawn fibers seems to be highly contributed by crystal lamella oriented along the as-spun fiber axis. The lamellae break-up induced crystalline orientation along the fiber axis at higher drawing ratio, accompanying a decrease in ΔH. It is noteworthy that 91 % crystallinity was obtained by hot-drawing nanofibers at small drawing ratio of 1.5.

In addition to large scale nanofibers (500nm) used in the above studies, molecular structure of hot-drawn small scale nanofibers (< 100nm) was investigated. As the results, 80 % crystallinity was enhanced in the small scale nanofibers at drawing ratio of 1.4. The high efficiency of hot-drawing on structure development might be due to nanometer scale effects. The packed molecular chains in small dimension induce high molecular interaction / shear force between molecular chains, affecting polymer crystallization kinetics.

Structure-properties of hot-drawn nanofibers were discussed by tensile tests using single nanofibers. Hot-drawing was successfully conducted using as-spun at 63m/min (540nm). The resultant hot-drawn nanofibers showed a significant increase in tensile properties, i.e. 6.6 in modulus, 230 MPa in strength and 0.26 in strain at break.

According to the post-processing studies, it was indicated that electrospun nanofibers has a great potential to show high performance by post-processing.

CHAPTER VI

CONCLUDING REMARKS AND RECOMMENDATIONS

The overall purpose of the work in this thesis was to investigate processing – structure – property relationship in electrospun nanofibers. This chapter discusses and summarizes the results of the research work described in the previous chapters. The major contributions of this work are reviewed and recommendations for future work are discussed.

6-1. Summary and Results

Fiber formation and patterning

In order to study the effects of processing parameters on molecular structure and tensile properties in electrospun fibers, an electrospinning setup was designed and developed (chap. 3). Unlike the standard setup, ambient conditions can be controlled using the developed setup.

The purpose in the first part of the work (processing studies) was to discuss the effects of electrospinning parameters on electrospun fiber morphology (fiber diameter and fiber uniformity). It was found that electrospun fiber diameter is

determined by mass of polymer in the spinning jet and the jet drawing ratio. Most of the electrospinning parameters were related with the jet drawing ratio and they are categorized in jet elasticity-, solidification time- and drawing force-related parameters. The tendencies to change fiber morphology were summarized in the processing map. The fiber morphology is highly contributed by polymer concentration, its molecular weight and solvent properties. Based on the systematic parameter studies, polymer nanofibers as small as 9nm in diameter were successfully produced. With the electrospinning setup developed in this study, 2D and 3D structures with electrospun aligned nanofibers were successfully produced (Chap. 3).

Structure formation / development via electrospinning

Structure formation / development in electrospun nanofibers were discussed using semi-crystalline rigid (PLLA), ductile (PCL) homopolymers and their block and random copolymers (Chap. 4). XRD and DSC analysis were conducted to investigate processing condition effects on the molecular structure.

For electrospun rigid polymer (PLLA) nanofibers, solvents properties and polymer concentration, which contribute to an electrical drawing of a jet, were found to affect molecular structure in amorphous region. Take-up velocity which is associated with

the mechanical drawing of the jet was the dominant parameter to develop crystalline structure. The crystalline structure appeared to be lamella oriented along the fiber axis at higher take-up velocity. On the other hand, crystalline structure was developed in electrospun ductile polymer (PCL) nanofibers via electrospinning process, but the crystallinity was independent of processing parameters like solvent properties and take-up velocity. Ductile polymer (PCL) has short crystallization time and low T_g which is lower than spinning temperature. Crystal formation of electrospun polymer fibers should be highly dependent on its crystallization rate and molecular mobility.

It was found that structure development of rigid (- LLA) units and ductile (- CL) is different in their block and random copolymers. Crystalline structure attributed to rigid (- LLA) units was developed in random units sequence (P(LLA-r-CL)) copolymer, while ductile (- CL) units were transformed into crystalline structure in block units sequence (P(LLA-b-CL) copolymer. The structure formation of ductile or rigid units is also highly reflected by their crystallization rate and molecular mobility. The mobility of ductile (- CL) units is high in block sequence (P(LLA-b-CL)) copolymer, while the mobility is restricted in random sequence (P(LLA-r-CL) copolymer. It would be concluded that crystalline structure is

developed by ductile units with high mobility and short crystallization rate in block sequence semi-ductile copolymer, whereas the ductile units support structure development of rigid units.

A disc collector was developed to conduct tensile tests using electrospun single nanofibers. As the results of tensile tests, crystallized PLLA nanofibers (as-spun at 630m/min) showed higher tensile modulus, strength but lower strain at break than that of amorphous PLLA nanofibers (as-spun at 63m/min).

Structure formation / development via post-processing

Structure formation / development of the electrospun nanofibers were discussed by applying post-processing to the as-spun PLLA nanofibers. Based on XRD and DSC analysis, the model of structure formation in hot-drawn nanofibers was suggested. The results of structure analysis indicated that crystalline formation via post-processing is highly dependent on initial molecular structure before the post-processing. Via annealing process, amorphous fibers (as-spun at 63m/min) has a high potential for the development of highly crystallized structure which is corresponding to isotropic crystalline structure.

On the other hand, crystallized fibers (as-spun at 630m/min) have a preferential structure to facilitate crystallization via hot-drawing. The crystalline structure in hot-drawn fibers seems to be crystal lamella oriented along the fiber axis. The lamellae break-up induced crystalline orientation along the fiber axis at higher drawing ratio, accompanying a decrease in ΔH. It is noteworthy that 91 % crystallinity was obtained by hot-drawing nanofibers (with around 500nm in a fiber diameter) at small drawing ratio of 1.5.

In addition to large scale nanofibers (500nm) used in the above studies, molecular structure of hot-drawn small scale nanofibers (< 100nm) was investigated. As the results, 80 % crystallinity was obtained in the small scale nanofibers at drawing ratio of 1.4. The high efficiency of hot-drawing on structure development might be due to nanometer scale effects. The packed molecular chains in small dimension induce high molecular interaction / shear force between molecular chains, affecting polymer crystallization kinetics.

Structure-properties of hot-drawn nanofibers were discussed by tensile tests using single nanofibers. Hot-drawing was successfully conducted using as-spun at 63m/min (540nm). The resultant hot-drawn nanofibers showed a significant increase

in tensile properties, i.e. 6.6 GPa in modulus, 230 MPa in strength and 0.26 in strain at break.

6-2. Review of Contributions

The major contribution of this thesis are summarized here.

- Development of the disc collector to prepare electrospun single nanofiber samples. The tensile test using electrospun single nanofibers is the effective way to discuss structure-properties relationship of the nanofibers.
- Development of the processing map which summarizes the effects of processing parameters on the morphology of electrospun nanofibers. The processing map may provide operators the idea that how each of processing parameter affects morphology of electrospun fibers.
- Development of 2D and 3D structures with aligned nanofibers. The structures would be good candidates for tissue engineering scaffolds to guide cell growth and filtration media to control filtration efficiency, respectively.
- Finding of the way for producing nanofibers with desired molecular structure and tensile property of electrospun nanofibers by controlling the dominant electrospinning / post-processing parameters. Nanofibers could be engineered to meet the demands from a wide range of application area based on the finding.

- Finding of the nanometer size effects on structure formation / development of electrospun nanofibers. This may leads to a new concept to understand polymer structure formation / development and contributes to polymer science.

6-3. Recommendations for Future Work

There are several interesting directions for future work in the areas of research presented in this thesis.

The mechanisms responsible for changes in electrical drawing ratio of a spinning jet could not be elucidated from the present study. Future work would be needed to identify the parameters which change the electrical drawing ratio. Repulsion force induced by static charges on the jet and electric force may determine the drawing ratio affected by ambient temperature, spinning voltage and solution properties. The charge level of the jet is likely measured by static voltmeter. The modeling based on the measurement might be helpful to understand the relationship between static charges on the jet and the drawing ratio. The jet is also mechanically drawn at higher take-up velocity. The continuous scanning of a spinning jet by X-ray may account for how take-up manner affects the jet drawing.

For fabrication of 2D and 3D architectures with electrospun aligned nanofibers, it still remains a concern for the size of architectures. If the stage fixed on edge of disc collector is large, electrospun nanofibers cannot be deposited on the whole stage surface area and mostly deposited at center line along edge of the disc collector. Another way must be concerned in order to fabricate 2D and 3D architectures with large surface area. During electrospinning using the disc collector, nanofibers move to the edge of the collector. Hence, if the stage can keep sliding vertically on the edge of the disc collector, it may help to cover the whole surface area of the stage with electrospun nanofibers, thus fabrication of 2D and 3D structures might be available.

In the morphology studies, we successfully controlled electrospun fiber diameter ranging from 9nm to around 3μm. However, structure-properties relationship in electrospun fibers with less than around 150nm in a diameter could not be investigated due to insufficient resolution of tensile tester. The tensile tester with higher resolution or another type of characterization apparatus would be required to identify the relationship.

6-4. Conclusion

The studies on processing-structure-properties relationship (PSP relationship) of electrospun nanofibers indicated that polymer fibers have great potential to develop / improve its molecular structure and mechanical properties if it is shrunk into smaller size. This would lead to further expansion of the material design. Further investigation on PSP relationship of nanofibers could give a new concept to create great performance polymer fibers.

Refereces

1. Brooman R A, *English Patent* 1845; 10: 582
2. Ziabicki A and Jarecki L, *In High Speed Fiber Spininng John Wiley and Sons, New York* 1985; 225
3. Yazdanian M, Ward I M and Brody H, *Polymer* 1985; 26: 1779
4. Clauss B and Salem D R, *Polymer* 1992; 33: 3193
5. Shimizu J, Okui N and Kikutani T, *SEN-I GAKKAISHI.* 1979; 35: 35-41
6. Lu F-M and Spruiell J E, *J. Appl. Polym. Sci.* 1987; 34: 1541
7. Dees J R and Spruiell J E, *J. Appl. Polym. Sci.* 1974; 18: 1053
8. Joseph E and Spruiell J E, *Polym. Eng. Sci.* 1975; 15: 660
9. Takasaki M, Ito H and Kikutani T, *J. Macromole. Sci.* 2003; 42: 59
10. Takarada W, Ito H, Kikutani T and Okui N, *J. Appl. Polym. Sci.* 2001; 80: 1582
11. Takarada W, Ito H, Kikutani T and Okui N, *J. Appl. Polym. Sci.* 2001; 80: 1575
12. Schmack G, Tandler B, Vogel R, Beyreuther R, Jacobsen and Fritz H-G, *J. Appl. Polym. Sci.* 1999; 73: 2785
13. Schmack G, Tandler B, Optiz G, Vogel R, Komber H, Hauβler, Voigt D, Weinmann S, Heinemann M and Fritz H-G, *J. Appl. Polym. Sci.* 2004; 91: 800
14. Lu F-M and Spruiell J E, *J. Appl. Polym. Sci.* 1987; 34: 1521
15. Peterlin A, *J. Polym. Sci. part C*, 1965; 9: 61

16. Stein R S and Wilkes G L, *In Structure and Properties of Oriented Polymers, John Wiley and Sons, New York,* 1975; 36

17. Keller A and Machin, *J. Macromol. Sci.* 1967; B1: 41

18. Kools F, *in Proceedings of the 4th International Conference, Polypropylene fibers and Textiles, Nottingham, U.K* 1987; 6/1

19. Capaccio F and Ward I M, *Polymer* 1975; 16: 239

20. Samuels R J, *J. Polym. Sci. part A* 1965; 3: 1741

21. Sadler D M and Barham P J Polymer 1990; 31: 36

22. Shimizu J, Toriumi K and Tamai K, *Sen-I Gakkaichi*, 1977;33: T-208

23. Shimizu J, Okui N and Kikutani T, *In High Speed Fiber Spininng John Wiley and Sons, New York* 1985; 429

24. Misra S, Lu F-M, Spruiell J E and Richeson G C, *J. Appl. Polym. Sci*. 1995; 56: 1761

25. Clauss B and Salem D R, Macromolecules 1995; 28: 8328

26. Abbott L E and White J L, *Appl. Polym. Symp.* 1973; 20: 247

27. Khaled M and Spruiell J E, J. Polym. Sci. Part B 1998; 36: 1005

28. Postema A R, Luiten A H, Ooster H and Pennings A J, *J. Appl. Polym. Sci.* 1990; 39: 1275

29. Fambri L, Pegoretti A, Fenner R, Incardona S D and Migliaresi, *Polymer* 1997;

38: 79

30. Postema A R, Luiten A H and Pennings A J, *J. Appl. Polym. Sci.* 1990; 39: 1265

31. Leenslag J W and Pennings A J, *Polymer* 1987; 28: 1965

32. Horacek I and Kalisek V, *J. Appl. Polym. Sci.* 1994; 54: 1751

33. Postema A R and Pennings A J, , *J. Appl. Polym. Sci.* 1989; 37: 2351

34. De Santis P and Kovacs A J, *Biopolymers* 1968; 6: 299

35. Kalb B and Pennings A J, *Polymer* 1980; 21: 607

36. Eling B, Gogolewski S and Pennings A J, Polymer 1982; 23: 1587

37. Huang Z M, Zhang Y Z, Kotaki M and Ramakrishna S, *Compos. Sci. Technol.*, 2003; 63: 2223

38. Formals A, *Process and Apparatus for Preparing Artificial threads, U.S. Patent No. 1,975,504* 1934

39. Shenoy S L, Bates W D, Frisch H L and Wnek G E, *Polmyer* 2005; 46: 3372

40. Kameoka J, Orth R, Yang Y, Czaplewski D, Mathers R, Coates F and Craighead H G, *Nanotechnology* 2003; 14: 1124

41. Megelski S, Stephens J S, Chase D B and Rabolt J F, *Macromoleucles* 2002; 35: 8456

42. Fong H and Reneker D H, *Polymer*, 1999; 40: 4585

43. Baumgarten P K, *J. Colloid. Interf. Sci.* 1971; 36: 75

44. Jarusuwanapoom T, Hongrojjanawiwat W, Jitjaicham S, Wannatong LO, Nithitanakul M, Pattamaprom C, Koombhongse P, Rangkupan R and Supaphol P, *Euro. Poly. J.* 2005; 41: 409

45. Demir M M, Gulgun Yilgor I, Yilgor E and Erman B, Polymer 2002; 43: 3303

46. Deitzel J M, Kleinmeyer J, Harris D and Tan N C B, *Polymer* 2001; 42: 261

47. Zhong X H, Kim K S, Fang D F, Ran S F, Hsiao, B. S and Chu B, *Polymer* 2002; 43: 4403

48. Son W K, Youk J H, Lee T S and Park W H, Polymer 2004; 45: 2959

49. Lee K H, Kim H Y, Ra Y M and Lee D R, Polymer 2003; 44: 1287

50. Wannatong L, Sirivat A and Supaphol P, *Polym. Int.* 2004; 53: 1851

51. Taylor G, *Proc. R. Soc. Lond. A.* 1964; 280: 383

52. Lee J S, Choi K H, Ghim H D, Kim S S, Chun D H, Kim H Y and Lyoo W S, *J. Appl. Polym. Sci.* 2004; 93: 1638

53. Buchko C J, Chen L C, Shen Y and Martin D C, *Polymer* 1999; 40: 7397

54. Zhao S L, Wu X H, Wang L G and Huang Y, *J. Appl. Polym. Sci.* 2004; 91: 242

55. Reneker D H, Yarin A L, Fong H and Koombhongse S, *J. Appl. Phys.* 2000; 87: 4531

56. Ayutsede J, Gandhi M, Sukigara S, Micklus M, Chen H E and Ko F, *Polymer* 2005; 46: 1625

57. Rutledge G C, Li Y, Fridrikh S, Warner S B, Kalayci, V E and Patra P, *National Textile Cneter, 2000 Annual Report (M98-D1), National Textile Center,* 2001;1

58. Yuan X, Xhong Y, Dong C and Sheng J, *Polym. Int. in press*

59. Mit-uppatham C, Nithitanakul M and Supaphol P, *Macromol. Chem. Phys.* 2004; 205: 2327

60. Bognitzki M, Czado W, Frese T, Schaper A, Hellwig M, Steinhart M, Greiner A and Wendorf J H, *Adv. Mater.* 2001; 13: 70

61. Casper C L, Stephens J S, Tassi N G, Chase D B and Rabolt J F, *Macromolecules* 2004; 37: 573

62. Koombhongse S, Liu W and Reneker D H, *J. poly. Sci. Polym. Phys*. 2001; 39: 2598

63. Li D and Xia Y, *Nano Lettter* 2004; 4: 933

64. Li D, Ouyang F, McCann J T and Xia Y, *Nano Letter ASAP article* 2005

65. Boland E D, Wnek G E, Simpson D G, Palowski K J and Bowlin G L, *J. Macromol. Sci. Pur Appl. Chem.* 2001; A38: 1231

66. Matthews J A, Wnek G E, Simpson D G and Bowling G L, *Biomolecules* 2002; 3: 232

67. Sundaray B, Subramanian V, Natarajan T S, Xiang R Z, Chang C C and Fann W S, *Appl. Phys. Lett.* 2004; 84: 1222

68. Katta P, Alessandro M, Ramsier R D and Chase G G, *Nano Letter* 2004; 4: 2215

69. Li D, Wang Y and Xia Y, *Nano Letter* 2003; 3: 1167

70. Dersch R, Liu T, Schaper A K, Greiner A and Wendorf J H, J. Polym. Sci. Part B 2003; 41: 545

71. Li D, Wang Y and Xia Y, *Adv. Mater.* 2004; 16: 361

72. Teo W E, Kotaki M, Mo X M and Ramakrishna S, *Nanotechnology* 2005; 16: 918

73. Zong X, Ran S, Fang D, Hsiao B S and Chu B, *Poylmer* 2003; 44: 4959

74. Fennessey S F and Farris R J, *Polymer* 2004; 45: 4217

75. Tan E P S and Lim C T, *Appl. Phy. Lett.* 2004; 84: 1603

76. Reneker DH, Chun I. Nanotechnology 1995; 7: 216-223.

77. Hou H, Jun Z, Reuning A, Schaper A, Wendorff JH, Greiner A. Macromolecules 2002; 35: 2429-2431.

78. Mo XM, Xu CY, Kotaki M, Ramakrishna S. Biomaterials 2004; 25: 1883-1890.

79. Ian MS, Solvent Recovery Handbook second edition, Brackwell Science, CRC Press

80. Bruno TJ, Svoronos PDN, CRC Handbook of Basic Tables for Chemical Analysis, CRC Press

81. International Programme on Chemical Safety

82. Deitzel J M, Kleinmeyer J D, Hirvonen J K and Tan N C B, *Polymer* 2001; 42: 8163

83. Jaeger R, Schonherr H and Vancso G J, *Macromolecules* 1996; 29: 7634

84. Buer A, Ugbolue S C and Warner S B, *Textile Res. J.* 2001; 71: 323

85. Zong X, Kim K, Fang D, Ran S, Hsiao B S and Chu B, *Polymer* 2002; 43: 4403

86. Mo X M, Xu C Y, Kotaki M and Ramakrishna S, *Biomaterials* 2004; 25: 1883

87. Tan S-H, Inai R, Kotaki M and Ramakrishna S 2004 *Polymer* 2005; 46: 6128-6134

88. Spruiell J E andWhite J L, *Polym. Eng. Sci.* 1975; 15: 660

89. Radhakrishnan J, Ito H, Kikutani T and Okui N, *Polym. Eng. Sci.* 1999; 39: 89

90. Cho H H, Kim K H, Kang Y A, Ito H and Kikutani T, *J. Appl. Polym. Sci.* 2000; **77:** 2267

91. Mezghani K and Spruiell J E, *J. Polym. Sci. B* 1998; 36: 1005 (Nanotech ref22

92. Schmack G, T¨andler B, Optiz G, Vogel R, Komber H, H¨außler H, Voigt D, Weinmann S, Heinemann M and Fritz H-G, *J. Appl. Polym. Sci.* 2004; 91: 800

93. Fischer E W, Sterzel H J and Wegner G, *Kolloid-Z.u.Z.Polym.* 1973; 251: 980

94. Crescenzi V, Manzini G, Calzolari G and Borri C, *Eur. Polym. J.* 1972; 8: 449

95. Tsuji H, Mizuno A and Ikada Y, *J. Appl. Polym. Sci.* 2000; 76: 947-953

96. Inai R, Kotaki M and Ramakrishna S, *Nanotechnology* 2005; 16: 1-6

97. Fong H, Chun I and Reneker D H, *Polymer* 1999; 40: 4585-4592

98. Hoogsten W, Postema A R, Pennings A J, tenBrinke G and Zugenmaier P, *Macromolecule* 1990; 23: 634

99. Mezghani K and Spruiell J E, *J. Polym. Sci. B* 1997; 36: 1005

100. Wei M, Shuai and Tonelli A E, *Biomacromolecules* 2003; 4: 783-792

101. Mark J E, Polymer Data Handbook; Oxford University Press: New York, 1999

103.Hoogsteen, Postema, Pennings, Brinke and ZugenmaierClauss, *Macromolecules* 1990; 23: 634

104. Brizzolara, Cantow, Diederichs, Keller and Domb, *Macromolecules* 1996; 29: 191

105. Puiggali, Ikada, Cartier, Okihara, Lotz, *Polymer* 2000; 41: 8921

106. Tsuji and Ikada, *Polymer* 1995; 36: 2709

107. Kwan Lee, Hee LEE and Jin, *European Polymer Journal* 2001; 37: 907

108. Clerk E S, *in Structure and Properties of Polymer Films, Plenum, New York,* 1973; 267